EVALUATION OF LARGE SCALE SEISMIC TESTING METHODS FOR ELECTRICAL SUBSTATION SYSTEMS

PEER Lifelines Project 410

Principal Investigator: R.L.Nigbor, USC

Research Assistant: Elena Kallinikidou, USC

University of Southern California Report CE-5060-1
October 12, 2004

ACKNOWLEDGMENTS

This project was sponsored by the Pacific Earthquake Engineering Research Center's Program of Applied Earthquake Engineering Research of Lifeline Systems supported by the California Energy Commission, the California Department of Transportation, and the Pacific Gas and Electric Company.

This work made use of the Earthquake Engineering Research Centers Shared Facilities supported by the National Science Foundation under award number EEC-9701568 through the Pacific Earthquake Engineering Research Center (PEER). Any opinions, findings, and conclusions or recommendations expressed in this material are those of the author(s) and do not necessarily reflect those of the National Science Foundation.

This report was prepared as a result of work sponsored by the California Energy Commission (Commission). It does not necessarily represent the views of the Commission, its employees, or the State of California. The Commission, the State of California, its employees, contractors, and subcontractors make no warranty, express or implied, and assume no legal liability for the information in this report; nor does any party represent that the use of this information will not infringe upon privately owned rights. This report has not been approved or disapproved by the Commission nor has the Commission passed upon the accuracy or adequacy of the information in this report.

The financial support of the PEARL sponsor organizations including the Pacific Gas & Electric Company, the California Energy Commission, and the California Department of Transportation is acknowledged.

Finally, the assistance of Professor Joel Conte and his graduate student Hemangi Pandit with the nonlinear SDOF modeling and analysis are gratefully acknowledged.

CONTENTS

LIST OF FIGURES

LIST OF TABLES

NOMENCLATURE

α = post-yield / pre-yield stiffness ratio: strain-hardening (or softening) ratio

Cy: strength coefficient (yield strength / weight)

E_D (t): energy dissipated by viscous damping

E_I (t): input energy to the structure due to the excitation (relative)

E_K (t): kinetic energy (relative)

E_S (t): elastic strain energy

E_Y (t): hysteretic energy (yielding)

$f_s(u(t),\dot{u}(t))$: restoring force for an elastoplastic system

fy: yield strength

u_m: peak absolute deformation of an elastoplastic system

u_y: yield deformation of an elastoplastic system

$\mu = \frac{u_m}{u_y}$: ductility factor of an elastoplastic system

m: system's mass

w: system's weight

k: system's stiffness

c: viscous damping coefficient

$c_{cr} = 2\sqrt{k \cdot m}$: critical damping coefficient

ξ: damping ratio

$\omega_n = \sqrt{\frac{k}{m}}$: natural frequency

$T_n = \frac{2\pi}{\omega_n}$: natural period of vibration

$\omega_D = \omega_n \sqrt{1-\xi^2}$: damped frequency

u (t): relative displacement with respect to the base at time t

$\dot{u}(t)$: relative velocity with respect to the base at time t

$\ddot{u}_s(t)$: support acceleration at time t

1. INTRODUCTION

The need for continuous experimental research in earthquake engineering is imperative in our pursuit to advance in the seismic engineering and construction practices, and as a result, enhance public safety and reduce economic losses in future earthquakes.

The Northridge earthquake (1994) as well as more recent major earthquakes in Turkey (Izmit 1999) Taiwan (Chi-Chi, 1999) and Japan (Kobe, 1995) have showed that the reliability of an electrical power transmission and distribution substation system depends upon not only the seismic response of its individual components but also upon the dynamic interaction between interconnected equipment.

Structural damage initiation, propagation and collapse mechanisms are very difficult to model analytically, and even then large–scale experimental verifications are essential, a fact which leads to the need for experimental testing facilities. Based on the facilities' capabilities, the structural systems and components can be tested as close to their prototype size and boundary conditions as possible.

This report is organized into four sections. Section 1 focus on an overview of the following three large-scale seismic testing methods:

- Current state of shake table facilities in the United States and Japan
- The use of underground explosive blasts for the simulation of earthquake ground motion based on data from the Nevada Test Institute (NETI) facility at the Nevada Test Site
- The use of uncontrolled mining explosions for the simulation of earthquake ground motion based on data from the Black Thunder Mine (BTM) event of April 3rd, 1997.

Section 2 includes an analytical comparison of the different testing methods based on their waveform characteristics (peak values: acceleration, velocity, displacement; Duration, Arias intensity, Cumulative absolute velocity, Fourier Spectra). The response of single degree of freedom (SDOF) linear and nonlinear systems to the selective waveforms is also investigated. The comparison is based on response, constant ductility and energy spectra.

Section 3 addresses the current testing needs for electrical substation systems and components.

Section 4 presents the comparison between the current seismic testing needs and existing capabilities.

2. OVERVIEW OF LARGE SCALE SEISMIC TESTING METHODS

2.1. Introduction

In this study, the main source of information regarding the state of Shake table facilities for earthquake engineering research in the United States was the EERI report:
" Assessment of Earthquake Engineering Research and Testing Capabilities in the United States", September 1995 [Ref.1] and the SRI International report: " Directory of International Earthquake Engineering Research Facilities", October 2001 [Ref.23].
Additional data on the recent and future upgrades for the US testing facilities have been obtained online from the NEES web page: *http://nees.ucsd.edu* .

2.2. Evaluation of existing Shake table Facilities in the US

In terms of major facilities, there are presently in the U.S. five shake tables, three reaction walls, four geotechnical centrifuges, and sixteen floor reaction systems. In the rest of the world, there are fourteen shake tables (twelve in Japan), seven reaction walls (six in Japan), eleven geotechnical centrifuges and twenty floor reaction systems [Ref.1].

The largest shaking tables in the U.S. are at the University of California at Berkeley (20ft x 20ft), the State University of New York at Buffalo (12ft x 12 ft), the University of Illinois at Urbana-Champaign (12ft x 12ft), the U.S. Army Civil Engineering Research Laboratory (USA CERL) (12ft x 12 ft) and the University of California at San Diego (10ft x 16ft), however, they are considered as small to medium sized tables. The payload capacity of these tables range from 15,000 to 120,000 lbs. Recent upgrades to the tables at Berkeley and USA CERL provide capability to excite test structures with three-dimensional earthquake motions. A review of the shake table testing facilities in U.S. is given in Tables 2-1 and 2-2. [Ref.2].

Currently, shake table tests are essential for the validation of various innovative structural control concepts, such as base-isolation systems, passive, active, and hybrid energy-dissipating devices. Furthermore, they are useful for testing equipment and non-structural components in buildings as well as nuclear containment vessels. However, due to the limited size and capacity of the shake tables in US, the specimens have to be scaled by a large factor and be tested at higher frequencies.

In general, most facilities have been utilized far less than they could if sufficient research funds were available. There is also a need for upgrading these facilities using state of the art equipment. The capital costs for upgrade of existing facilities in U.S. is estimated at $60 million spread over a five to ten year period (data for 1995). The costs of research, operation and maintenance of these facilities are estimated at $40 to $50 million per year [Ref.1].

Table 2-1 List of Major U.S. Shake Table Facilities

Institution	State	Payload (metric tn)	Size (m x m)	DOFs	Freq. Range (Hz)	Max Stroke (m)	Max Velocity (m/s)	Comments
EERC, University of California Berkeley	California	45.36	6.1x6.1	6	0-15	0.127	0.762	
State university of New York at Buffalo	New York	50	3.6x3.6	5	0.1-50	0.15	1.25	Plan to install a second table on rails for rapid relocation.
University of California San Diego	California	32.66	3.0x4.9	1	0-50	0.152	0.89	
University of Nevada at Reno	Nevada	45	4.3x4.5	2	0.1-30	0.3	1	University of Nevada at Reno has two 45 tn shake tables relocatable on a 45m x 17m strong floor.
University of IL at Urbana-Campaign	Illinois	4.5	3.7x3.7	1	0.1-50	0.05	0.381	
U.S.Army, Civil Engineering Research Lab, Illinois	Illinois	45.36	3.6x3.6	3	0.1-60	0.3	1.3	
Wyle	Alabama	27	6.1x6.1	2	0-100	0.152	0.89	

Table 2-2 Smaller U.S. Shake Tables (Partial List)

Rice University	Texas	0.68	1.52x1.52	1	0-75	0.076	0.89	
ANCO	Colorado	1.8	1.56diam	6	0-40	0.1	2.3	
Arizona State University	Arizona		3x3					
Cornell University	New York	2.7	2.1x1.5	3	0-50	0.076	0.8	
Drexel University	Pennsylvania	0.41	1.2x1.8	1	0-2000	0.06		
Stanford University	California	2.2	1.5x1.5	1	0-50	0.032	0.635	
University of Ca. at Irvine	California	9.1	3x3	4	0-50	0.254	0.254	Under construction
University of Ca. at Los Angeles	California	0.51	1x2	1	0-30	0.037	2.54	
University of Southern California	California							
University of Washington	Washington	9	2.4x1.8	1	0-1000	0.038		
Union Carbide, Oak Ridge	Tennessee	7	1.83x1.83	3	0.1-20	0.193	0.3	
Westinghouse	Pennsylvania	3.1	3.1x3.1	2	0-500	0.61	2.54	
NASA	Alabama	.907	3.0x4.5	6		2.44	0.1	
Wyle	California	13.2	2.4x2.4	2	0-70	0.3	1.17	3 additional smaller tables

2.3. Assessment of the need for a large scale US test facility

The Loma Prieta, Northridge, and Kobe earthquake caused extraordinary damage in urban areas where the performance of many engineered structures was poor. Large structures such as bridges and buildings, components for large industrial facilities such as chemical plants, power generation facilities and lifelines require large-scale experimentation to fully understand their seismic behavior. Earthquake simulation testing facilities with the capability to test large structures are necessary to further explore earthquake mitigation solutions.

One large facility is needed to test the structures with plan dimensions on the order of 50 feet. In addition, two regional shaking table facilities are needed where structures of approximately one half this size can be tested [Ref.1]. The use of a series of small-sized tables linked together in synchronization to excite a large-scale specimen, instead of a single large shaking table should be considered.

Costs to develop a single national testing facility with a large shaking table and / or large reaction wall are estimated in excess of $400 million. Annual operating costs for a national facility are estimated in excess of $100 million. For a fraction of the operating costs associated with a single large facility, a number of research and testing programs could take place at regional centers and smaller institutions that could possibly yield a larger amount of research information than a single large facility. Any decision about future implementation of a large-scale facility should be based on a detailed feasibility study and on a comprehensive national plan for experimental research

As stated by the MTS enterprise (a U.S. based enterprise which has supplied over 140 custom engineered shaking table systems around the world), the Tadotu Facility can provide useful insight for a futuristic view of structural experimental facilities. It is likely that future facilities will be similar in appearance and scope and will require similar budgets to operate [Ref. 4].

A conceptual design for a large U.S. test facility was conceived by MTS enterprise for the EERI in 1982 [Ref. 4]. The facility was designed to have two testing areas:
A 20 m x 20m six degree of freedom shaking table that could subject 2000 ton specimens, 30 meters high to 1g acceleration, 1.5 m/sec velocity and 1m stroke and
A 46 m x 61m strong floor surrounded on three sides with strong walls 30 meter tall.

The cost estimate in 1984 was $130 million. The future implementation of the facility is unknown.

2.4. Japan's large scale seismic testing facilities

In Japan, many seismic test facilities currently exist in universities, national institutes and also in industrial enterprises. In this section two extraordinarily large-scale testing facilities in Japan will be discussed; the one at Tadotsu (a project of NUPEC, Nuclear Power Engineering Company) and the other at Tsukuba (a project of BRI, Building Research Institute) [Ref. 3].

For the facility at Tadotu on Shikoku Island, the primary consideration was the implementation of full-scale experiments for equipment and if possible for structures of NPP (Nuclear Power Plants). The table is 15m x 15m, biaxial and can subject 1000ton specimens to 1.84g horizontally and .92g vertically acceleration. The system uses gas charged accumulator banks to reduce the approximately 50,000 Kw peak power required if only hydraulic pumps were used. The initial cost of the Tadotu facility was approximately $300 million U.S. in 1982 (the facility was completed in November 1982). A total of twenty-three shaking table experiments were performed during this 13-year period. The cost of each experiment averaged around $ 40 million U.S. and the maintenance costs alone over the 13-year period was approximately $100 million U.S. [Ref. 3].

The 15m x 15m, 1000ton payload shake table of NUPEC (Nuclear Power Engineering Test Center) in Tadotu, Japan, seems despite its worldwide unique capacities, significantly underutilized due to high operational cost and test complexities. The utilization of shake tables in this country varies from 30% to 50%.
The second facility is the structural test laboratory at the Building Research Institute at Tsukuba (BRI). The hydraulic actuators controlled by electronic servo-controllers have capacity of 1000kN in force and 1m stroke. The capacity of the reaction wall is 40 MN for shear and 720 MN x m for bending moment. Each one of the two test floors can accommodate structures with 300m2 floor area and 25 meter height. The magNeTIc response type displacement transducers (DLT) can measure displacement up to +1m with accuracy of 0.01mm. The cost to complete the BRI facility was about 45 million U.S. dollars and the yearly maintenance cost $0.35 million U.S. in 1994. In the early 1980s, the first U.S.-Japan joint research project took place at the BRI with a full-scale test of a 7-story reinforced concrete building [Ref. 3]. A list of shake table testing facilities in Japan is given in Table 2-3.

Table 2-3 List of Major Shake Tables in Japan

Criterion: Payload >=20 tons or Area >=10m2

Institution	Payload (ton)	Size (m x m)	DOFs	Freq. Range (Hz)	Max Stroke (m)	Max Velocity (m/s)
Aichi Institute of Technology	136.1	11x6	1	3.3-13.3	0.007	
Building Research Institute	18.13	3x4	3	0-50	0.1	
Fujita Corporation	25	4x4	1		0.5	1.5
Hazama Corp. Ltd	80	6x4	3	0-50	0.3	
Hitachi Engineering Corp.	20	4x4	1	0-30		
Kajima Corp. Tokyo	50	5x5	6	0-60	0.2	1
Kumagai-Gumi Corp. Ltd	63.5	5x5	6	0-70	.26	
Kyoto University	13.6	5x3	6	0-50	.30	1.5
National Research Institute of Agriculture Engineering	45.4	6x4	3	0-40	0.15	0.75
National Research Institute for Earth Science and Disaster Prevention	1088	20x15	3	0-15	1.0	2.0
Nishimatsu construction Corp.		5.5x5.5	6			
Nuclear Power Engineering Corp	1000	15x15	1horiz &vert	0-30	0.2	0.75
NYK Corporation Ltd	20	2.6x2.6	6	0-80	0.2	0.6
NRC for Disaster Prevention, Tsukuba	500	15x15	1horiz &vert	0-50	0.03	0.37
Obahashi-Gumi Corporation	45.35	5x5	3			
Public Works Research Institute	272.11	8x8	1horiz &vert	0-50	0.6	2.0
Sanryo Heavy Industries Corp	90.7	6x6	6	0-50	0.3	
Shimizu Corp	10.88	5x4	2	0-50	0.1	
Taisei Corp Ltd	20	4x4	1horiz &vert		0.4	
Tobishima Corp Ltd	20	4x4	3	0-30	0.2	

2.5. Simulation of strong ground motion with explosive sources

Dynamic testing of as-built structures with underground blasts is perhaps the closest form of testing to a natural earthquake. Three different types of blasts can be used for such dynamic testing:

- The first type is the one in which explosions were not designed to simulate any desired kind of ground motion or were not intended primarily to excite any particular structure. Underground nuclear explosions have been shown to be comparable to strong-motion earthquakes and therefore provide an opportunity for obtaining data on structural response to strong ground motion. Other explosions such as in mining may be taken advantage of for testing nearby structures. The obvious disadvantage is that only structures located within the region of measurable ground motions arising from the explosions can be tested

- The second type of blast tests is the one in which explosions are designed specifically for exciting the test structure but not designed to simulate earthquake-like ground motions on structural response. Such tests have been performed infrequently and mostly on Nuclear Power Plant (NPP) buildings. It is unlikely that detonation of high explosives would become an acceptable source of exciting as-built structures because of the safety aspect and the potential damage it may cause to the test structure. However, small explosive charges, the energy of which would not be enough to cause any damage to the tested structure, may be acceptable as excitation source.

- The third type of explosion technique is implemented with arrays of sequentially fired explosives to simulate earthquake-like ground motions. These explosion induced motions have to be similar to the natural earthquake ground motions in certain essential aspect, that depend partly on the dynamic characteristics of the structure to be tested. A discussion on the simulation criteria is given by Higgins [Ref.12]. Although this technique has the potential to become a field technique for proof testing, its utility can only be fully established only after the successful demonstration of in-situ testing.

2.5.1. Response of Structures to Underground Nuclear Explosions

Blume reported on a number of studies on the response of many high-rise buildings in Las Vegas to ground motion originated by underground nuclear explosions, where the distance of the explosion site varied from 81 to 181 miles. The buildings studied varied in height up to 32 stories and most of them were of reinforced concrete construction [Ref. 6,7,8].

In some cases three components of acceleration and three components of displacement at the top of the buildings were recorded. In other cases, velocity meters at the top, at two or

three intermediate levels, at the basement and on the ground surface were used to measure response. Discussing the results, Blume observed that generally the response tended to peak at or close to natural periods. The maximum responses of six of the buildings to the explosions were compared with those to two distant earthquakes. The comparisons showed that the explosions produced larger response.

Blume also studied the natural periods of the buildings associated with the maximum response. Natural periods of the buildings were observed to be generally non-constant and period changes were considered to be not necessarily indicative of damage. In many buildings period and damping tended to increase with time, loading, amplitude, and with prior history of loading.

The author also used the results to obtain approximate mode shapes and to study modal contribution from different modes to peak amplitudes. He concluded there was no reason that the findings based on response to underground nuclear explosions should not be applicable to the problem of response to natural earthquake.

Continuing the above studies, Blume compared measured responses to those of the same buildings to the 1971 San Fernando earthquake with an epicentral distance of 235 miles. One of the nuclear explosions located at about half this distance from the buildings caused peak accelerations of almost up to twice the San Fernando earthquake response amplitudes. He also compared the fundamental periods of the buildings and found them to be similar at peak response.

2.5.2. Simulation of earthquake strong-motion by Underground Explosive Blasts

Bleiweis et al. reported on the simulation of strong-motion earthquake effects on structures using explosive blasts [Ref. 8]. A series of dynamic blasts was detonated 100ft from the test structure, a three-story single-bay steel frame supported on a concrete base. Accelerations were measured at different levels of the structure, the base and the free field. Based on the results the authors state that varying the charge size and using time delays had only a small effect on the frequency response of the base of the structure. The frequency content was more sensitive to distance and depth of the charge placement. The natural frequencies and mode shapes for the structure's three flexural modes were found to be very close to those obtained from steady-state shaker tests. The damping estimates were made from the power spectra of blast-response records, using the half-power method.

Another test with buried explosive charges is that of the proof testing of a circuit breaker in an electric substation reported by Taylor et al. [Ref. 9]. One of the objectives of the test was to demonstrate that the explosives test method could be performed safely in an electrical substation, in the presence of energized equipment. Accelerometers were placed at the free field, on the circuit breaker itself and on the foundation; also a tri-axial strong-motion seismograph and a peak-shock recording device were mounted on the foundation.

The instrumentation was designed to give response spectra and the Fourier Transform of the records. Since this was a proof test, the functional performance was of primary interest and it appears that the response records were not used for determining the dynamic characteristics of the circuit breaker. The authors conclude that the seismic proof testing using buried explosive charges is promising as a method of in situ testing of large structures and also provides a more realistic simulation of the earthquake response since it includes the effects of soil and foundation.

Higgins et al. [Refs. 10,11,12], describe the potential and feasibility of underground explosions for simulating natural earthquake ground motions in vibration tests. These authors state that the underground detonation of high explosives is the best available means of simulating the effect of earthquake ground motions on soil and soil-structure systems and state that explosives in various arrays can produce motions with amplitudes and frequency content in the range of those expected in large earthquakes. They conclude that enhancement of the time duration and number of motion cycles of explosive experiments is feasible and practical with time-sequenced explosions.

Bruce and co-writers [Refs. 13,14] describe another effort on earthquake simulation using controlled explosives. The technique produces earthquake-like ground motion by detonation of a planar array of vertical line sources placed in the soil near the test structure. The reported tests involved 1/3-scale array sources and the emphasis in this test series was on the simulation technique itself rather than the structural response aspect. They note that simulation with large displacements is limited to low frequencies (2-3 Hz) and that producing significant ground motion in very stiff soil or rock site might be impractical with their technique. This technique, which later was given the name RESCUE, will be described in more detail in the next section of this report.

2.6. Nevada Testing Institute

The Nevada Testing Institute (NeTI), a non-profit institution located in the state of Nevada, is founded to facilitate the use of the Nevada Test Site (NTS) by researchers primary in University Institutions in U.S. and abroad. The main objective of NeTI is to develop advanced testing capabilities for the testing of earthquake hazard mitigation design and technologies related to civil, structural and seismic resistant engineering systems. Using the Repeatable Earth Shaking by Controlled Underground Expansion (RESCUE) technique for producing strong ground motion developed by SRI International, the NeTI is developing a full-scale strong ground motion testing facility.

2.6.1. The RESCUE technique

The RESQUE technique addresses the need to study the response of large and full-scale structures under strong ground motion loading that includes significant realistic soil-structure interaction. The RESCUE technique can be used in two ways. First, large and

full-scale structures of interest will be constructed on a permanent soil test bed that is loaded dynamically by RESCUE sources (NeTI facility at NTS). Second, RESCUE can be fielded around existing structures to test the dynamic response of actual full-scale structures in situ [Ref. 5].

The RESCUE technique produces ground motion by simultaneously expanding a planar array of buried vertical sources. The RESCUE source design consists of a rubber bladder around a steel rectangular mandrel. Propellant is burned in steel canisters to produce high-pressure gas, which is subsequently vented in a controlled manner into the source module to produce low-pressure gas (up to 1 Mpa). This causes the rubber bladder to expand and move the soil, which excites the structure. Because the sources generate low pressure, they do minimal damage to the surrounding soil, allowing for sequential pulses of ground motion to be applied to the soil. Each pressure pulse typically produces two cycles of ground motion due to the elastic rebounding response of the soil medium.

The RESCUE technique provides complete control over the applied pressure pulse characteristics. The peak pressure is controlled by the propellant quantity; the pulse rise time is controlled by the canister vent area; the pulse duration is controlled by the opening time of the source vents; the time between consecutive pressure pulses is controlled by the propellant ignition time (Ref. 5, Fig 1-3 shows the full-scale soil island test bed that is currently planned to be constructed at the NTS). The test bed is 46m x 46m and is designed to accommodate full-scale structures, such as wood, steel or concrete framed, storage tank facilities, buried pipelines, electrical switchyard equipment or large-scale models of nuclear reactors. Each of these types of structures can be tested to failure without causing damage to the facility.

To simulate ground motion that is representative of near-fault long-period type motion, the RESQUE sources can generate a sequence of two pressure pulses with a decreased delay time, between the first and second pressure pulse, thus producing one long-duration pressure pulse.
To generate vibratory motion, the RESCUE sources can be placed in trenches opposite each other and to produce a combined motion in two orthogonal directions they can be buried in adjacent trenches. They also generate a vertical component that is 10 to 20% of the magnitude of the horizontal component. However, by placing the RESCUE source in the ground such that the bladder surface applying pressure against the soil is at an acute angle with respect to the horizontal plane, the vertical motion can be amplified (Illustrations of the RESQUE sources can be found in Ref. 5).

2.6.2. Tests performed with the RESCUE technique

Seven tests were performed at SRI's remote test site (CHES) and five tests were performed at the NTS with a 1/7-scale prototype RESCUE source. For applied pressure levels of up to 0.6 Mpa, peak 1/7 scale ground motions of 5.8 g, 60 cm/sec and 4.8 cm

were obtained, which correspond to 0.8 g, 60 cm/sec and 34 cm. Considering that the RESCUE source can generate up to 1 Mpa peak pressure the maximum full-scale ground motion can reach values up to 1.0to 2.0 g, 100 to 140 cm/sec and 60 to 100cm. A summary of the test results is presented in Table 2-4.

Table 2-4 Summary of 1/7 scale ground motion generated at SRI's CHES and NTS

Test	Soil type	Applied Pressure (Mpa)	Gauge Location (from source)	Peak Ground Motion			Peak Spectral Value and Period		
				Accel.	Velocity	Displ	Accel.	Velocity	Displ.
				(g)	(cm/s)	(cm)	(g)	(cm/s)	(cm)
SRI 5	Stiff clay	0.21	1.5 m Free - field	3	28	0.8	7@ 0.04 sec	50 @ 0.08s	0.8 @ 0.16s
SRI 6	Stiff clay	0.28	1.5 m Free - field	5.8	56	1.3	13 @ 0.04s	112 @ 0.08s	2.5 @ 0.25 s
NTS 2	Weak compacted silty-sand	0.3	3.6 m Soil Island	1.3	28	1.4	3.2 @ 0.04s	58 @ 0.2 s	2.3 @ 0.4 s
NTS 3	Weak compacted silty sand	0.44	3.6 m Soil Island	2.6	48	3.8	5.1 @ 0.05s	92 @ 0.2s	4.8 @ 0.6 s
NTS 4	weak compacted silty sand	0.44	3.6 m Soil Island	2.6 to 4.5	50	2.8	7.4 @ 0.02s	87 @ 0.2 s	3.8 @ 0.7 s
NTS 5	weak compacted silty sand	0.6	3.6 m Soil island	4	60	4.8	5.8 @ 0.02s	112 @ 0.2 s	5.8 @ 0.5 s

The tests depicted the following characteristics of the RESQUE technique:

- The RESQUE technique provides the capability for tailoring the applied peak pressure, pressure pulse shape and generated ground motion and is able to generate large ground motions with respect to acceleration, velocity and displacements.

- The RESQUE technique applied pressure loads are reproducible with respect to propellant quantity and also timing and firing sequence.

- The RESQUE hardware is durable, can be used for multiple tests and is easily transported.

2.6.3. Development of the Nevada Seismic Testing Center

SRI's RESQUE technique along with the existing testing and construction capabilities at the NTS, allows for the development of a strong ground motion testing center that will enable seismic testing to be performed on large and full-scale structures. The center will be able to accommodate multistory buildings, nuclear reactor structures, highway overpass structures, fluid storage tanks, electrical switchyard equipment and buried pipelines.

One of the main advantages of the proposed facility at the NTS (Fig. 2-1) is the implementation of multiple test beds of different sizes and soil types, which along with the versatility of the RESQUE technique in producing a wide variety of ground motion types, offers the research community an efficient multi-faceted testing capability. This overcomes the inefficiencies of tying up a limited testing facility with one long-term research project. The full development of the Center is projected to be a five-year process that includes the final design performance testing of full-scale RESQUE sources in the year 2000, construction of the first full-scale test bed in the year 2001, and final development of the Center through the year 2004.

Figure 2-1 Proposed Nevada Seismic Testing Center at the Nevada test Site

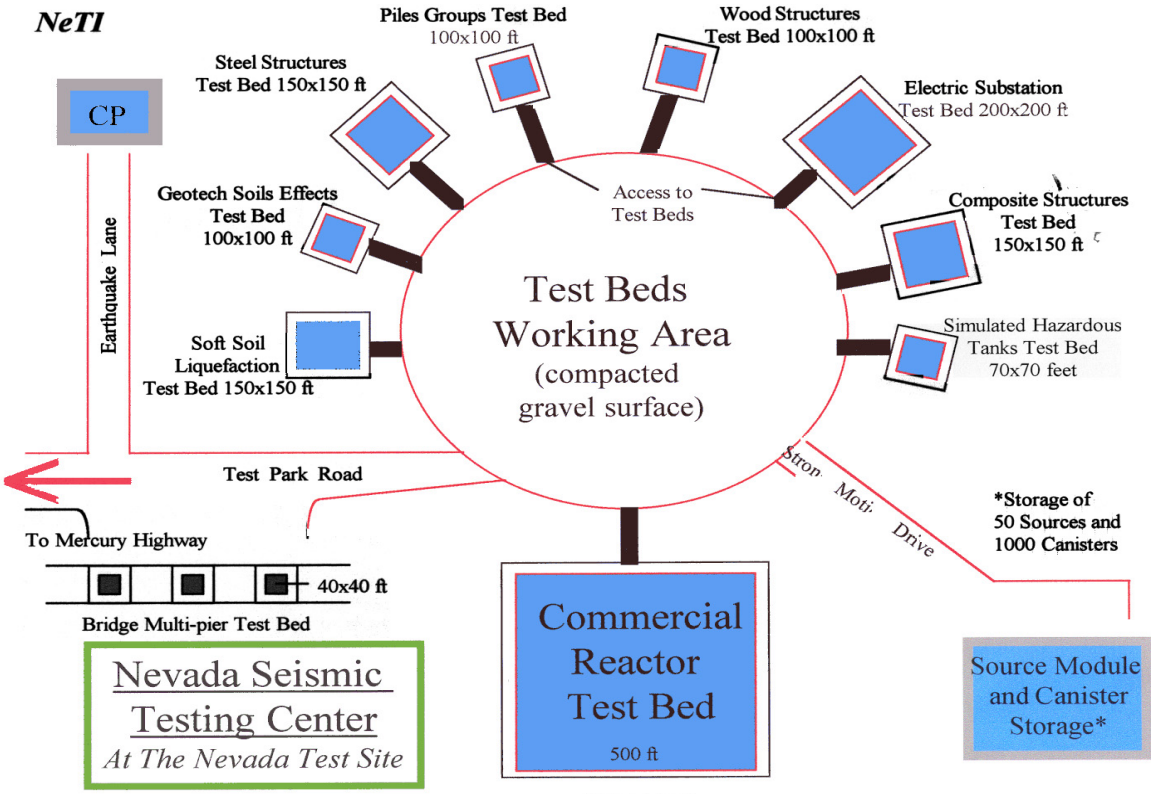

Figure 11

2.7. Black Thunder Coal Mine Event – Background Information

For the Black Thunder coal event of April 3,1997 the length of the explosive array was 1280 m and the total weight of explosive estimated at 2.95 kilotons. The rows in the explosive array were triggered at 35-millisecond delays. The strong ground motion duration due to this detonation was about 6.0 seconds. A total of 25 accelerometers were fielded for this event. The accelerometers recorded radial, transverse and vertical measurements at 50, 100, 150, 200, 300, 400 and 500 m ranges from the explosive array.

Based on the data from Ref. 24, it is noted that for this event uncertainties in the baseline correction for the ground accelerations are not expected to affect the response spectra values for frequencies greater than about 1.5 Hz, but may have an effect on the spectral ordinates for the low-frequency range. The estimation error for the spectral ordinates and also for the peak ground accelerations, velocities and displacements due to baseline correction uncertainties is not given in the ARA report [Ref.24].

3. ANALYTICAL COMPARISON OF DIFFERENT TESTING METHODS

3.1. Introduction

To compare quantitatively the waveforms from the testing methods with the recorded earthquake records, first we examine the Fourier spectra for all the records and then the response spectra for single degree of freedom (SDOF) linear and nonlinear systems. The following three testing methods are investigated in this study: 1) Shake table (10" and 2" displacement limit); 2) Nevada Test Institute; 3) Black Thunder Mine event of April 3rd, 1997. The earthquake records used in the analysis were from the Landers and Northridge earthquake.

The response spectra (absolute acceleration, relative values: displacement, velocity) for a linear SDOF system and also the constant ductility spectra, energy time histories and response spectra for an elasto-plastic SDOF system were calculated and the results will be discussed in the following paragraphs.

3.2 Record Description

The following four groups of acceleration time history records are included in this study: (1) Earthquake; 2) Shake Table (10 in. displacement limit, 2 in. displacement limit, Telcordia record); 3) NETI; 4) Black Thunder Mine. The record ensemble with additional information on the data sources, filtering and duration is given in Tables: 3-1, 3-2.

The PEER Strong Motion Database (*http://peer.berkeley.edu)* was the source of the earthquake acceleration data in the first group. From the six near field records (Table 3-1: R1-R6) two are from the Landers earthquake (1992/06/28) and four from the Northridge earthquake (1994/01/17).

To simulate the waveforms for the two different shake tables (displacement limit of 10 and 2 in.), the six earthquake records from the first group were processed twice (High Pass Ormsby filter) (Tables 3-1, 3-2: R7-R18).

Table 3-1 Records (1-14) that contributed to the analysis

Records	Name	Type	Recording Source /Station	Data Source	Magnitude (M)	Focal Depth (Km)	Distance to Fault (Km)	Filtering	# Points	DT sec	Duration sec
1	Landers/ LCN260	EQ/Landers (1992/06/28)	SCE/ 24 Lucerne	PEER SMDB	7.3	9	1.1	HP 0.0 - LP 60.0	9625	0.005	48.12
2	Landers/ LCN345	EQ/Landers (1992/06/28)	SCE/24 Lucerne	PEER SMDB	7.3	9	1.1	HP 0.0 - LP 60.0	9625	0.005	48.12
3	Northr/ SCS142	EQ/Northridge (1994/01/17)	DWP/74Sylmar Convert.Sta.	PEER SMDB	6.7	19	6.2	unknown	8000	0.005	39.995
4	Northr/ SCE018	EQ/Northridge (1994/01/17)	DWP/75Sylmar Convert.Sta. East	PEER SMDB	6.7	19	6.1	unknown	8000	0.005	39.995
5	Northr/ RRS-288	EQ/Northridge (1994/01/17)	DWP/77 Rinaldi Receiving Sta.	PEER SMDB	6.7	19	7.1	unknown	2990	0.005	14.945
6	Northr/ PAR-L	EQ/Northridge (1994/01/17)	SCE/ 0 Pardee	PEER SMDB	6.7	19	-	HP 0.5 - LP 20	4425	0.005	22.12
7	Landers/ LCN260	Shake Table, 10" limit	SCE/ 24 Lucerne	PEER SMDB modified	7.3	9	1.1	HP 0.3	9625	0.005	48.12
8	Landers/ LCN345	Shake Table, 10" limit	SCE/24 Lucerne	PEER SMDB modified	7.3	9	1.1	HP 0.05	9625	0.005	48.12
9	Northr/ SCS142	Shake Table, 10" limit	DWP/74Sylmar Convert.Sta.	PEER SMDB modified	6.7	19	6.2	HP 0.3	8000	0.005	39.995
10	Northr/ SCE018	Shake Table, 10" limit	DWP/75Sylmar Convert.Sta. East	PEER SMDB modified	6.7	19	6.1	HP 0.3	8000	0.005	39.995
11	Northr/ RRS-288	Shake Table, 10" limit	DWP/77 Rinaldi Receiving Sta.	PEER SMDB modified	6.7	19	7.1	HP 0.5	2990	0.005	14.945
12	Northr/ PAR-L	Shake Table, 10" limit	SCE/ 0 Pardee	PEER SMDB modified	6.7	19	-	HP 0.05	4425	0.005	22.12
13	Landers/ LCN260	Shake Table, 2" limit	SCE/ 24 Lucerne	PEER SMDB modified	7.3	9	1.1	HP 0.8	9625	0.005	48.12
14	Landers/ LCN345	Shake Table, 2" limit	SCE/24 Lucerne	PEER SMDB modified	7.3	9	1.1	HP 0.4	9625	0.005	48.12

Table 3-0 Records (15-28) that contributed to the analysis

Records	Name	Type	Recording Source /Station	Data Source	Magnitude (M)	Focal Depth (Km)	Distance to Fault (Km)	Filtering	# Points	DT sec	Duration sec
15	Northr/ SCS142	Shake Table, 2" limit	DWP/74Sylmar Convert.Sta.	PEER SMDB modified	6.7	19	6.2	HP 1.4	8000	0.005	39.995
16	Northr/ SCE018	Shake Table, 2" limit	DWP/75Sylmar Convert.Sta. East	PEER SMDB modified	6.7	19	6.1	HP 1.3	8000	0.005	39.995
17	Northr/ RRS-288	Shake Table, 2" limit	DWP/77 Rinaldi Receiving Sta.	PEER SMDB modified	6.7	19	7.1	HP 1.6	2990	0.005	14.945
18	Northr/ PAR-L	Shake Table, 2" limit	SCE/ 0 Pardee	PEER SMDB modified	6.7	19	-	HP 1.3	4425	0.005	22.12
19	Telcordia	Shake Table	Synthetic	Telcordia GR-63-CORE	n.a.	n.a.	n.a.	-	6145	0.005	30.72
20	Measured NTS-5	NETI	NETI	Gefken transmittal 4/2001	n.a.	n.a.	n.a.	-	520	0.005	2.595
21	Scaled NTS-5	NETI	NETI	Gefken transmittal modified	n.a.	n.a.	n.a.	-	3638	0.005	18.185
22	Synthesized NTS	NETI	Synthesized	Gefken transmittal 4/11/2001	n.a.	n.a.	n.a.	-	10733	0.005	53.66
23	50m radial	Black Thunder Mine	BTM/ARA	ARA Report	n.a.	n.a.	n.a.	LP 80	1501	0.005	7.5
24	50 m vertical	Black Thunder Mine	BTM/ARA	ARA Report	n.a.	n.a.	n.a.	LP 80	1501	0.005	7.5
25	100 m radial	Black Thunder Mine	BTM/ARA	ARA Report	n.a.	n.a.	n.a.	LP 80	1501	0.01	15.01
26	200m radial	Black Thunder Mine	BTM/ARA	ARA Report	n.a.	n.a.	n.a.	LP 80	1501	0.01	15.01
27	300m radial	Black Thunder Mine	BTM/ARA	ARA Report	n.a.	n.a.	n.a.	LP 80	1501	0.01	15.01
28	500 m radial	Black Thunder Mine	BTM/ARA	ARA Report	n.a.	n.a.	n.a.	LP 80	1501	0.01	15.01

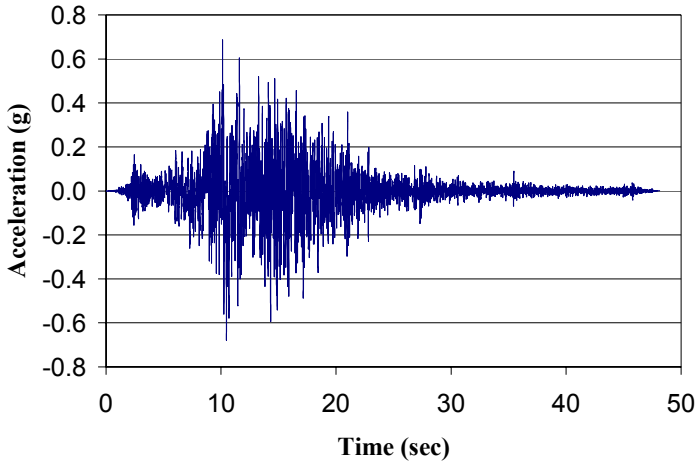

Figure 3-1 Landers Earthquake, Lucerne Valley Record

The Telcordia record (Table 3-2: R19) is an industrial standard for seismic testing of telecommunication equipments. The test procedure, described in the document "Network Equipment –Building System (NEBS) Requirements: Physical Protection" by Telcordia Technologies [Ref.16, section 5.4], subjects equipment to follow the prescribed motion of the synthesized waveform by means of a shaker table. The acceleration time history waveform VERTEQII has been synthesized from several earthquakes and for different building types and soil site conditions. The Telcordia record for earthquake risk zone 4 (Fig. 3-2), which has the highest acceleration among the risk zones, participated in this analysis.

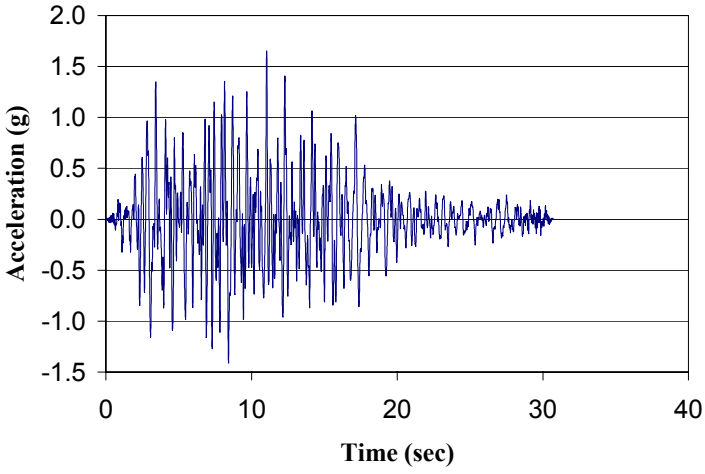

Figure 3-0 Telcordia Time History

From the three acceleration data records in the third group, two correspond to the Nevada Test Site test series:

- (R20) NTS, measured 1/7 scale prototype RESQUE source (Fig. 3-3)
- (R21) calculated corresponding full-scale acceleration time history

The third record (R22, Fig. 3-4)) is a full-scale, multi-pulse, synthesized acceleration time history, which corresponds to the detonation of a series of RESQUE sources (provided by Mr. P. Gefken).

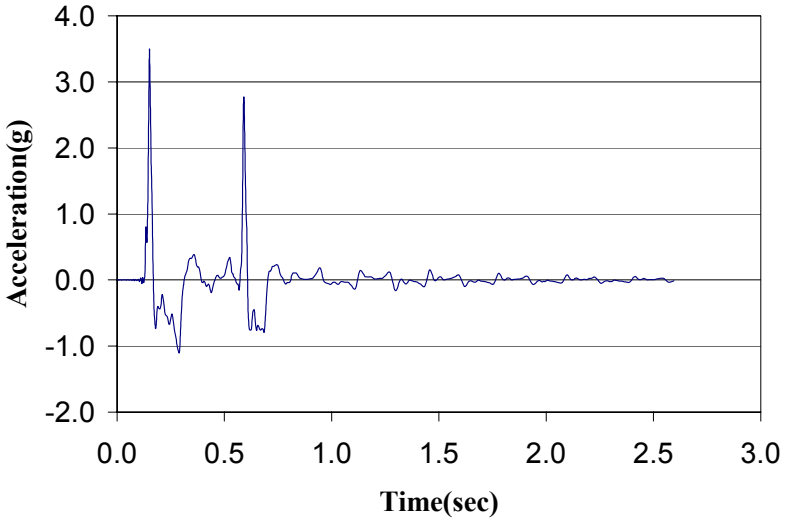

Figure 3-3 Nevada Test Site NTS –5 measured (1/7 scale RESQUE source)

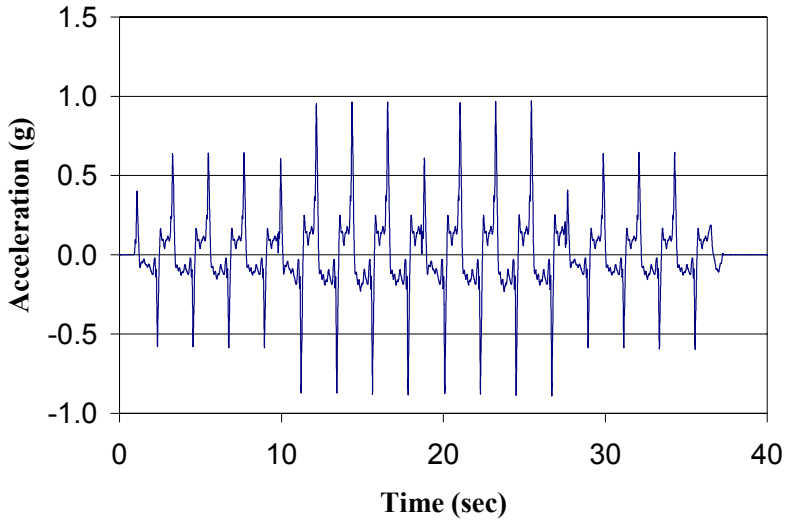

Figure 3-4 Synthesized Multi Pulse NETI record

The fourth group of data consists of ground accelerations recorded during the Black Thunder Coal Mine event of April 3,1997 [Ref. 24]. The locations of the ground motion recording stations in this study with respect to the explosive array source are the following: vertical (50 m); radial (50, 100, 200, 300, 500 m.)

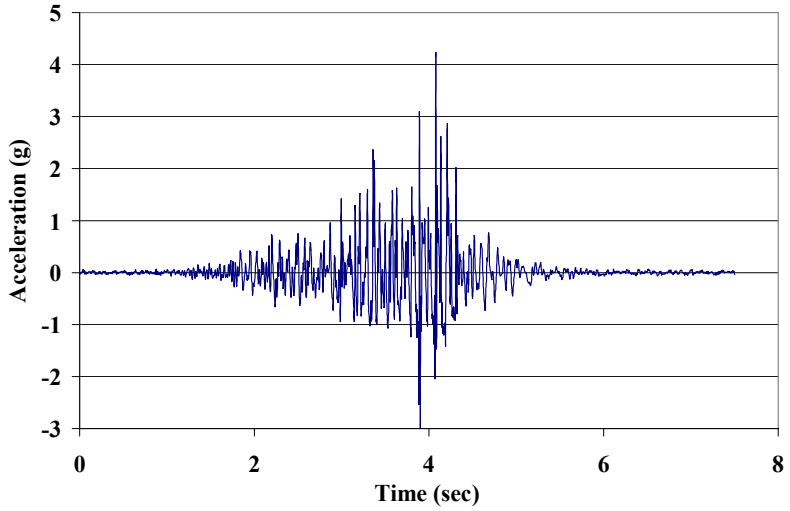

Figure 3-5 Black Thunder Mine 50 vertical (April 3rd 1997)

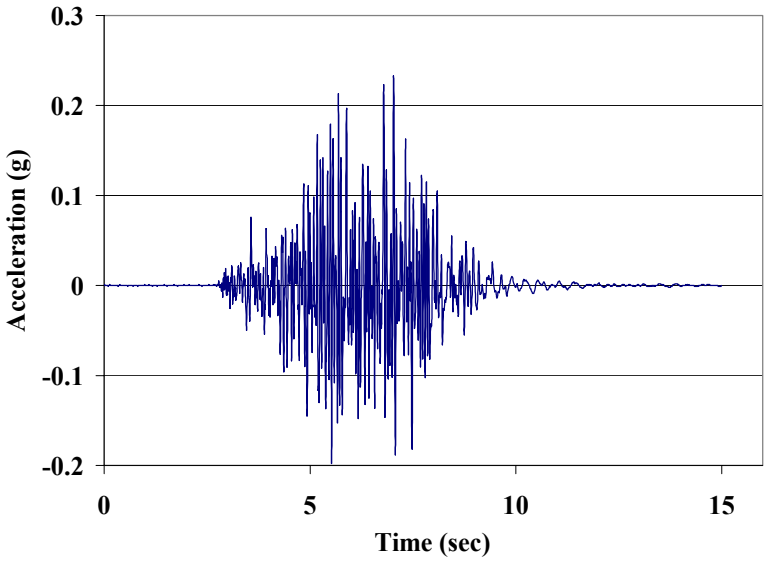

Figure 3-6 Black Thunder Mine 500 radial (April 3rd 1997)

3.3 Records characteristics

Table 3-3 includes the following records characteristics:

- The peak absolute acceleration (PA), velocity (PV) and displacement (PD) of the recorded time histories.

- The bracketed duration [D]. To measure bracketed duration corresponding to a given acceleration level, the first and last occurrences of accelerations equal to or larger than a prescribed value are marked on the acceleration trace. The time duration between these two markings is called bracketed duration (Bolt 1969; Page and others 1972). In this study, the bracketed duration corresponding to 0.05g acceleration is evaluated for the record ensemble.

- The Arias Intensity (AI) given by:

$$AI_{ij} = \pi / 2g \int_0^{t0} a_i(t) a_j(t) dt \qquad (3.3.1.)$$

where to: the record duration

$a_i(t), \alpha_j(t)$: the acceleration amplitudes of the orthogonal components

This parameter (Arias, 1970) is a measure of seismic intensity and has a tensorial character (nine components). In this study the scalar value is used [Ref.17].

- The Cumulative Absolute Velocity (CAV) defined as the area under the absolute acceleration versus duration curve is given by:

$$CAV = \int_o^{t0} |\alpha(t)| dt \qquad (3.3.2.)$$

Kennedy and Reed originally proposed this parameter in a study sponsored by the Electrical Power Research Inst. [Ref.18, EPRI NP-5930, 1988]. It was used as an indicator for potential damage in nuclear power plants.
Later on, the method of calculating CAV was modified to remove the dependence on records of long duration containing low (non-damaging) accelerations [Ref.19, EPRI TR-1000829, 1991]. The method to standardize the CAV calculation, which is adopted in this study, consists of calculating incrementally the parameter in 1 sec intervals. Each interval contributes to the sum only if it has at least one peak that exceeds the fixed level of acceleration 0.025g.

Table 3-3 Records characteristics

PA: Peak absolute acceleration
PV: Peak absolute velocity
PD: Peak absolute displacement
[D]: 0.05g Bracketed duration
AI: Arias Intensity
CAV: Cumulative absolute velocity

Records	Name	Type	PA (g)	PV (cm/s)	PD (cm)	[D] (sec)	AI (gsec)	CAV (gsec)
1	Landers/LCN260	EQ/Landers (1992/06/28)	0.727	146.5	262.7	33.255	0.711	2.535
2	Landers/LCN345	EQ/Landers (1992/06/28)	0.789	32.4	69.8	33.32	0.671	2.511
3	Northr/SCS142	EQ/Northridge (1994/01/17)	0.897	102.8	47.0	27.29	0.538	1.653
4	Northr/SCE018	EQ/Northridge (1994/01/17)	0.828	117.5	34.2	17.055	0.458	1.424
5	Northr/RRS-288	EQ/Northridge (1994/01/17)	0.838	166.1	28.8	13.095	0.751	1.675
6	Northr/PAR-L	EQ/Northridge (1994/01/17)	0.657	75.2	13.2	17.945	0.315	1.138
7	Landers/LCN260	Shake Table, 10" limit	0.685	78.06	25.89	33.255	0.689	2.51
8	Landers/LCN345	Shake Table, 10" limit	0.789	27.19	23.66	33.2	0.671	2.511
9	Northr/SCS142	Shake Table, 10" limit	0.892	85.75	20.2	27.64	0.537	1.636
10	Northr/SCE018	Shake Table, 10" limit	0.831	103.54	22.66	17.245	0.456	1.425
11	Northr/RRS-288	Shake Table, 10" limit	0.818	138.93	24.99	13.305	0.737	1.66
12	Northr/PAR-L	Shake Table, 10" limit	0.657	75.21	13.15	17.945	0.315	1.138
13	Landers/LCN260	Shake Table, 2" limit	0.689	36.23	4.52	33.255	0.662	2.469
14	Landers/LCN345	Shake Table, 2" limit	0.788	20.41	4.97	33.32	0.669	2.507
15	Northr/SCS142	Shake Table, 2" limit	0.594	40.87	4.56	12.84	0.233	1.009
16	Northr/SCE018	Shake Table, 2" limit	0.807	46.59	4.87	13.8	0.347	1.217
17	Northr/RRS-288	Shake Table, 2" limit	0.622	53.34	4.79	13.3	0.405	1.352
18	Northr/PAR-L	Shake Table, 2" limit	0.508	33.87	4.88	17.385	0.145	0.804
19	Telcordia time history	Shake Table Standard	1.65	103.1	12.78	29.98	7.151	8.072
20	Measured NTS-5	NETI	3.467	58.1	4.68	2.3	0.511	0.362
21	Scaled NTS-5	NETI	0.543	58.2	32.77	3.93	0.072	0.3
22	Synthesized NTS	NETI	0.97	122.8	50.82	36.215	2.9	5.972
23	50m radial	Black Thunder Mine	2.871	18.95	2.09	7.365	1.363	1.286
24	50 m vertical	Black Thunder Mine	4.163	31.81	1.82	7.245	2.054	1.581
25	100 m radial	Black Thunder Mine	1.902	27.92	2.39	5.64	1.295	1.382
26	200 m radial	Black Thunder Mine	0.761	11.31	1.55	5.42	0.212	0.628
27	300 m radial	Black Thunder Mine	0.374	8.43	0.64	5.53	0.097	0.455
28	500 m radial	Black Thunder Mine	0.231	3.33	0.63	5.29	0.036	0.278

Peak Acceleration (PA) - Figure 3.7:

For the earthquake records (R1 –R6), the PA values ranged from 0.657 g (R6) to 0.897 g (R3). The PA values for the shake table with 10" displacement limit (R7-R12) were almost equal to the corresponding earthquake records. For the shake table with 2" displacement limit (R13-R18), the PA values ranged from 0.508 g (R18) to 0.807 g (R16). The reduction percentages for the PA values relative to those from the earthquake records were:
R13 / 5.23 %; R14 / none; R15 / 33.78 %; R16 / 2.54 %; R17 / 25.77 %; R18 / 22.68 %.

The PA for the Telcordia record (R19, shake table waveform) was 1.65g, almost 1.85 times larger than the largest PA earthquake value.
Amongst the NETI group of records, the highest PA value (3.467 g) originated from the measured NETI record (R20). The PA value from the scaled NETI (R21) was 6.4 times smaller (0.543 g) than the measured NETI as expected. The PA of 0.97 g from the synthesized multi-pulse NETI (R22) was closer to the largest earthquake value.

Finally, the largest PA value (4.163 g) from the record ensemble originated from the 50 m vertical BTM (R24). For the BTM 300 m and 500 m records the PA values were considerably smaller than those from the earthquake group (43% and 65% respectively smaller than the lowest PA earthquake value).

Peak Velocity (PV) - Figure 3.8:

For the earthquake records (R1-R6), the PV values ranged from 32.4 cm/sec (R2) to 166.1 cm/sec (R5), which was the largest among the record ensemble. The PVs for the shake table with 10" limit (R7-R12), which ranged from 27.19 cm/sec (R8) to 138.93 cm/sec (R11), were decreased from the equivalent earthquake values by the following reduction percentages:
R7 / 46.72%; R8 / 16.08%; R9 / 16.58%; R10 / 11.88%; R11 / 16.36%; R12 / none.

For the shake table with 2" limit (R13-R18) the range of PV values was: 20.41 cm/sec (R14) to 53.34 cm/sec (R17); the corresponding reduction percentages were larger:
R13 / 75.27%; R14 / 37%; R15 / 60.24%; R16 / 60.35%; R17 / 67.88%; R18 / 54.96%.

The PV for the Telcordia record was 103.1 cm/sec. The measured and scaled NETI records (R20, R21) had the same PV value as expected (58.1 cm/sec, close to the lower earthquake range); the PV value for the synthesized NETI (R22) was 122.8 cm/sec close to the higher earthquake range.

The BTM group (R23-R28) had very low PV values; the largest among them was 31.81 cm/sec for the 50 m vertical (R24). For the 200 m, 300 m and 500 m BTM, the PVs were negligible.

Arias Intensity (AI) - Figure 3.9:

The AI for the earthquake (R1-R6) and the corresponding 10" shake table records (R7-R12) were practically equal, with values ranging from 0.315 gsec (R6) to 0.711 gsec (R1). For the 2" shake table (R13-18), the AI values were smaller than the earthquake AI values by the following reduction percentages:
R13 / 6.9%; R14 / none; R15 / 56.7%; R16 / 24.23%; R17 / 46.07%; R18 / 53.97%.

The largest AI value (7.151 gsec) from the record ensemble originated from the Telcordia record (R19), which exceeded by ten times the largest earthquake value. The second largest AI value (2.9 gsec) belonged to the synthesized NETI record (R22). The AI values for the measured (R20) and scaled NETI (R21) were 0.511 and 0.072 gsec respectively.

From the BTM group, the AI values for the 200, 300, 500 m (R26-R28) were much smaller than the earthquake records. The AI for the 100 m (R25) was between the earthquake limits with a value of 0.648 gsec. The 50 radial (R23) and 50 vertical (R24) had large AI values which exceeded by almost 2 and 3 times respectively the largest earthquake AI.

Cumulative Absolute Velocity (CAV) –Figure 3.9:

Although the CAVs were higher than the AIs values for the record ensemble, the observations for the AIs values can be applied to the description of the CAVs values.

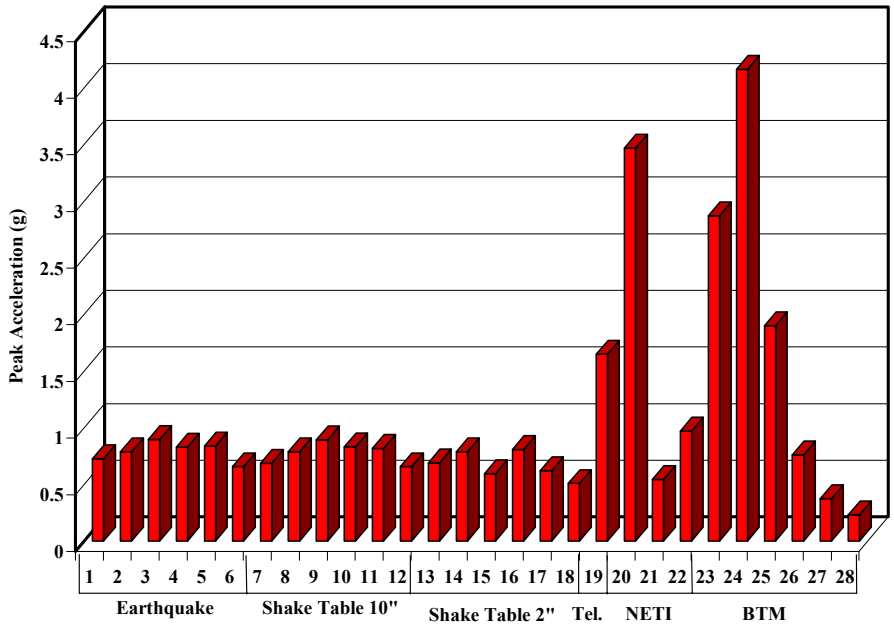

Figure 3-7 Peak acceleration values for the record ensemble

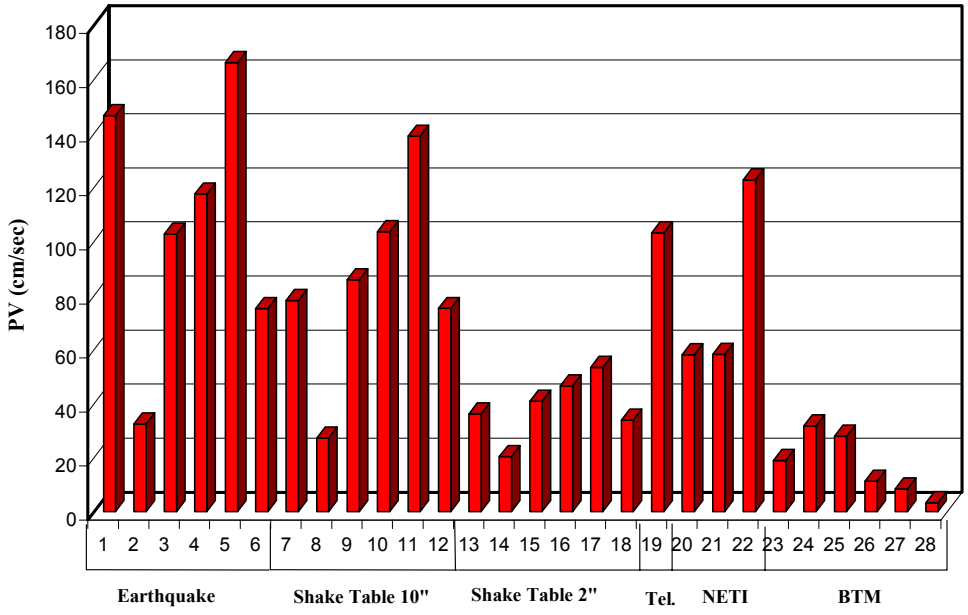

Figure 3-8 Peak Velocity Values for the record ensemble

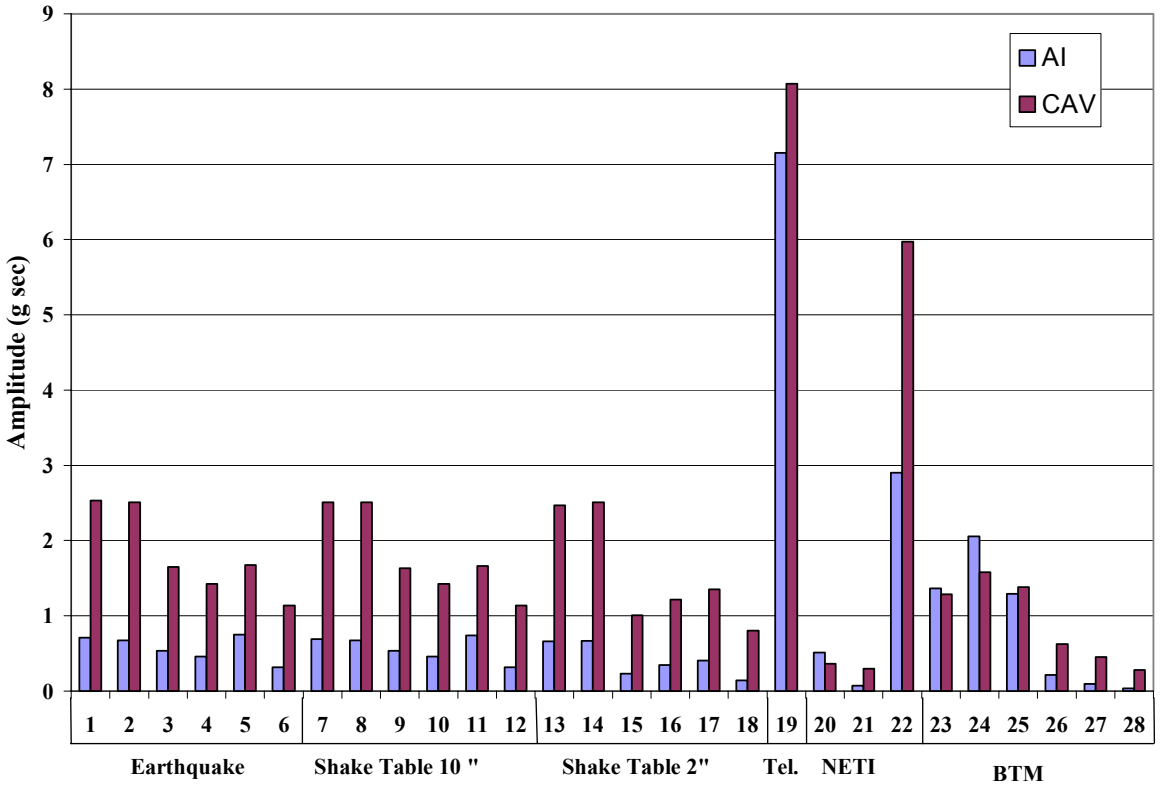

Figure 3-9 Arias Intensity (AI) and Cumulative Absolute Velocity (CAV) for the record ensemble

3.4 Fourier Analysis for the record ensemble

The discrete Fourier transforms for the record ensemble were calculated with the Fast Fourier Transform (FFT) algorithm to examine the frequency content of the acceleration time histories (ATH). Fig. 3-10 through 3-12 illustrate selective Fourier amplitude graphs in log-normal scale.

In Fig.3-10 the Fourier spectra for the earthquake records R5-Northr/RRS-288 and R1-Landers/LCN260 are presented. The spectrum for R5-Northr/RRS-288 peaks between 0-5 Hz, whereas R1-Landers/LCN260 has a broader frequency spectrum.

The Fourier amplitude values for both the R20-Measured NTS-5 and R23-BTM 50m radial records exceed the R5-Northr/RRS-288 values for frequencies larger than 2 Hz and 6 Hz respectively, and exhibit large amplitudes for higher frequencies (Fig. 3-11). The Fourier spectra for the NETI records R20-Measured NTS-5 and R22-Synthesized NTS depicted in Figure 3-12 differ significantly. The spectrum for the R20 record has peaks every 2 Hz (periodic behavior); even though the amplitudes for the R22 record fall under the R5-Northr/RRS-288 values, the two spectra have similar frequency bandwidths.

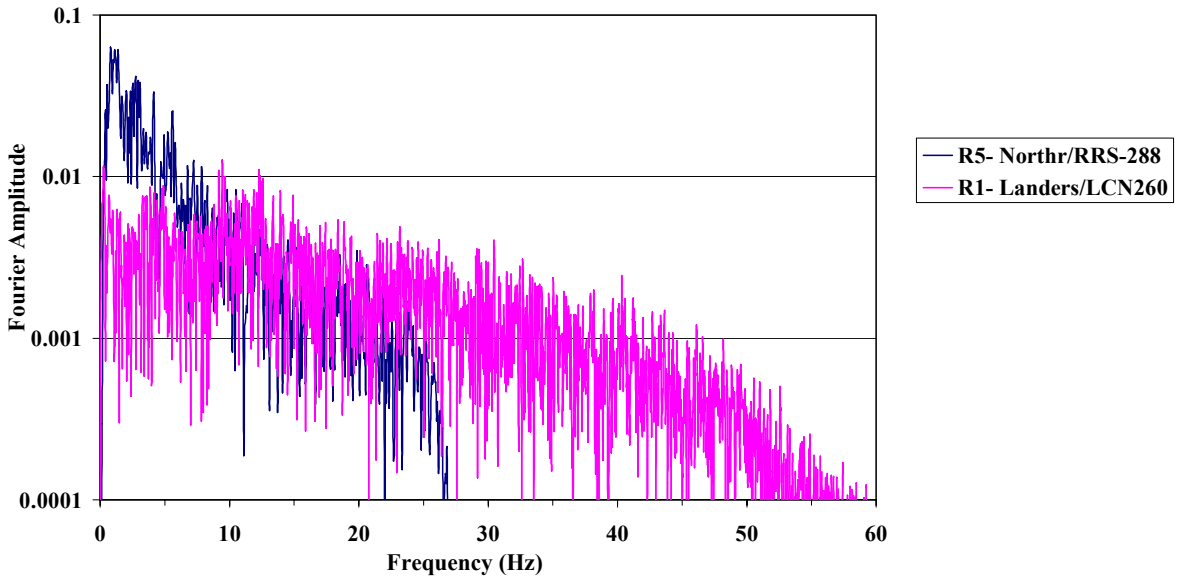

Figure 3-10 Fourier spectra for the records R1-Landers/LCN260,

R5-Northr/RRS-288

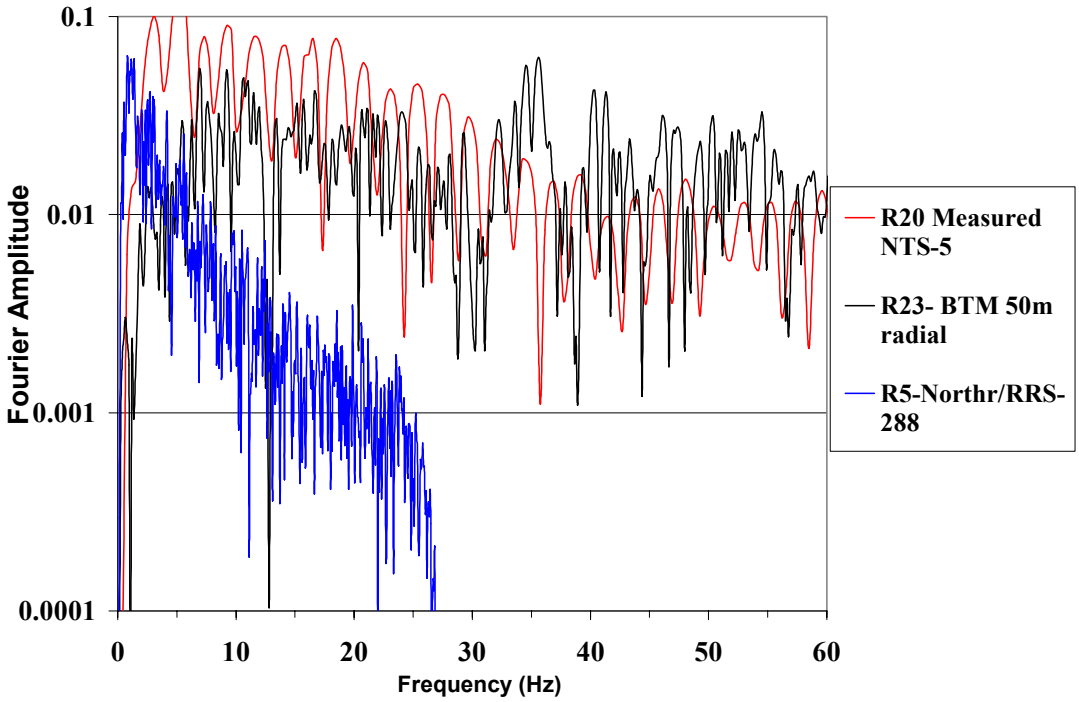

Figure 3-11 Fourier spectra for the records R5-Northr/RRS-288, R20-Measured NTS-5, R23-BTM 50 m radial

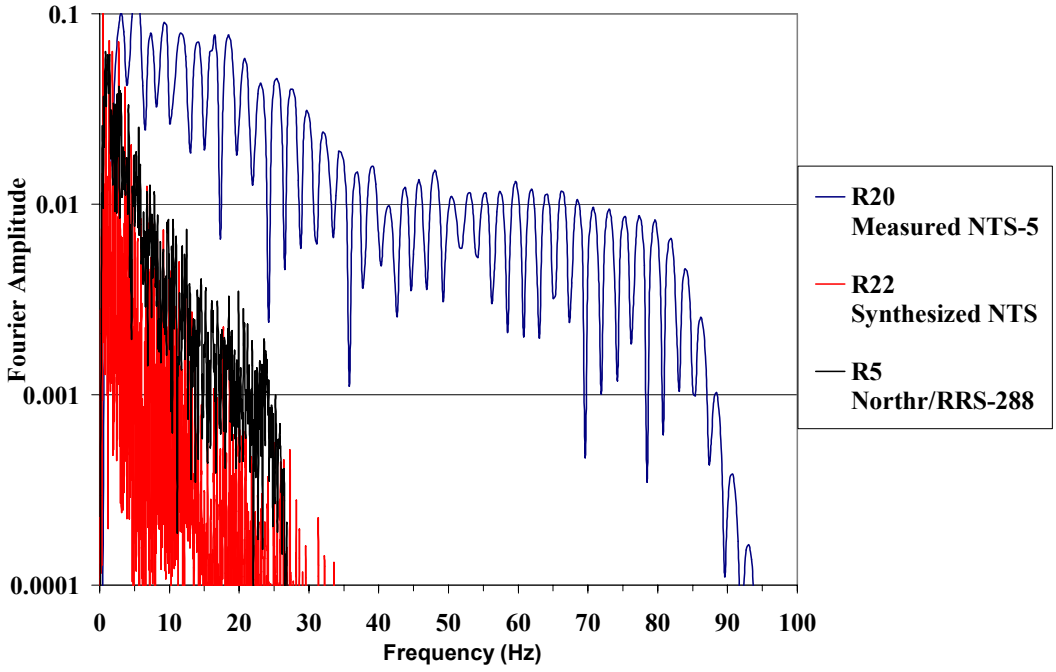

Figure 3-12 Fourier Spectra for the R5 –Northr/RRS-288 and the R20, R22 NETI records

3.5 Analysis for a linear sdof

The formulation of the equation of motion of a SDOF linear system subjected to base excitation in terms of the relative motion of the mass with respect to the motion of the support is given by:

$$\ddot{u}(t) + 2\xi\omega_n\dot{u}(t) + \omega_n{}^2 u(t) = -\ddot{u}_s(t) \tag{3.5.1}$$

The solution of the differential equation, Eq. (3.5.1) is obtained by numerical evaluation of the Duhamel's integral that is:

$$u(t) = -\frac{1}{\omega_d}\int_0^t \ddot{u}_s(\tau)e^{-\xi\omega_n(t-\tau)}\sin[\omega_D(t-\tau)]d\tau \tag{3.5.2}$$

The relative velocity $\dot{u}(t)$ is obtained by differentiating Eq. (3.5.2):

$$\dot{u}(t) = -\xi\omega_n u(t) - \int_0^t \ddot{u}_s(\tau)e^{-\xi\omega_n(t-\tau)}\cos[\omega_D(t-\tau)]d\tau \tag{3.5.3}$$

The absolute acceleration of the mass, is then given by:

$$\ddot{u}_t(t) = \ddot{u}_s(t) + \ddot{u}(t) = -\omega_n{}^2 u(t) - 2\xi\omega_n\dot{u}(t) \tag{3.5.4}$$

The maximum response in terms of the:
- absolute acceleration (SA: spectral acceleration)
- relative displacement (SD: spectral displacement)
- relative pseudovelocity (PSSV: pseudo spectral velocity)

is computed for a damping ratio of 5% critical damping and period values ranging from 0.02 to 10 sec. The three spectral quantities SD, PSSV and PSSA - pseudo spectral acceleration - are interrelated by the following equations:

$$PSSA = \omega^2 SD \qquad (3.5.5) \qquad\qquad PSSV = \omega SD \quad (3.5.6)$$

For long-period systems (T_n>2.0 sec), the pseudo spectral velocity (PSSV) is less than the peak relative velocity ($\dot{u}_o$). For short-period systems, the PSSV exceeds the $\dot{u}_o$ values with the differences increasing as the period becomes shorter. Over the medium-period range (0.2 < T_n< 2.0 sec) the PSSV can be taken as an approximation to the $\dot{u}_o$ values for small damping values (ξ<0.2) [Ref. 25, Section 6.12.1]

The difference between the pseudo spectral acceleration (PSSA) and the spectral acceleration (SA = peak relative displacement u_0) is small for short-period systems (T_n<=5.0 sec) and is of some significance only for long-period systems with large values of damping (ξ>0.1) [Ref. 25, Section 6.12.2].

In Table 3.4 SA, SV, and SD values for the selective periods: 0.2, 0.3, 1.0, 3.0 sec are presented for the record ensemble.

Discussion

Figures 3.13 – 3.17 depict the SA values for period values 0.02 –10 sec and 5% cr. damping for the record ensemble. The SA values for the earthquake records (R1-R6) and the corresponding large shake tables (R7-R12) are almost identical as it can be seen in Fig. 3.13 and 3.14. The SA spectrum for the R19 Telcordia record envelopes the large shake table spectra with particularly high values for periods ranging from 0.1 – 1.0 sec. For the smaller shake tables (R13-R18), the SA values are slightly smaller than those from the corresponding earthquake records for period less than 1.0 sec. For larger period values (>1.0 sec) the difference between the SA values increases.

In Fig. 3.16 the three NETI (R20-R22) SA spectra are compared with the maximum and minimum SA values from the earthquake records. The measured NETI (R20) spectrum exceeds the maximum earthquake boundary only for period values smaller than 0.3 sec; whereas the SA values for the synthesized NETI (R22) fall between the two earthquake boundaries, and the scaled NETI (R21) spectrum has values closer to the minimum earthquake boundary.

The SA spectra for the BTM records (R23-R28) show that before the threshold period of 0.20 sec, the acceleration amplitudes are larger than the maximum earthquake boundary for the 50 m. and 100 m. records, and also for period values > 0.22 sec the SA values are below the minimum earthquake boundary for all the BTM records (Fig. 3.17).

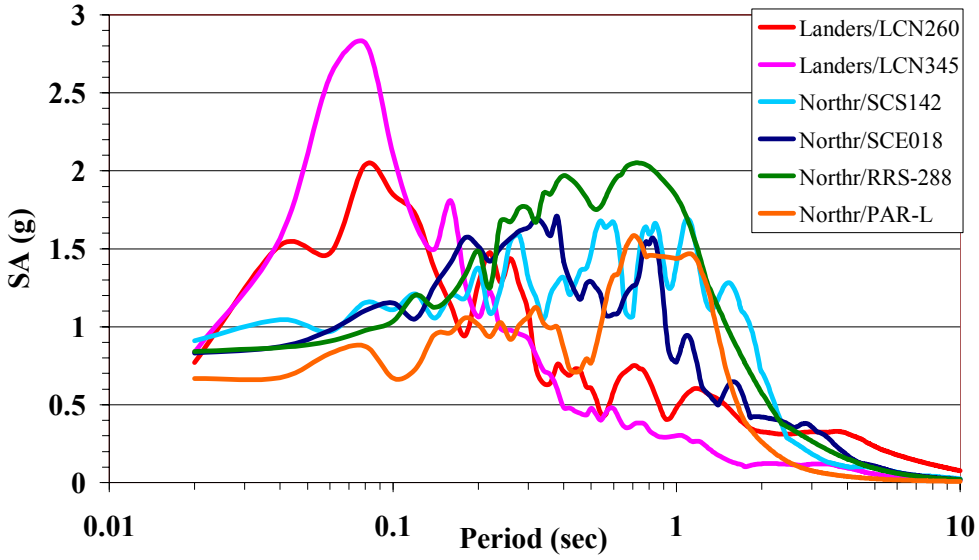

Figure 3-13 Spectral Acceleration for a linear SDOF (5 % cr. damping)

Earthquake Records

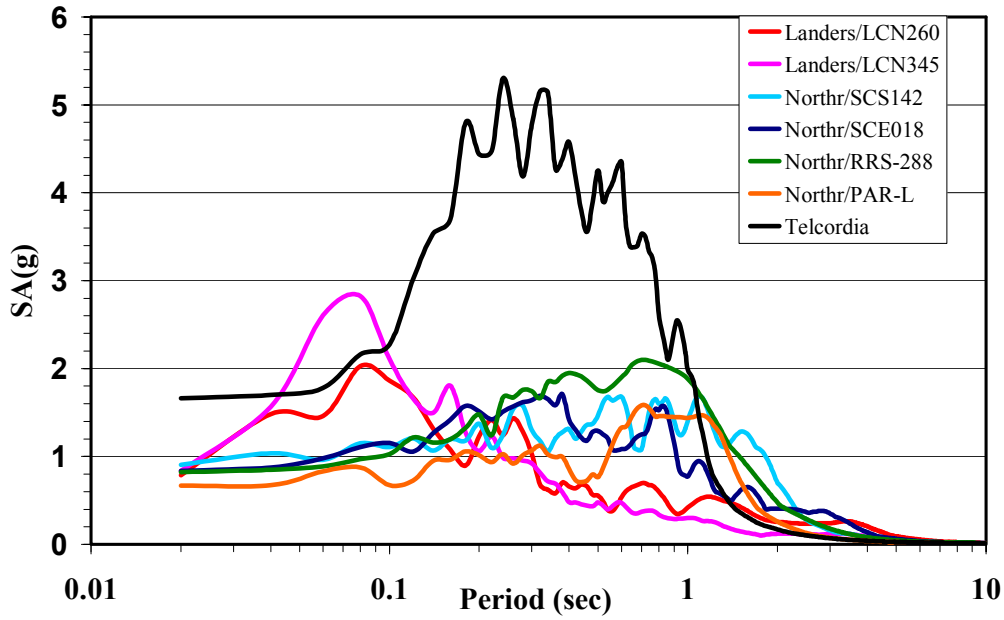

Figure 3-14 Spectral Acceleration for a linear SDOF (5% cr. Damping)

Shake Table 10" displacement limit and Telcordia records

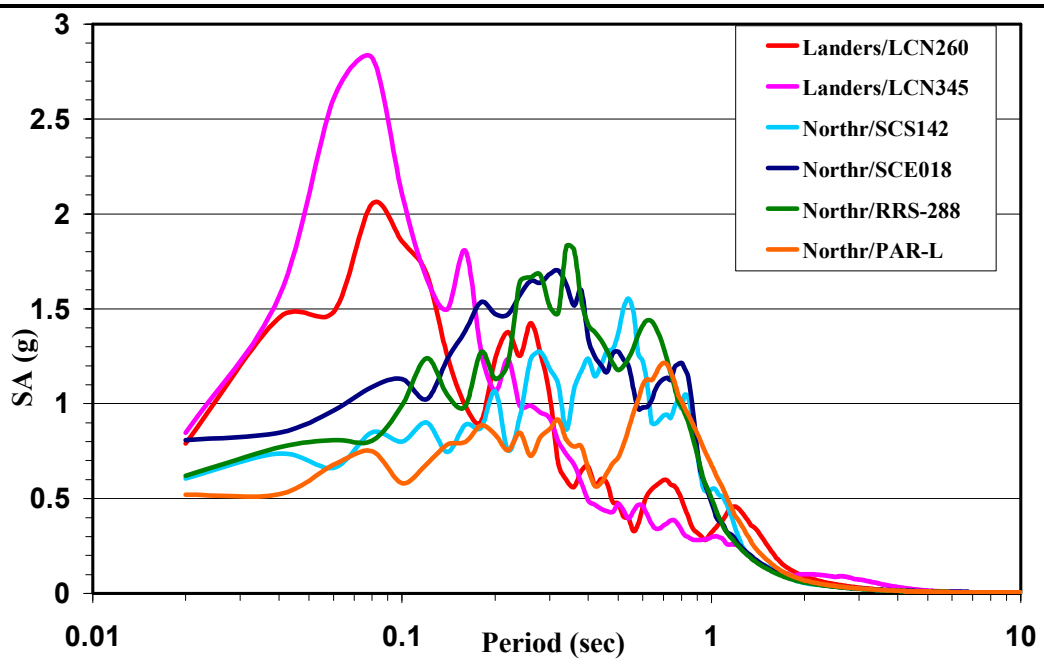

Figure 3-15 Spectral Acceleration for a linear SDOF (5% cr. Damping)

Shake Table 2" displacement limit records

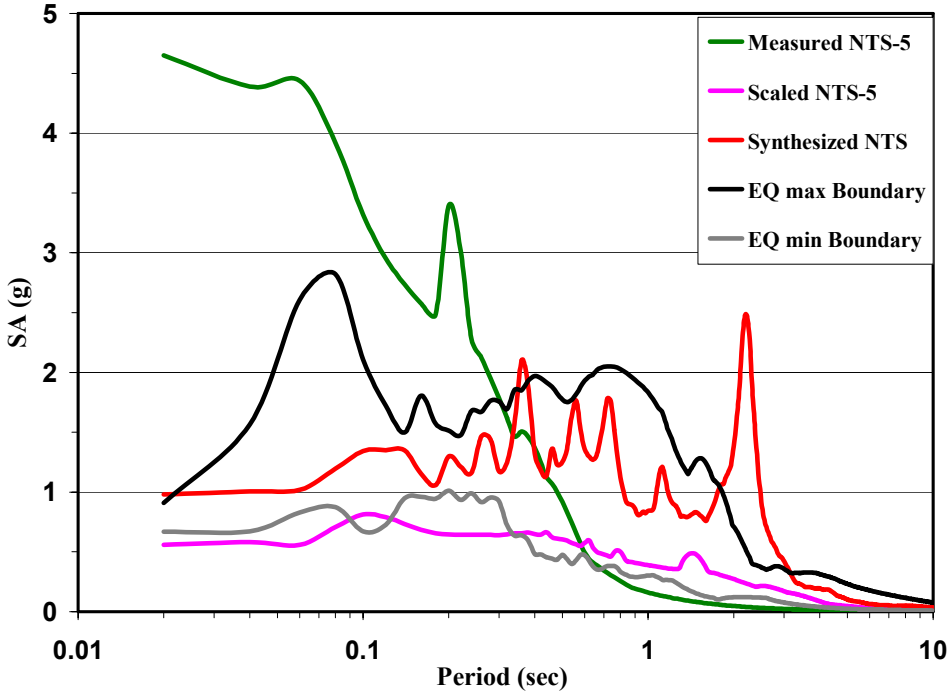

Figure 3-16 Spectral Acceleration for a linear SDOF (5% cr. Damping)

NETI records

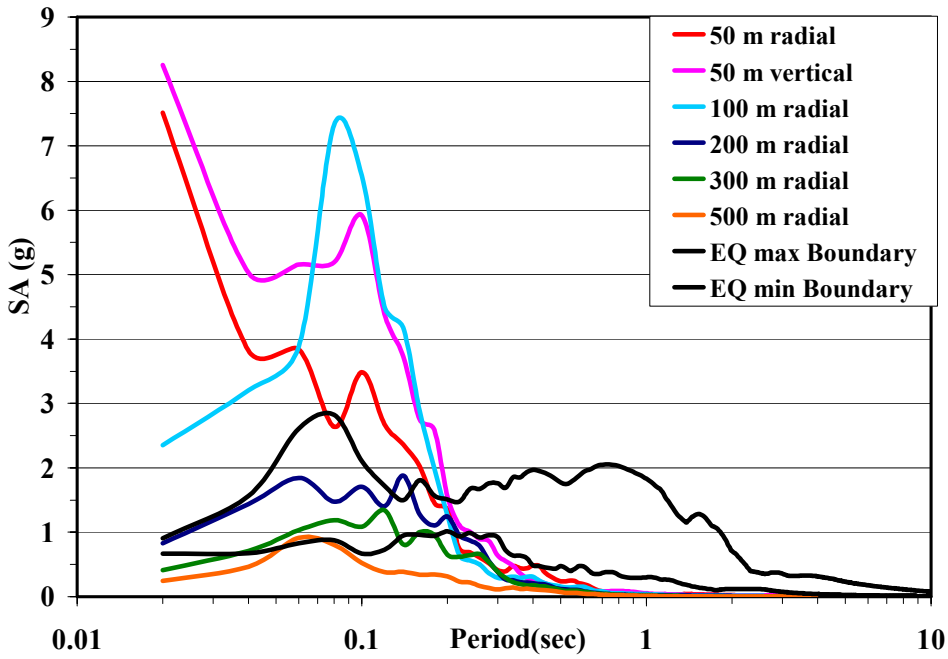

Figure 3-17 Spectral Acceleration for a linear SDOF (5% cr. Damping)

BTM records

Table 3.4 Spectral values for a linear system with 5% critical damping

SA3: Spectral acceleration for period 3 sec
SA1: Spectral acceleration for period 1 sec
SA.3: Spectral acceleration for period .3 sec
SA.2: Spectral acceleration for period .2 sec
SD3: Spectral displacement for period 3 sec
SD.3: Spectral displacement for period .3 sec
SV3: Pseudo spectral velocity for period 3 sec
SV1: Pseudo spectral velocity for period 1 sec
SV.3: Pseudo spectral velocity for period .3 sec
SV.2: Pseudo spectral velocity for period .2 sec
SD1: Spectral displacement for period 1 sec
SD.2: Spectral displacement for period .2 sec

Records	Name	Type	SA3 g	SA 1 g	SA .3 g	SA.2 g	SV3 cm/sec	SV1 cm/sec	SV.3 cm/sec	SV.2 cm/sec	SD 3 cm	SD 1 cm	SD .3 cm	SD.2 cm
1	Landers/ LCN260	EQ/Landers (1992/06/28)	0.326	0.478	1.087	1.276	151.937	74.267	50.646	39.721	72.54	11.82	2.42	1.264
2	Landers/ LCN345	EQ/Landers (1992/06/28)	0.119	0.301	0.923	1.063	55.417	46.768	42.890	32.926	26.46	7.44	2.05	1.05
3	Northr/ SCS142	EQ/Northridge (1994/01/17)	0.184	1.403	1.307	1.377	86.004	217.973	61.075	42.905	41.06	34.7	2.92	1.36
4	Northr/ SCE018	EQ/Northridge (1994/01/17)	0.358	0.772	1.637	1.513	166.715	119.867	76.398	47.128	79.6	19.08	3.65	1.5
5	Northr/ RRS-288	EQ/Northridge (1994/01/17)	0.266	1.834	1.759	1.486	122.335	284.913	82.149	46.319	58.41	45.34	3.92	1.47
6	Northr/ PAR-L	EQ/Northridge (1994/01/17)	0.076	1.439	1.066	1.012	34.217	223.595	49.772	31.536	16.34	35.58	2.38	1
7	Landers/ LCN260	Shake Table, 10" limit	0.241	0.419	1.034	1.228	111.756	65.025	48.139	38.221	53.36	10.35	2.3	1.22
8	Landers/ LCN345	Shake Table, 10" limit	0.118	0.301	0.922	1.063	55.178	46.790	42.865	32.902	26.34	7.45	2.05	1.05
9	Northr/ SCS142	Shake Table, 10" limit	0.159	1.401	1.303	1.373	74.414	217.771	60.910	42.784	35.53	34.66	2.91	1.36
10	Northr/ SCE018	Shake Table, 10" limit	0.351	0.771	1.639	1.515	163.678	119.802	76.496	47.202	78.15	19.07	3.65	1.5
11	Northr/ RRS-288	Shake Table, 10" limit	0.178	1.884	1.746	1.478	81.598	292.761	81.556	46.091	38.96	46.59	3.89	1.47
12	Northr/ PAR-L	Shake Table, 10" limit	0.076	1.439	1.066	1.012	34.202	223.613	49.769	31.541	16.33	35.59	2.37	1
13	Landers/ LCN260	Shake Table, 2" limit	0.031	0.323	1.039	1.238	13.960	50.005	48.373	38.539	6.66	7.96	2.31	1.23
14	Landers/ LCN345	Shake Table, 2" limit	0.073	0.297	0.922	1.065	34.015	45.783	42.840	32.985	16.24	7.29	2.04	1.05
15	Northr/ SCS142	Shake Table, 2" limit	0.025	0.55	1.184	1.066	10.507	85.319	55.209	33.197	5.02	13.58	2.64	1.06
16	Northr/ SCE018	Shake Table, 2" limit	0.026	0.478	1.684	1.472	10.384	74.197	78.517	45.818	4.96	11.81	3.75	1.46
17	Northr/ RRS-288	Shake Table, 2" limit	0.024	0.5	1.511	1.131	10.502	77.366	70.456	35.144	5.01	12.31	3.36	1.12
18	Northr/ PAR-L	Shake Table, 2" limit	0.026	0.675	0.867	0.836	11.638	104.816	40.479	26.012	5.56	16.68	1.93	0.83
19	Telcordia time history	Shake Table Standard	0.07	1.994	4.771	4.441	29.310	306.295	256.328	152.768	14.11	49.18	10.62	4.4
20	Measured NTS-5	NETI	0.023	0.161	1.783	3.393	9.448	24.505	83.039	105.582	4.51	3.9	3.96	3.36
21	Scaled NTS-5	NETI	0.172	0.389	0.64	0.645	79.970	60.462	29.880	20.098	38.18	9.62	1.43	0.64

22	Synthesized NTS	NETI	0.423	0.84	1.172	1.3	196.845	130.645	54.689	40.450	93.98	20.79	2.61	1.29
23	50m radial	Black Thunder Mine	0.016	0.035	0.412	1.354	7.628	4.863	19.009	42.160	3.64	0.77	0.91	1.34
24	50 m vertical	Black Thunder Mine	0.014	0.052	0.636	1.56	6.587	7.285	29.573	48.355	3.14	1.16	1.41	1.539
25	100 m radial	Black Thunder Mine	0.006	0.039	0.29	1.265	2.658	4.807	13.404	39.676	1.269	0.765	0.64	1.263
26	200 m radial	Black Thunder Mine	0.005	0.023	0.384	1.245	2.151	3.242	17.853	38.464	1.027	0.516	0.852	1.224
27	300 m radial	Black Thunder Mine	0.003	0.017	0.387	0.651	1.189	2.683	18.022	20.158	0.568	0.427	0.86	0.642
28	500 m radial	Black Thunder Mine	0.002	0.012	0.111	0.313	0.653	1.852	5.196	9.630	0.312	0.295	0.248	0.306

3.6 Analysis for an elastoplastic sdof system

In this section, analytical expressions are derived for the dynamic response of a bilinear elastoplastic (α = 0.0) SDOF system (Fig. 3.18).

The governing equation for an inelastic system is given by:

$$m\ddot{u}(t) + c\dot{u}(t) + f_s(u(t),\dot{u}(t)) = -m\ddot{u}_s(t) \qquad (3.6.1)$$

For a certain deformation *u(t)*, the restoring $f_s(u(t),\dot{u}(t))$ depends on the prior history of motion of the system and whether the deformation is currently increasing ($\dot{u}(t) > 0$) or decreasing ($\dot{u}(t) < 0$). To identify the system parameters that influence the deformation response *u(t)*, Eq.(3.6.1) is divided by *m* to obtain:

$$\ddot{u}(t) + 2\xi\omega_n\dot{u}(t) + \omega_n{}^2 u_y \widetilde{f}_s(u,\dot{u}) = -\ddot{u}_s(t) \qquad (3.6.2)$$

where the function: $\widetilde{f}_s(u,\dot{u}) = \dfrac{f_s(u,\dot{u})}{f_y}$ (3.6.3)

describes the force deformation relation in dimensionless form. Eq. (3.6.2) indicates that for a given support acceleration at time t, the system response depends on three system parameters: ω_n, ξ, and u_y, in addition to the force-deformation diagram.

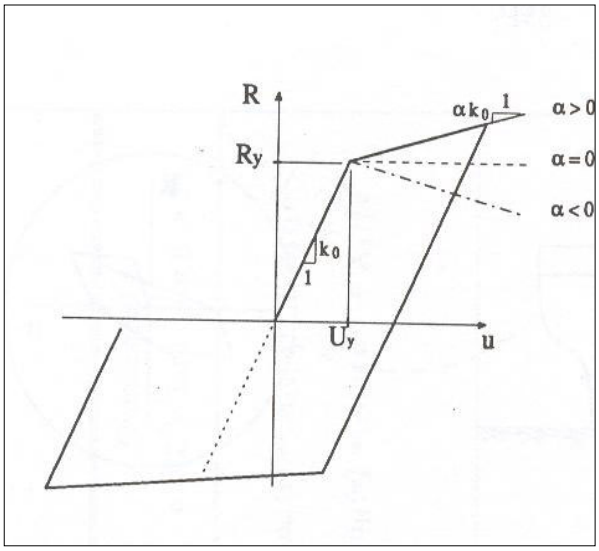

Figure 3-18 Bilinear Hysteretic Model

Eq. (3.6.2) can be rewritten in terms of the displacement ductility factor $\mu(t)$ by substituting:

$$u(t) = u_y \mu(t) \qquad \dot{u}(t) = u_y \dot{\mu}(t) \qquad \ddot{u}(t) = u_y \ddot{\mu}(t) \qquad (3.6.4)$$

which gives:

$$\ddot{\mu}(t) + 2\xi\omega_n \dot{\mu}(t) + \omega_n{}^2 \tilde{f}_s(\mu, \dot{\mu}) = -\frac{\omega_n{}^2 \ddot{u}_s(t)}{C_y . g} \qquad (3.6.5)$$

where the coefficient C_y is given by: $$C_y = \frac{f_y}{m \cdot g} \qquad (3.6.6)$$

The acceleration, displacement and velocity values for the elastoplastic SDOF system are derived by analytical integration of the equation of motion, by assuming the piecewise linearity of the force-deformation relationship and the excitation time histories. (For a detailed explanation on the derivation of the inelastic SDOF response see Ref.21, Appendix 2).

Discussion

In this study the analysis for an elastoplastic system was performed for period values ranging from 0.02 to 3.0 sec and the following parameters:
Strength Coefficient Cy = *0.25,* Damping ratio ξ = *0.05* C_{cr}, Weight = 1.0,
Hardening ratio $\alpha = 0$

The peak absolute values for the acceleration, displacement and ductility factor for selective period values (T= 3.0, 1.0, 0.3, 0.2 sec) are given in Table 3-5. The peak absolute accelerations (PA) for the earthquake (R1-R6) and the corresponding large shake tables (R7-R12) have almost equal values; for the small (R8-R13) shake table records the PAs are slightly reduced. The Telcordia (R19), measured NETI (R20), and the BTM (R23, R24, and R25) records, they all have larger PA values than the earthquake records (Fig. 3-19).

The large peak absolute displacement (PD) values that are illustrated in Fig. 3-20 imply significant inelastic behavior. The synthesized NETI (R22) has the largest PD values and the BTM (R23-R28) records the smallest among the record ensemble.

The ductility demand for short period systems (T < 0.3 sec) is very large for the given strength coefficient (*Cy* = 0.25). This result implies that these systems should be designed for a yield strength f_y the same as the strength required by the system to remain elastic; otherwise the inelastic deformation and ductility demand may be excessive.

Table 3.5 Peak absolute values for an elastoplastic system with 5% critical damping.

PA 3, PA 1, PA .3,PA .2: Peak absolute acceleration for period 3.0, 1.0, 0.3, 0.2 sec (g)
PD 3, PD 1, PD.3, PD .2: Peak absolute displacement for period 3.0, 1.0, 0.3, 0.2 sec (cm)
Duct 3, Duct 1, Duct .3, Duct .2: Maximum ductility for period 3.0, 1.0, 0.3, 0.2 sec

Records	Name	Type	SA3	SA 1	SA .3	SA .2	SD 3	SD 1	SD .3	SD .2	Duct3	Duct1	Duct.3	Duct.2
1	Landers/LCN260	EQ/Landers (1992/06/28)	0.795	0.744	0.841	0.823	74.43	18.14	3.43	3.1	1.331	2.956	22.893	12.482
2	Landers/LCN345	EQ/Landers (1992/06/28)	0.807	0.853	0.909	0.861	26.46	7.57	2.16	1.08	0.473	1.219	3.873	4.336
3	Northr/SCS142	EQ/Northridge (1994/01/17)	0.996	1.09	0.589	0.567	41.06	32.1	10.1	8.67	0.734	5.168	18.069	34.915
4	Northr/SCE018	EQ/Northridge (1994/01/17)	1.029	1.062	0.916	0.799	63.56	26.45	11.4	10.77	1.137	4.258	20.387	43.343
5	Northr/RRS-288	EQ/Northridge (1994/01/17)	1.05	1.017	0.959	0.896	58.42	31.24	25.3	18.34	1.045	5.029	45.253	73.825
6	Northr/PAR-L	EQ/Northridge (1994/01/17)	0.708	0.895	0.466	0.363	16.34	22.62	7.78	5.28	0.292	3.641	13.919	21.274
7	Landers/LCN260	Shake Table, 10" limit	0.821	0.779	0.809	0.802	53.36	13.18	2.2	2.5	0.954	2.122	3.923	10.06
8	Landers/LCN345	Shake Table, 10" limit	0.807	0.853	0.908	0.86	26.35	7.57	2.17	1.04	0.471	1.219	3.877	4.191
9	Northr/SCS142	Shake Table, 10" limit	0.998	1.096	0.583	0.566	35.53	35.1	10.28	7.49	0.635	5.651	18.39	30.142
10	Northr/SCE018	Shake Table, 10" limit	1.021	1.065	0.901	0.773	70.42	27.34	11.7	10.96	1.26	4.401	20.909	44.095
11	Northr/RRS-288	Shake Table, 10" limit	0.969	1.014	0.944	0.882	38.96	28	21.55	18.9	0.697	4.507	38.548	76.047
12	Northr/PAR-L	Shake Table, 10" limit	0.708	0.896	0.466	0.363	16.33	22.62	7.78	5.29	0.292	3.642	13.925	21.281
13	Landers/LCN260	Shake Table, 2" limit	0.702	0.802	0.783	0.78	6.66	7.67	2.79	2.59	6.665	7.672	2.787	2.589
14	Landers/LCN345	Shake Table, 2" limit	0.795	0.856	0.917	0.859	16.24	7.32	1.94	1.12	0.29	1.179	3.468	4.51
15	Northr/SCS142	Shake Table, 2" limit	0.618	0.668	0.501	0.45	5.02	15.25	4.57	2.81	0.09	2.456	8.169	11.308
16	Northr/SCE018	Shake Table, 2" limit	0.83	1.045	0.822	0.817	4.96	12.11	10.08	9.32	0.089	1.95	18.032	37.491
17	Northr/RRS-288	Shake Table, 2" limit	0.632	0.802	0.763	0.617	5.01	11.52	4.1	4.39	0.09	1.855	7.34	17.678
18	Northr/PAR-L	Shake Table, 2" limit	0.528	0.661	0.542	0.294	5.56	11.62	3.42	1.15	0.099	1.871	6.113	4.631
19	Telcordia time history	Shake Table Standard	1.691	1.896	1.66	1.608	14.11	21.92	14.71	14.04	0.252	3.528	26.327	56.491
20	Measured NTS-5	NETI	3.461	3.445	3.349	3.245	4.51	3.9	2.81	2.56	0.081	0.628	5.02	10.291
21	Scaled NTS-5	NETI	0.532	0.522	0.322	0.28	38.18	10.02	3.58	2.51	0.683	1.614	6.406	10.086
22	Synthesized NTS	NETI	1.143	0.809	0.649	0.622	82.7	90.79	39.79	43.02	1.479	14.615	71.173	173.129
23	50m radial	Black Thunder Mine	2.878	2.88	2.776	2.942	3.64	0.77	0.99	0.84	0.065	0.125	1.769	3.39
24	50 m vertical	Black Thunder Mine	4.17	4.178	4.263	4.47	3.14	1.16	0.91	2.85	0.056	0.187	1.621	11.463
25	100 m radial	Black Thunder Mine	1.9	1.905	2.175	2.128	1.269	0.765	0.631	0.888	0.023	0.123	1.141	3.589
26	200 m radial	Black Thunder Mine	0.761	0.764	0.662	0.839	1.027	0.516	0.796	0.978	0.018	0.083	1.424	3.943
27	300 m radial	Black Thunder Mine	0.375	0.382	0.61	0.646	0.568	0.427	0.878	0.483	0.01	0.069	1.575	1.943
28	500 m radial	Black Thunder Mine	0.231	0.233	0.319	0.401	0.312	0.295	0.248	0.311	0.006	0.047	0.444	1.267

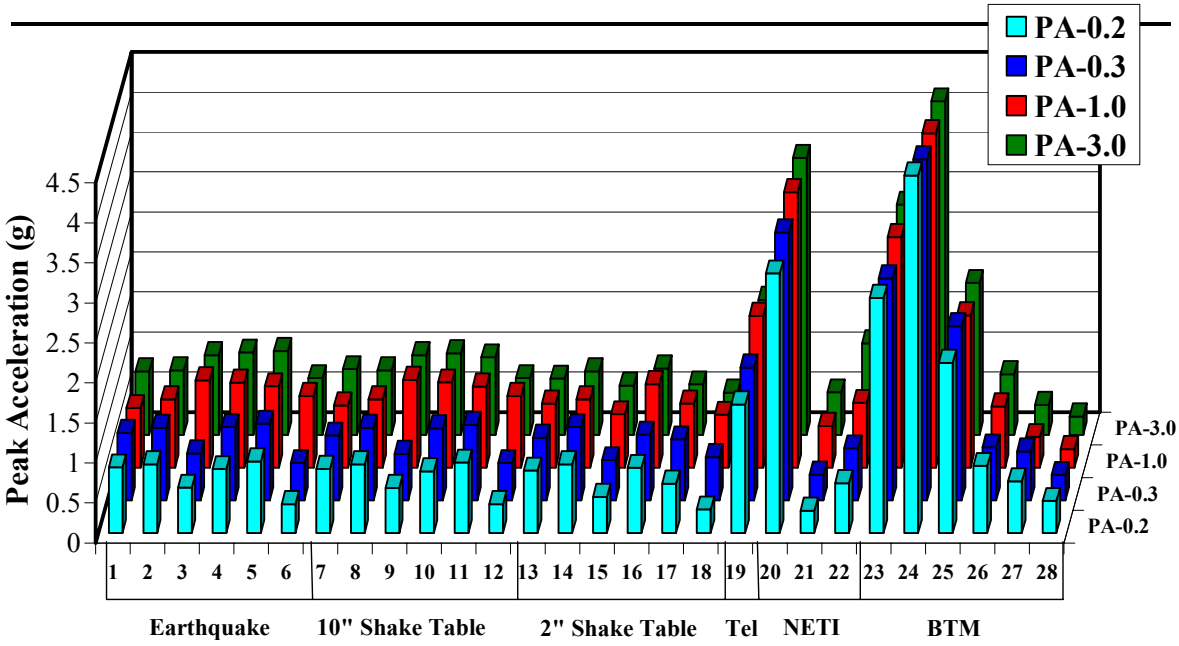

Figure 3-19 Peak acceleration values for an elastoplastic SDOF system (5% cr. damping)

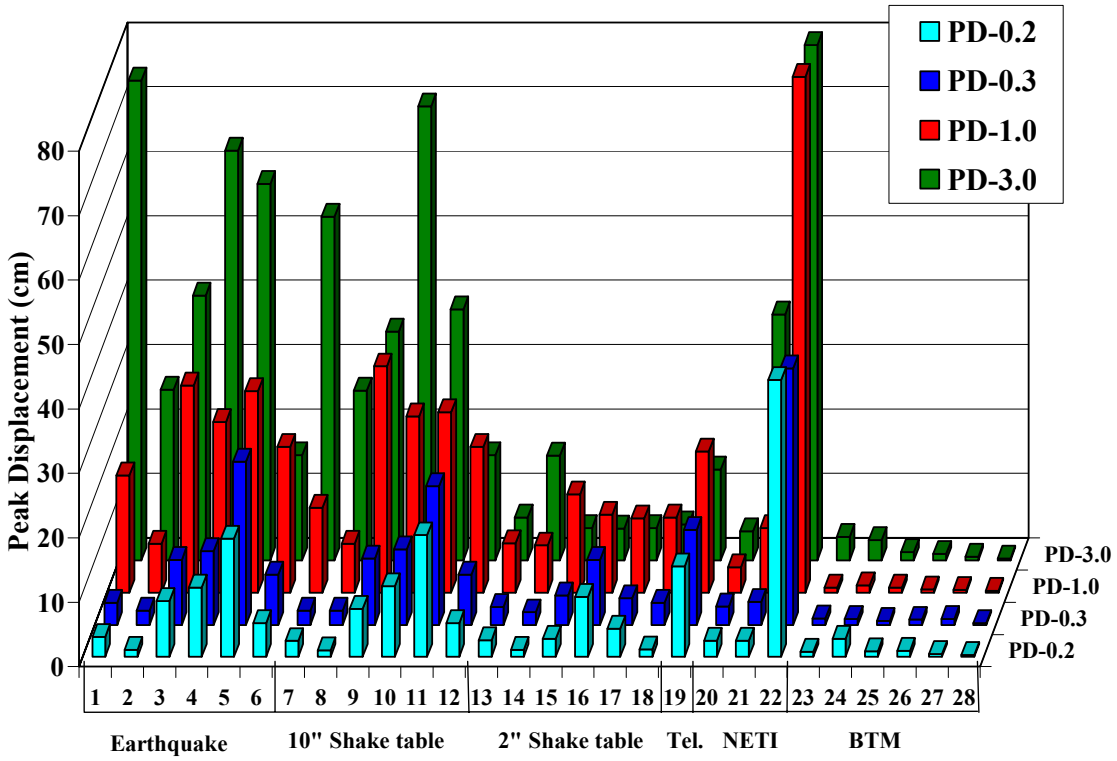

Figure 3-20 Peak displacement for an elastoplastic SDOF system (5% cr. damping)

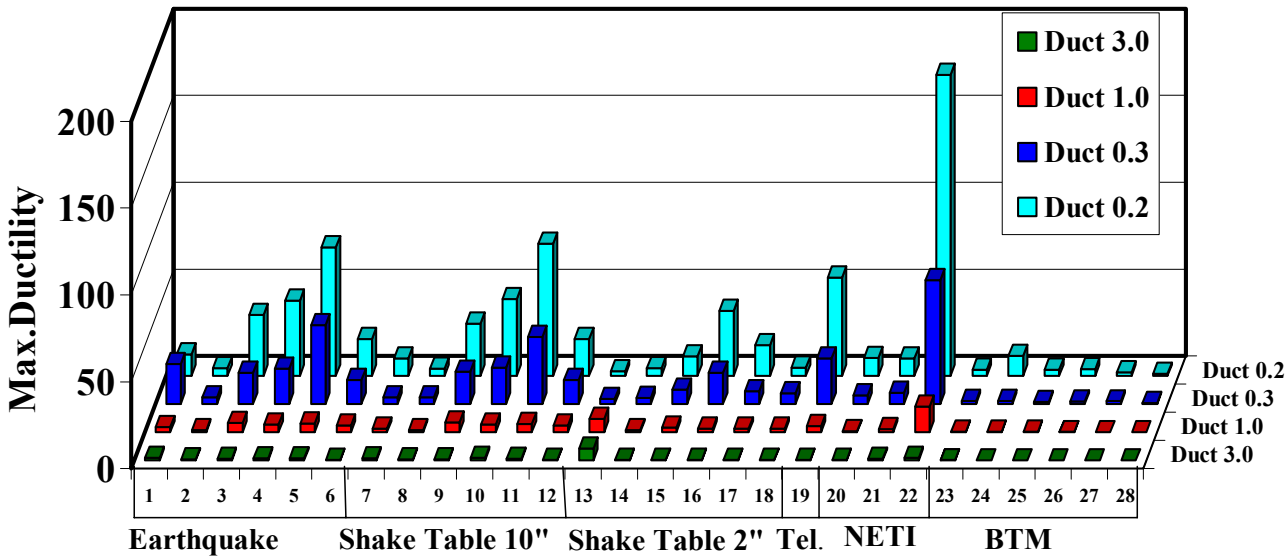

Figure 3-21 Maximum Ductility values for an elastoplastic SDOF system

(5% cr. damping)

3.6.1 Constant Ductility Spectra for an elastoplastic SDOF system

In design applications, the effect of yielding is to reduce the value of the design loads below those required for elastic behavior, the magnitude of this reduction being a function of the degree of inelastic behavior that can be tolerated by the system. The system's ductility capacity is given by the system's ductility factor μ. For a specified system's ductility capacity given by the ductility factor, the construction of the constant ductility spectra allows the determination of the yield strength fy, which is necessary to limit the ductility demand imposed by the excitation to the system's inherent allowable ductility.

In the present study constant ductility spectra for ductility factor $\mu = 4$, are constructed for the record ensemble and are presented in Fig. 3.22 – 3.27.
An interpolating procedure is necessary to obtain the yield strength of an elastoplastic system for a specified ductility factor since the response of a system with arbitrarily selected yield strength will seldom correspond to the desired ductility value. For further details on the construction of the Constant-Ductility Spectrum see Ref.25, Section7.5.3.

Discussion

The data from Fig.3.22 –3.27 demonstrate the strength demand imposed by the ground / shake table motion on a system with ductility capacity μ =4.0.

Fig.3.22 depicts the constant ductility spectra for the earthquake records (R1-R6). (R5) Northridge/RRS-288, imposed the highest strength demand to an elastoplastic system (μ =4.0) for period values 0.1-1.0 sec, whereas for period values 1.0 –10 sec, the strength demand from (R1) Landers/LCN260 exceeded that from all the other earthquake records.

In Fig.3.23, three constant ductility spectra for the Landers/LCN260 and the equivalent shake table records are compared (R1, R7, R13). It is observed that the 10" shake table spectrum values are slightly smaller than the earthquake spectrum values until the threshold period value of 2.0 sec, and for larger period values the difference increases. The smaller spectrum values are observed for the 2" shake table, where for period values larger than 0.5 sec the spectrum deviates significantly from the earthquake spectrum.

In Fig.3.24 it is of interest to note that the two spectra for the Northr/RRS-288 and the shake table 10" coincide through the period value 3.0 sec. The 2"shake table has significantly smaller values.

In Fig. 3.25 the Telcordia and the North/RRS 288 records are compared. The Telcordia record imposed the largest yield strength value from the record ensemble ($f_y max$ =*1*.981 W for period T = 0.25 sec*)* on the elastoplastic system under consideration, and it is the only record which its spectrum values exceeded those from the North/RRS record for the range of period values 0.1 – 0.9 sec.

Fig.3.26 depicts the constant ductility spectra for the NETI records. The yield strength values for the synthesized NETI record fluctuate between the North/RRS-288 values for the smaller period range (0.1 –1.0 sec) and exceed these values for the larger period range (1.0 – 10. sec). The measured NETI record spectrum exceeds the North/RRS spectrum only in the small period range (0.1 – 0.15 sec) and for the period range (0.15 –10.0 sec) the measured NETI spectrum values are almost 10 times smaller than the yield strength values for the North/RRS-288.

Finally the constant ductility spectra for the BTM records and the Northr/RRS-288 spectrum are presented in Fig.3.27. The Northr/RRS-288 spectrum envelopes all the BTM spectra for period values T > 0.15 sec and it is observed that the yield strength values for all the BTM records are significantly smaller the spectrum values for the Northr/RRS-288 record.

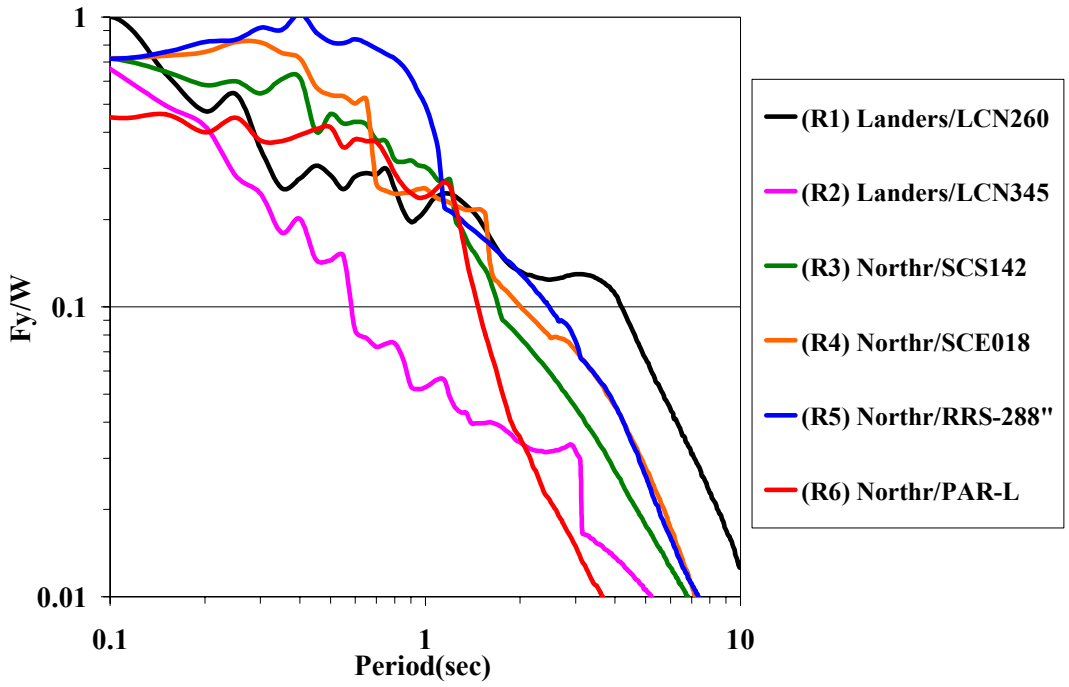

Figure 3-22 Constant ductility spectra for the earthquake records (R1-R6).

Ductility = 4.0

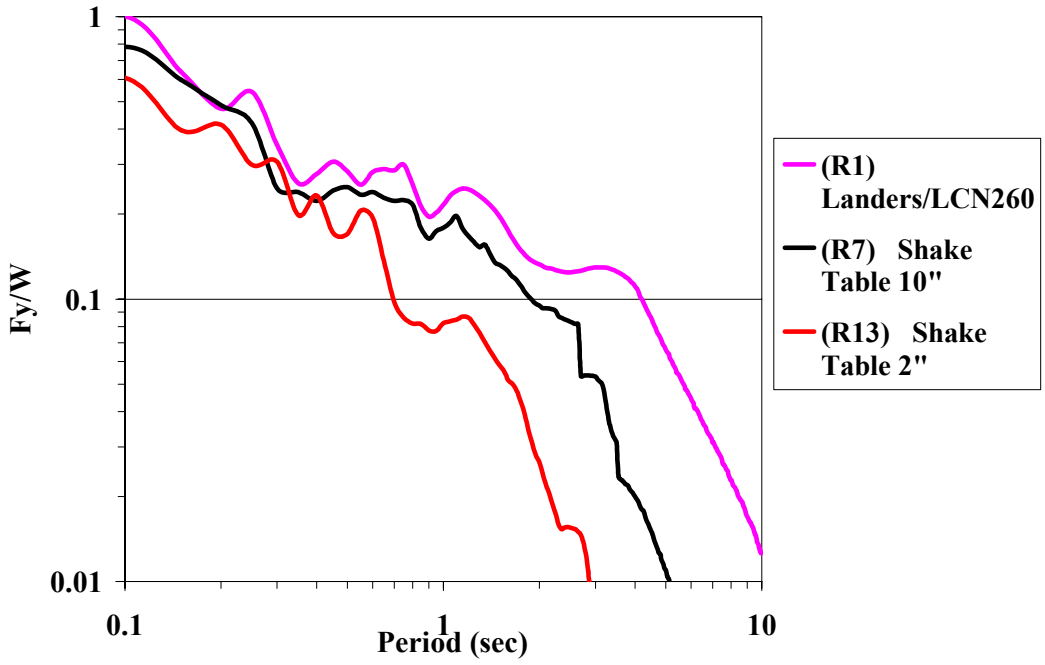

Figure 3-23 Constant ductility spectra for the Landers/LCN260 record (Ductility = 4.0)

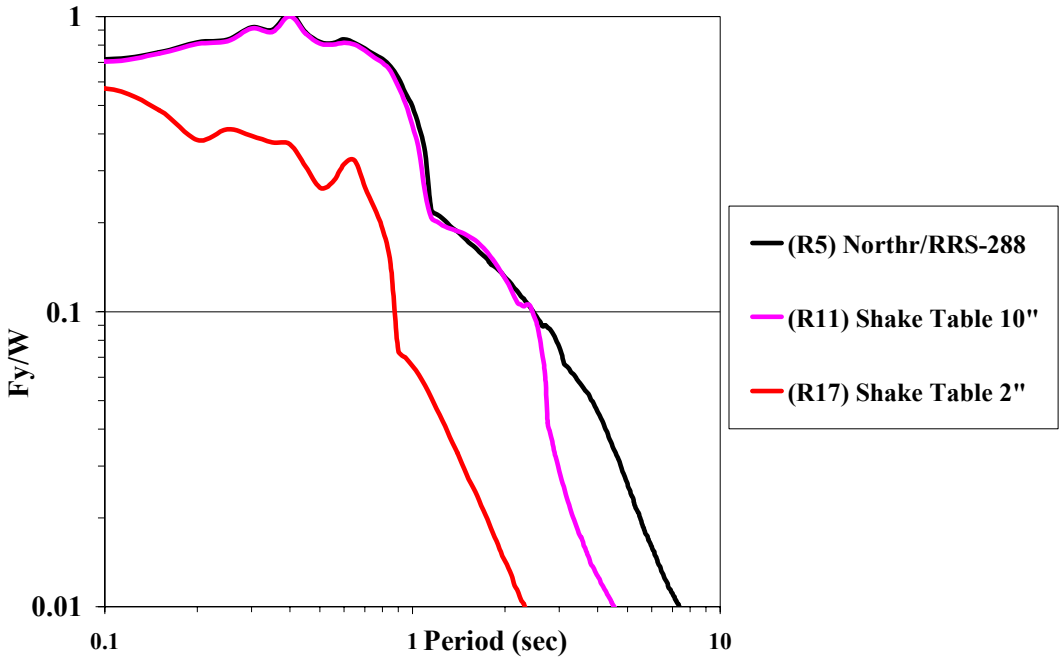

Figure 3-24 Constant ductility spectra for the Northr/RRS-288 record (Ductility = 4.0)

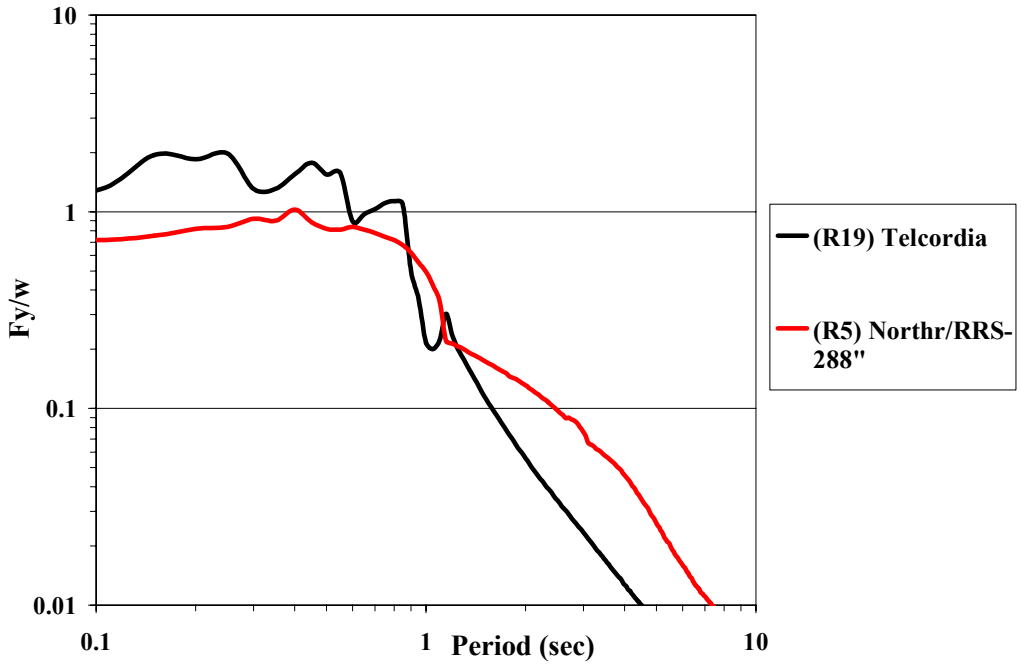

Figure 3-25 Constant ductility spectra for the Telcordia record (Ductility=4.0)

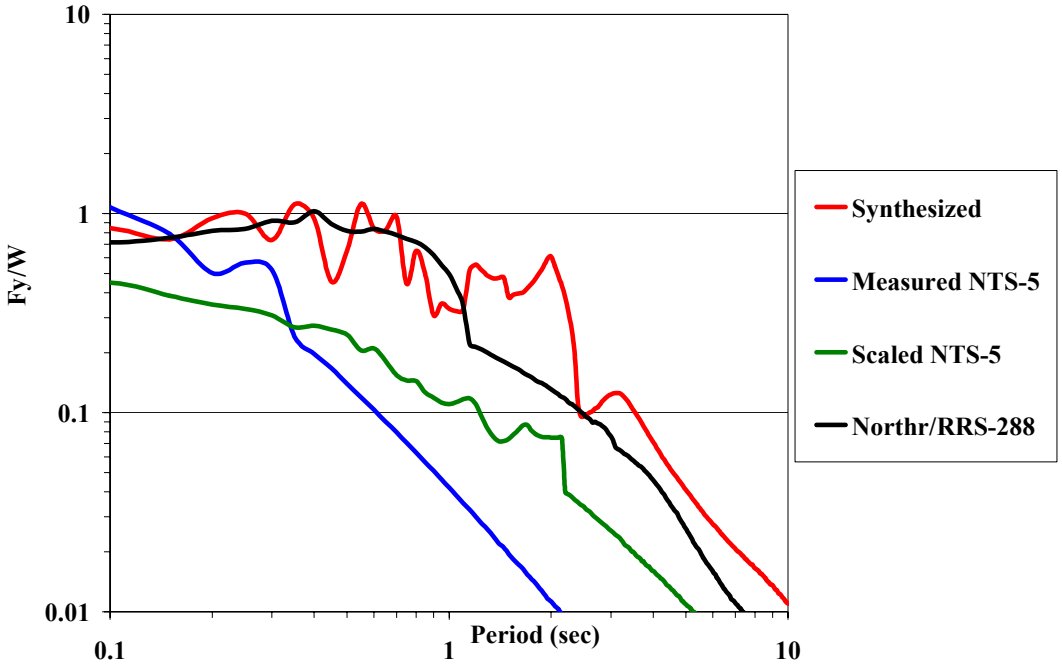

Figure 3-26 Constant ductility spectra for the NETI records (Ductility = 4.0)

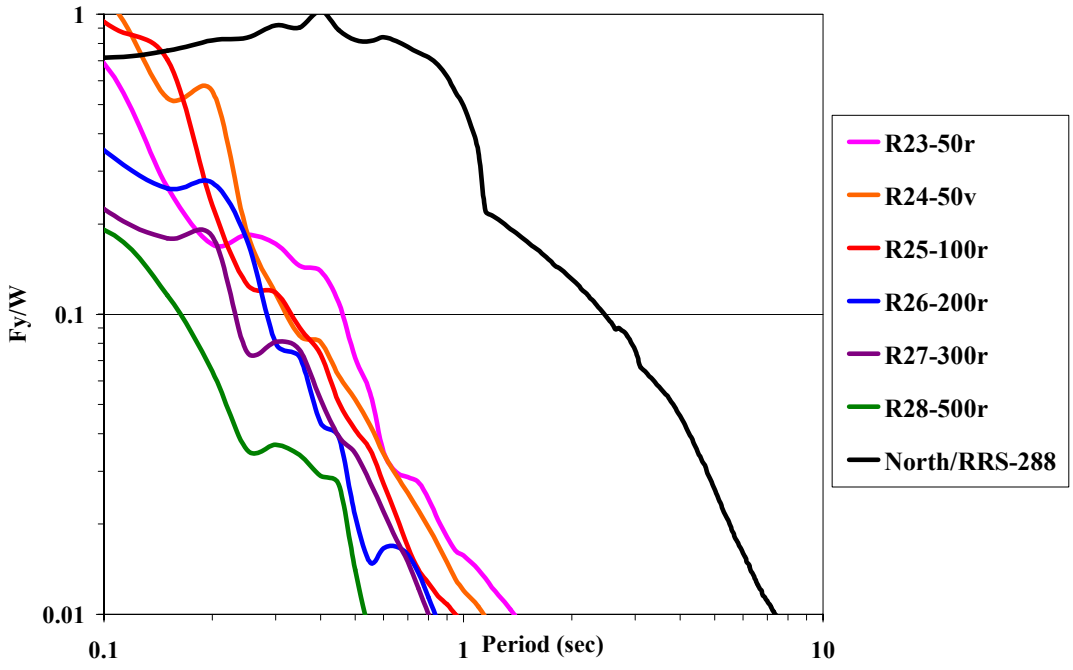

Figure 3-27 Constant ductility spectra for the BTM records (Ductility = 4.0)

3.6.2 Energy Balance Equation

Mainly both viscous damping and yielding dissipate the earthquake input energy to an inelastic system. The energy balance equation is obtained by integrating the equation of motion for a SDOF inelastic system, with respect to the relative displacement u(t) :

$$m\ddot{u}(t) + c\dot{u}(t) + fs(u(t), \dot{u}(t)) = -m\ddot{u}_g(t) \tag{3.6.7}$$

$$\int_0^u m\ddot{u}(t)du + \int_0^u c\dot{u}(t)du + \int_0^u f_s(u(t), \dot{u}(t))du = -\int_0^u m\ddot{u}_g(t)du \tag{3.6.8}$$

or by using the notation $du = \frac{du}{dt}dt = \dot{u}dt$ the above equation can be rewritten:

$$\int_0^t m\ddot{u}(t)\dot{u}dt + \int_0^t c\dot{u}(t)\dot{u}dt + \int_0^t f_s(u(t), \dot{u}(t))\dot{u}dt = -\int_0^t m\ddot{u}_g(t)\dot{u}dt \tag{3.6.9}$$

The right side of the equation is the total energy input to the structure $E_I(t)$. Since the term $\dot{u}$ is the relative velocity the corresponding input energy is also relative.

The first term on the left side of Eq. (3.6.9) is the kinetic energy of the mass associated with its motion relative to the ground:

$$E_K(t) = \int_0^t m\dot{u}(t)\ddot{u}(t)dt = \left|\frac{1}{2}m\dot{u}^2(t)\right|_0^t = \frac{1}{2}m\dot{u}^2(t) - \frac{1}{2}m\dot{u}^2(0) \tag{3.6.10}$$

The second term on the left side of Eq. (3.6.9) is the energy dissipated by viscous damping:

$$E_D(t) = \int_0^t c\dot{u}^2(t)dt \tag{3.6.11}$$

The third term on the left side of Eq. (3.6.9) is the sum of the energy dissipated by the recoverable elastic strain energy $E_S(t)$ and the irrecoverable hysteretic energy through yielding $E_Y(t)$.

Based on these energy quantities the energy balance equation of the system can be rewritten as:

$$E_I(t) = E_K(t) + E_D(t) + E_S(t) + E_Y(t) \quad (3.6.12)$$

To compute the energy terms, the integration over time has to be broken into the number of constant linear loading time intervals. A discussion on the analytical integration of motion and the evaluation of the energy terms can be found in Ref. 21.

3.6.3 Energy Time Histories

The energy time histories (kinetic, damping, elastic, yielding) were calculated for the record ensemble. The graphs (Fig. 3-29 through Fig. 3-56) depict the energy dissipation time histories (damping, damping + yielding, total input) for the following seven records:

- (R1) Earthquake - Landers / LCN260
- (R7) Shake Table 10" - Landers / LCN260
- (R13) Shake Table 2" - Landers / LCN260
- (R19) Telcordia
- (R20) Measured NTS-5
- (R22) Synthesized NTS
- (R23) Black Thunder Mine 50 m radial

For each record, the energy time histories for an elastoplastic system with 5% critical damping and strength coefficient equal to 0.25 (Cy = yield strength/ weight, weight =1.0) are presented for period values 0.2, 0.3, 1.0 and 3.0 sec.

The results show that the energy supplied to the elastoplastic system is being dissipated throughout the excitation time history mainly by viscous damping and hysteretic behavior (when yielding occurs). In addition, the input energy for the same record varies according to the system's period as it is expected. The system's period also affects the damping, inelastic and kinetic energy participation percentages to the total input energy dissipation.

Table 3.7 summarizes the maximum damping, yielding and total energy values at the end of the excitation, along with the participation percentages for the damping and yielding to the dissipation of the input energy for the aforementioned seven records.

For the earthquake record R1-Landers/LCN260, more than 50% of the input energy is being dissipated by hysteretic behavior for small period systems (T = 0.2, 0.3 sec). For the larger period range, the yielding percentage decreases while both the dissipating damping and kinetic energy increase. The same energy time history trends with the R1-Landers/LCN260 record are also observed for the corresponding 10" and 2" shake table records. It is interesting to note that for both shake table excitation records and period

value T =3.0 sec., no yielding occurs and the elastoplastic system dissipates the input energy mainly by damping and also kinetic and elastic energy by a smaller percentage.

For the R19-Telcordia record yielding is the main energy dissipater for period range T = 0.2 -1.0 sec. with a high percentage ratio ranging from 65% to 70%. For period value T = 3.0 sec. no yielding occurs.

The response of the elastoplastic system under consideration to the R20-NETI measured NTS-5 record exhibits high inelastic energy values for period T = 0.2, 0.3 sec. and no hysteretic behavior for period T >=1.0 sec. On the other hand, hysteretic behavior is observed for the R22-NETI synthesized record and period T =1.0 and 3.0 sec. In addition, the inelastic are higher than the damping percentages for systems with T < 1.0 sec.

From the BTM group of records, energy time history results for the R23-BTM 50 m. radial are presented. The lowest total energy input values from the seven records under consideration were observed for R23. Mainly damping is dissipating the excitation energy. There is a significant decrease in inelastic energy as the period increases and there is no nonlinear behavior for systems with T > 1.0 sec.

3.6.4 Total Input Energy for selective records

Figures 3-57 through 3-67 depict the total input energy time histories for the seven selective records (R1, R7, R13, R19, R20, R22, R23). Table 3.6 summarizes the total input energy reduction percentages for four period values (T = 0.2, 0.3, 1.0, 3.0 sec.) with respect to the earthquake Landers /LCN260 record (R1). The following observations can be made based on Figs.3.54 - 3.57 and Table 3.7:

10”(R7) and 2”(R13) Shake tables:
The 10” Shake table record has smaller reduction percentages values from the 2” Shake table for the four period values. For both records though, the energy results are the closest to the earthquake record (R1) as expected since their acceleration time histories are filtered versions of the (R1) record.

Telcordia (R19):
The input energy values for the Telcordia record exceed significantly the earthquake values for periods of 0.2, 0.3 and 1.0 sec. For the period of 3.0 sec a large reduction percentage of approximately 60% is observed with respect to the earthquake total energy input.

Measured NTS-5 (R21) and Synthesized NETI (R22):
The measured NTS-5 record has large reduction percentages for T = 0.2 and 0.3 sec.
For period values T = 1.0 and 3.0 sec the total input energy values are so minor that we can infer about the elastoplastic system that will remain undisturbed. On the other hand,

the input energy values originated from the synthesized NETI record exceed by 8 to 18 times the earthquake values for all the periods and are the largest among the record ensemble for T >1.0 sec.

50 m radial BTM (R23):
Finally, the smallest total input energy values and the largest reduction percentages from the group of seven records resulted from the BTM 50 m radial record. This result indicates that the intensity of the BTM explosion is too weak to produce significant excitation similar in magnitude to an earthquake excitation, for elastoplastic systems with period T > 0.2 sec.

3.6.5 Ratio of the hysteretic over the total dissipated energy

In Fig. 3-28 the graphs of the ratio of the hysteretic (E_Y) over the total dissipated energy ($E_K + E_D + E_S + E_Y$) at the end of the excitation for the seven selective records are presented. It is evident that the Synthesized NETI record (R22) has the largest ratio values for periods larger than 0.2 sec. High hysteretic ratio values are also observed for the measured NETI (R20) record for periods up to 0.6 sec.

The graphs for both the large (R7) and the small (R13) shake table records follow closely the corresponding earthquake Landers LCN/260 (R1) graph till the period of 0.3 sec approximately, and for larger period values (T >0.3 sec) fall under the earthquake graph. The Telcordia (R19) envelops the earthquake Landers LCN/260 (R1) graph for the period range of 0.3 - 1.1 sec, and for period values larger than 1.1 sec the ratio values decrease following a steep slope.

The smallest hysteretic ratios among the seven records are observed for the BTM 50 m radial (R23), which indicate that mainly kinetic and damping energy dissipate the excitation input. The graph also implies that systems with period values larger than 0.5 sec will behave linearly and remain in the elastic region.

Table 3-6 Total Input Energy reduction percentages for selective records with respect to (R1)

Records	Reduction percentages with respect to record (R1) (%)			
	0.2 sec	0.3 sec	1.0 sec	3.0 sec
(R7) Landers/LCN260	5.02	6.04	18.05	22.97
(R13) Landers/LCN260	5.12	8.08	35.55	98.61
(R20) Measured NTS -5	52.47	38.85	94.15	99.45
(R23) BTM 50 m radial	71.38	83.27	98.62	99.68

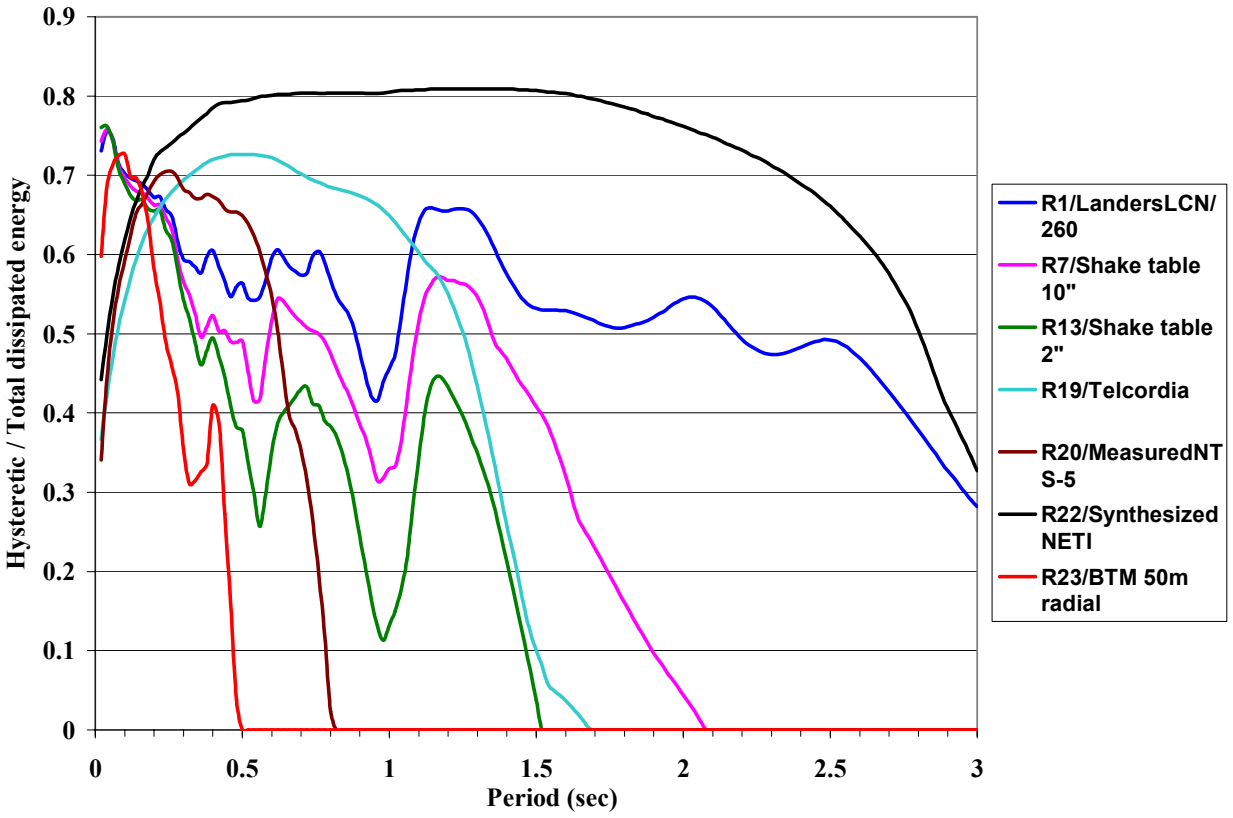

Figure 3-28 Ratio of the hysteretic energy over total dissipated energy at the end of the excitation for a selective group of records.

Table 3-7 Maximum Energy quantities at the end of excitation

Max Ed / unit mass: maximum damping energy / unit mass, at the end of excitation
Max Ey / unit mass: maximum yielding energy / unit mass, at the end of excitation
Max Ei / unit mass: maximum total input energy / unit mass, at the end of excitation

Records	Max Ed / unit mass 1000 (cm/sec)^2				Max Ey / unit mass 1000 (cm/sec)^2				Max Ei /unit mass 1000 (cm/sec)^2			
	0.2sec	0.3 sec	1.0 sec	3.0 sec	0.2sec	0.3 sec	1.0 sec	3.0 sec	0.2sec	0.3 sec	1.0 sec	3.0 sec
(R1) Landers/LCN260	1.86	2.05	3.551	11.563	3.818	3.002	2.98	4.542	5.679	5.052	6.532	16.118
Participation to the total input energy (%)	32.76	40.58	54.37	71.74	67.24	59.42	45.63	28.18				
(R7) Landers/LCN260	1.822	2.067	3.589	12.404	3.571	2.679	1.763	0	5.394	4.747	5.353	12.415
Participation to the total input energy (%)	33.78	43.54	67.04	99.91	66.20	56.43	32.93	0				
(R13) Landers/LCN260	1.86	2.128	3.653	0.224	3.528	2.515	0.556	0	5.388	4.644	4.21	0.224
Participation to the total input energy (%)	34.52	45.82	86.77	100	65.48	54.15	13.21	0				
(R19) Telcordia	52.628	45.969	35.549	6.518	96.522	104.197	65.829	0	149.15	150.17	101.802	6.518
Participation to the total input energy (%)	35.28	30.61	34.92	100	64.71	69.39	64.66	0				
(R20) Measured NTS -5	0.83	0.968	0.352	0.074	1.868	2.074	0	0	2.699	3.089	0.382	0.088
Participation to the total input energy (%)	30.75	31.34	92.15	84.10	69.21	67.14	0	0				
(R22) Synthesized	16.653	19.209	23.211	94.628	42.745	58.711	95.774	45.904	59.399	77.921	118.986	140.637
Participation to the total input energy (%)	28.03	24.65	19.51	67.28	54.86	75.35	80.49	32.64				
(R23) BTM 50 m radial	0.679	0.546	0.089	0.043	0.945	0.297	0	0	1.625	0.845	0.09	0.051
Participation to the total input energy (%)	41.78	64.61	98.88	84.31	58.15	35.15	0	0				

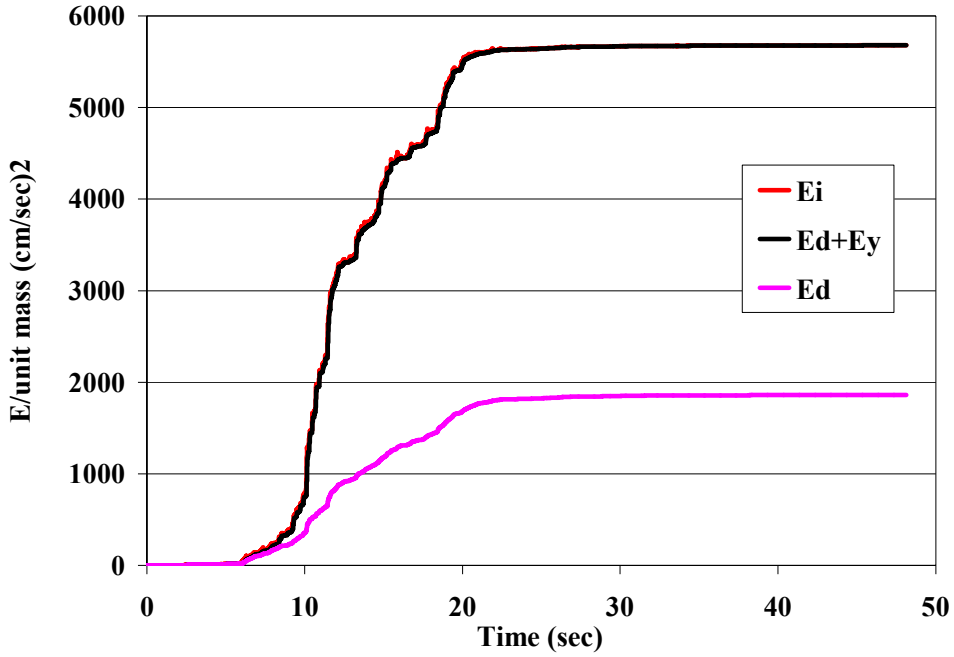

Figure 3-29 Time history of Energy dissipation for Record 1 –Landers/LCN260 (T=0.2 sec, 5% cr. damping, Cy=0.25)

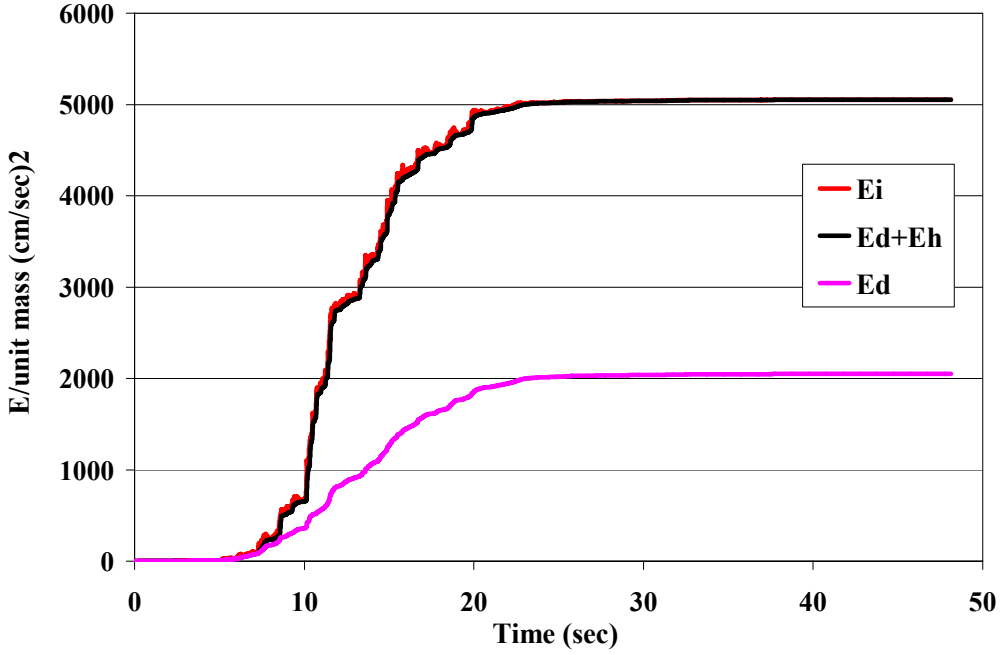

Figure 3-30 Time history of Energy dissipation for Record 1 –Landers/LCN260 (T=0.3 sec, 5% cr. damping, Cy=0.25)

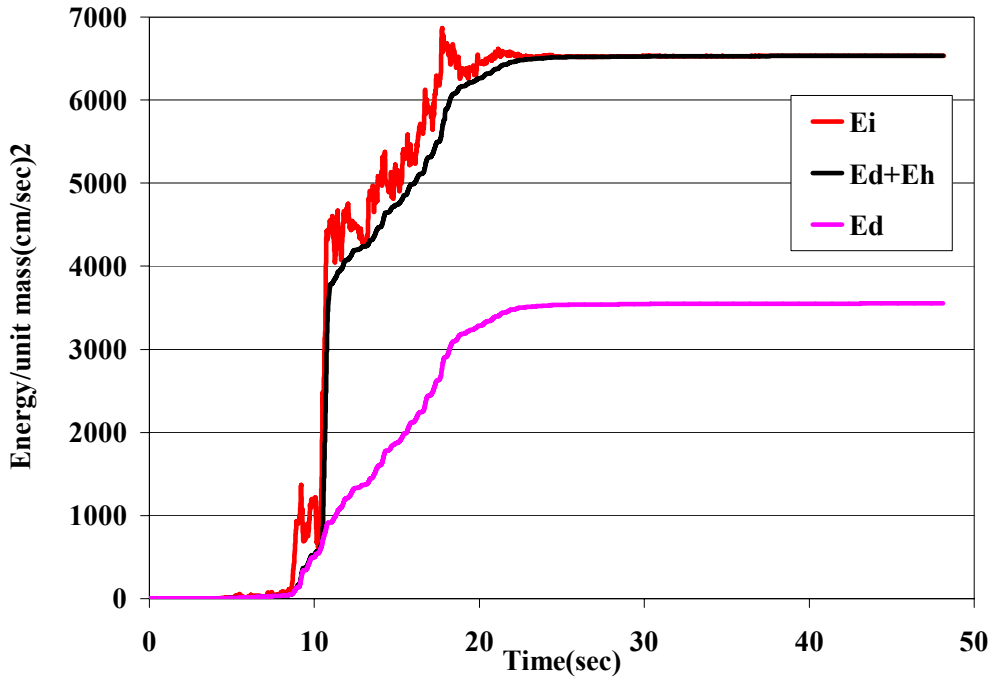

Figure 3-31 Time history of Energy dissipation for Record 1 –Landers/LCN260

(T=1.0 sec, 5% cr. damping, Cy=0.25)

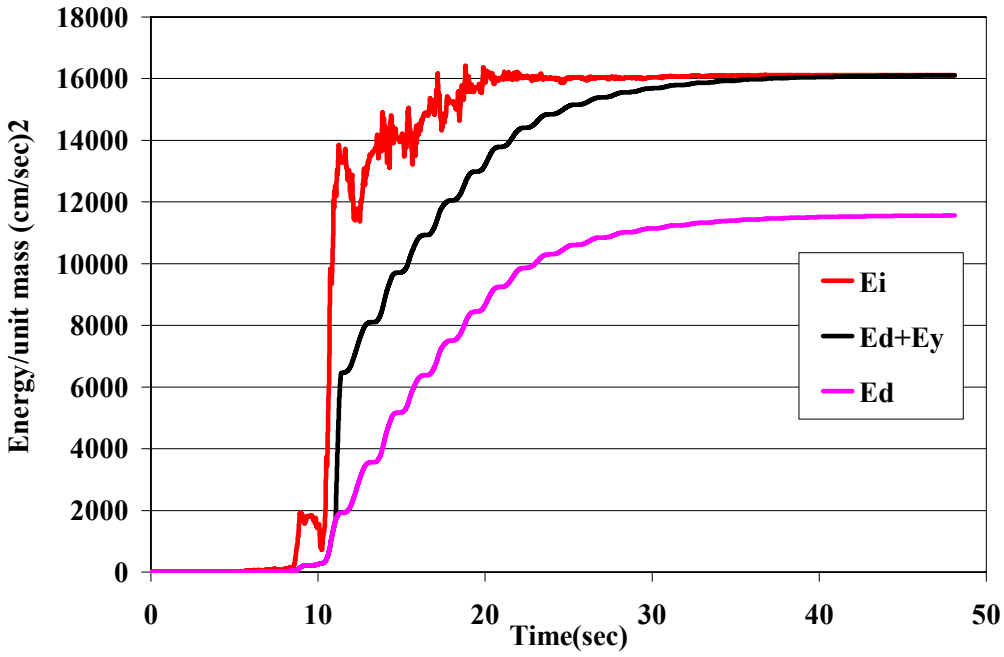

Figure 3-32 Time history of Energy dissipation for Record 1 –Landers/LCN260

(T=3.0 sec, 5% cr. damping, Cy=0.25)

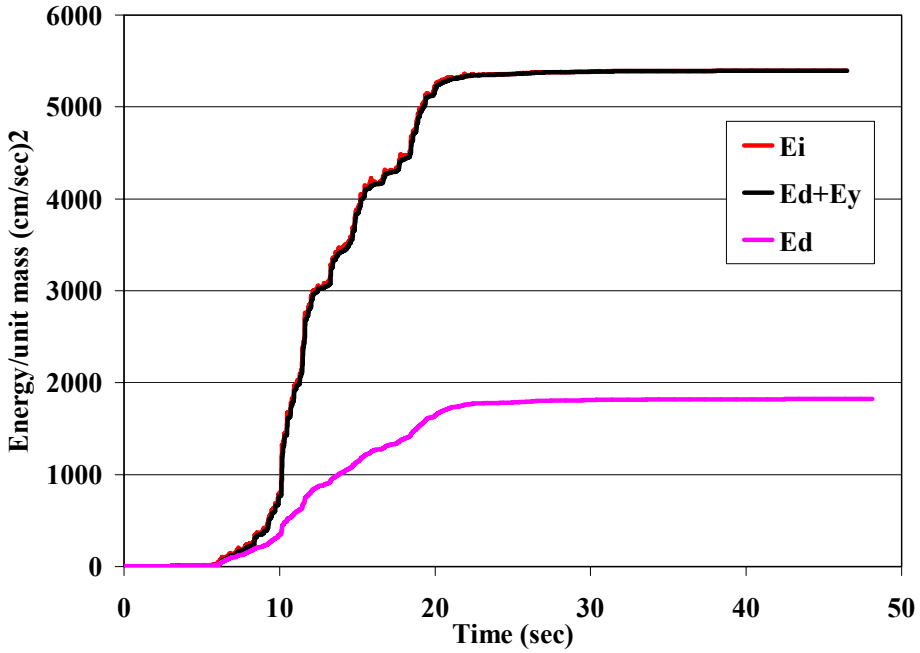

Figure 3-33 Time history of Energy dissipation for Record 7

Shake Table 10" (Landers/LCN260) - T=0.2 sec, 5% cr. damping, Cy=0.25

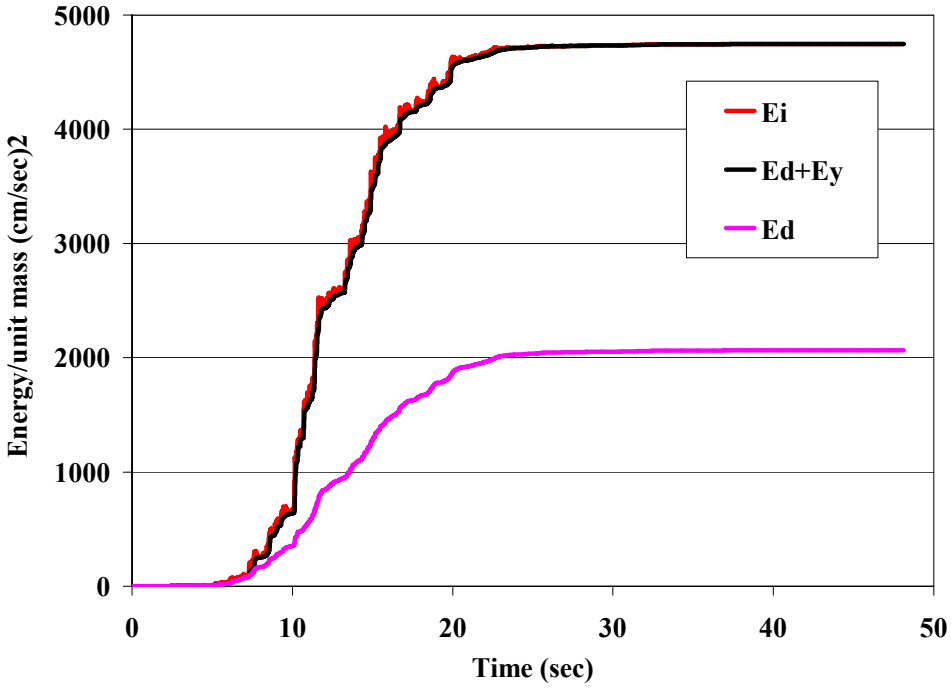

Figure 3-34 Time history of Energy dissipation for Record 7

Shake Table 10" (Landers/LCN260) - T=0.3 sec, 5% cr. damping, Cy=0.25

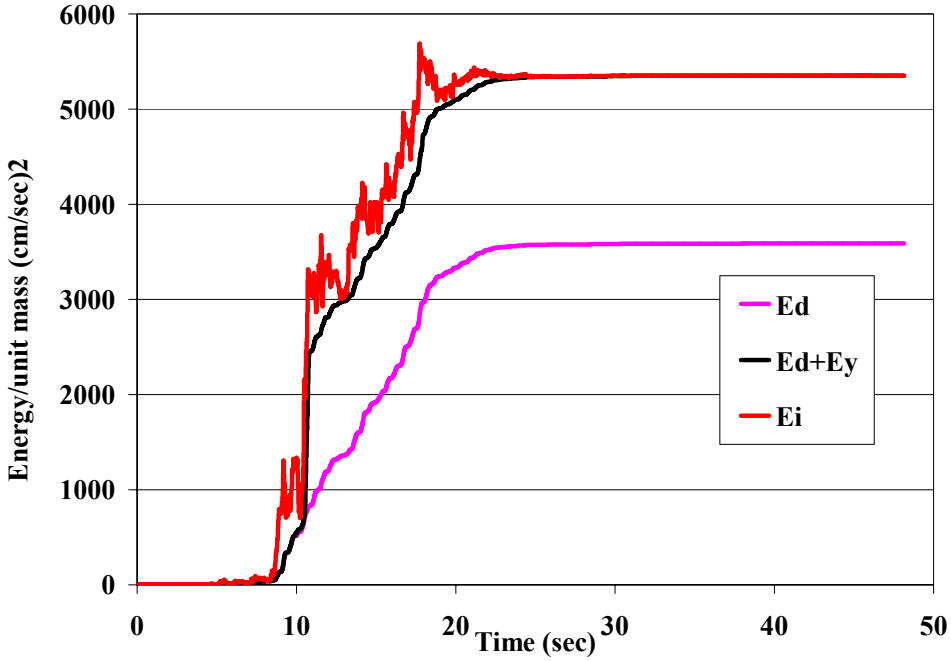

Figure 3-35 Time history of Energy dissipation for Record 7

Shake Table 10" (Landers/LCN260) - T= 1.0 sec, 5% cr. damping, Cy=0.25

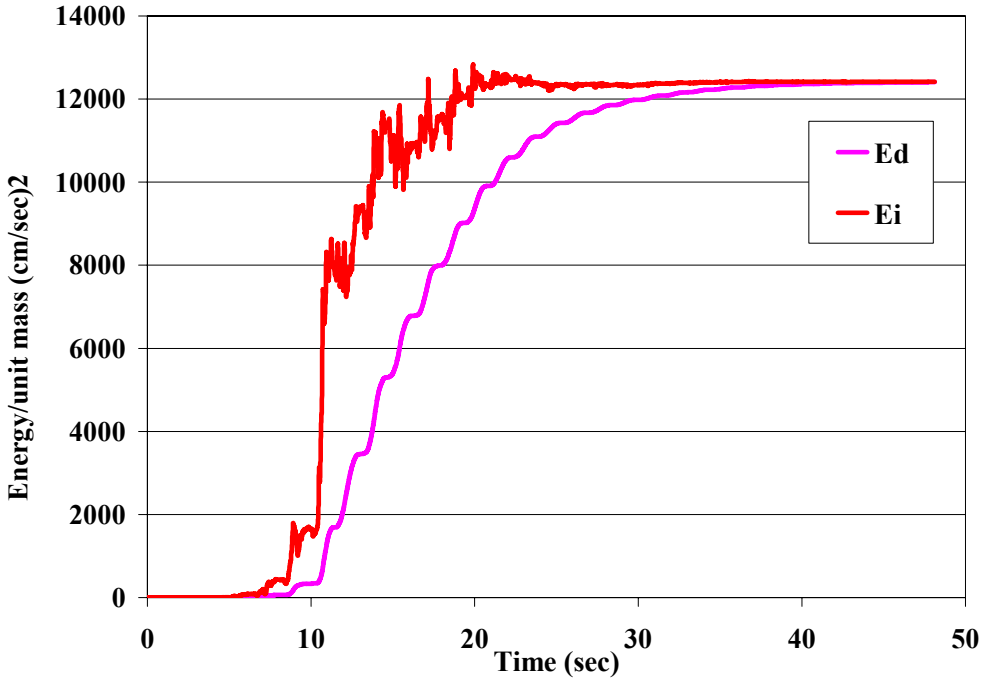

Figure 3-36 Time history of Energy dissipation for Record 7

Shake Table 10" (Landers/LCN260) - T= 3.0 sec, 5% cr. damping, Cy=0.25

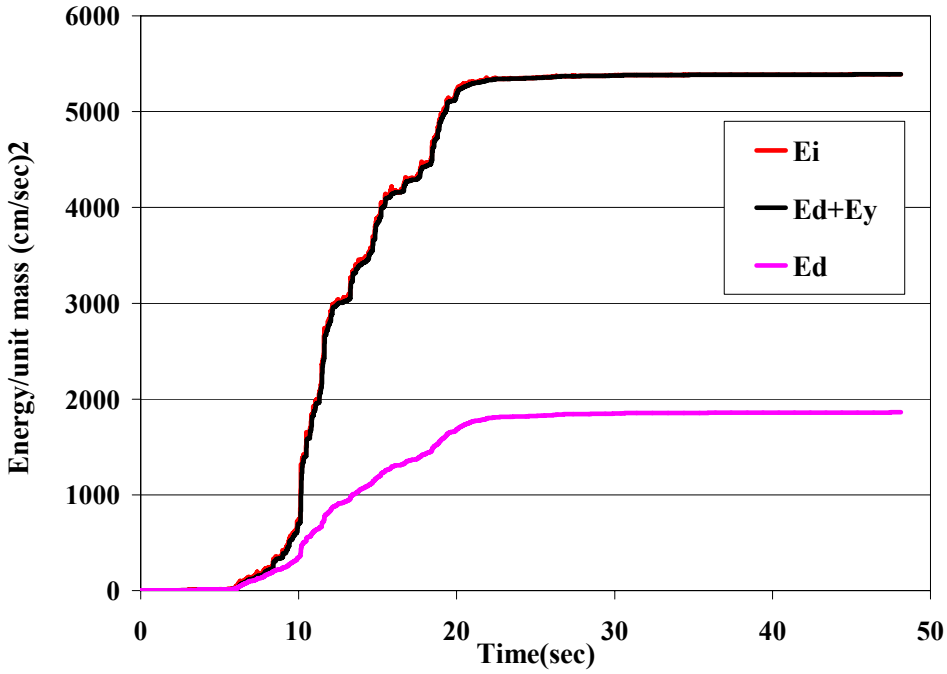

Figure 3-37 Time history of Energy dissipation for Record 13

Shake Table 2" (Landers/LCN260) - T= 0.2 sec, 5% cr. damping, Cy=0.25

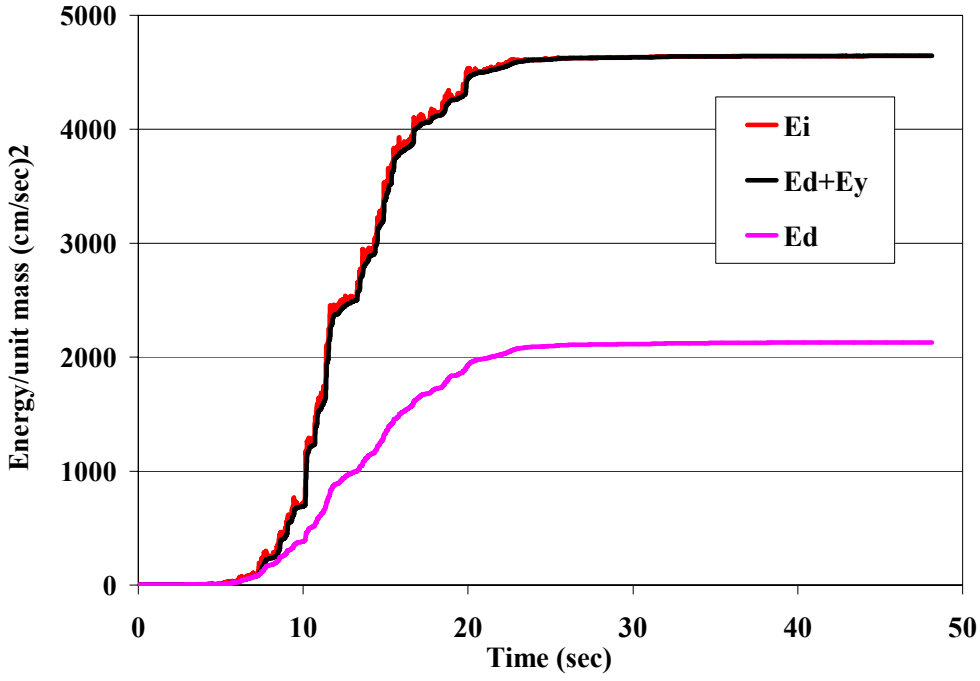

Figure 3-38 Time history of Energy dissipation for Record 13

Shake Table 2" (Landers/LCN260) - T= 0.3 sec, 5% cr. damping, Cy=0.25

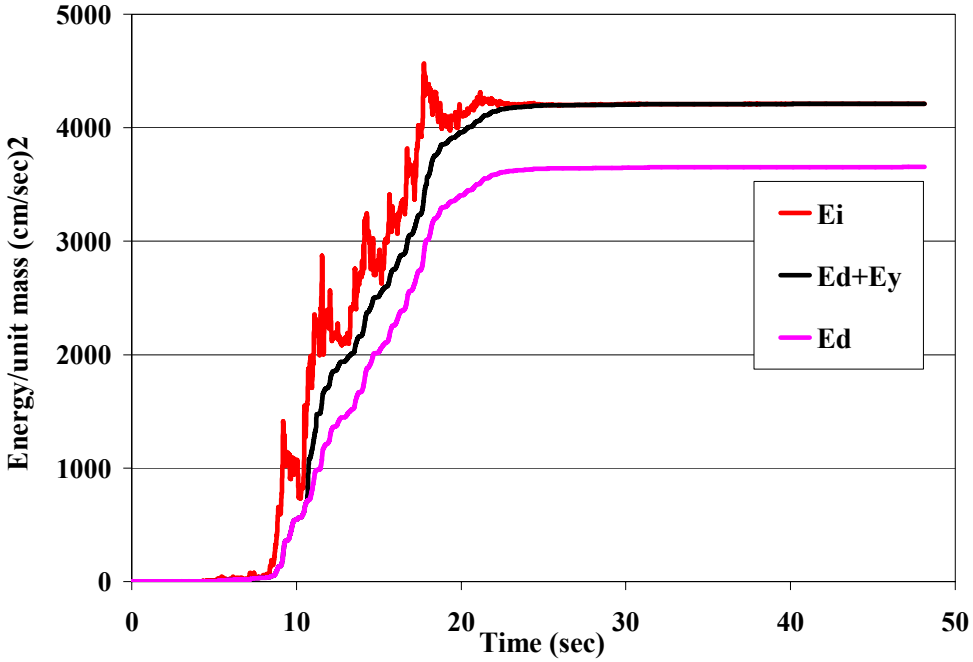

Figure 3-39 Time history of Energy dissipation for Record 13

Shake Table 2" (Landers/LCN260) - T= 1.0 sec, 5% cr. damping, Cy=0.25

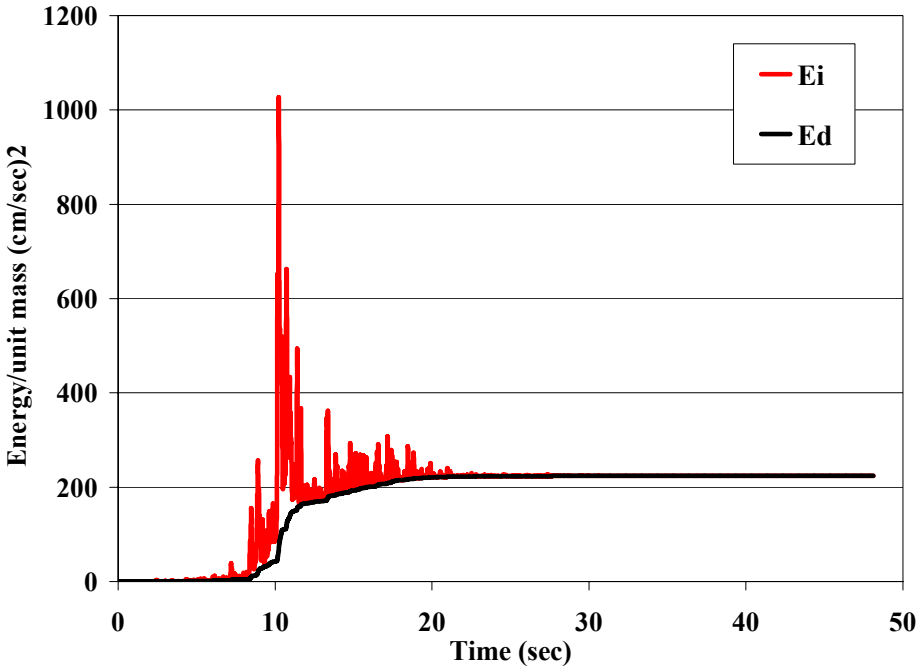

Figure 3-40 Time history of Energy dissipation for Record 13

Shake Table 2" (Landers/LCN260) - T= 3.0 sec, 5% cr. damping, Cy=0.25

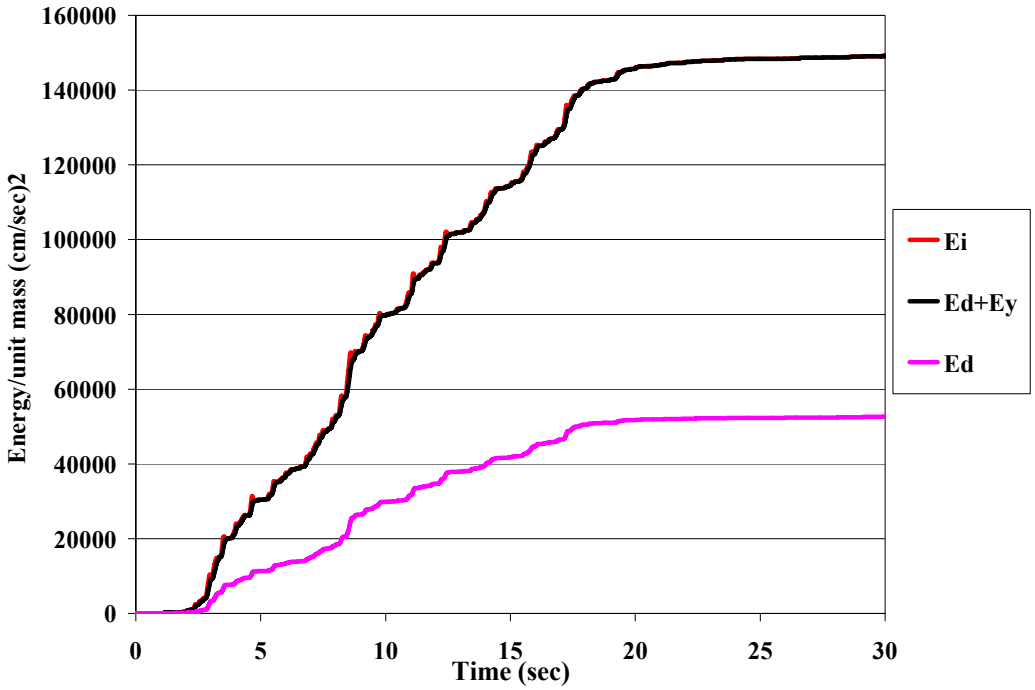

Figure 3-41 Time history of Energy dissipation for Record 19

Telcordia -T= 0.2 sec, 5% cr. damping, Cy=0.25

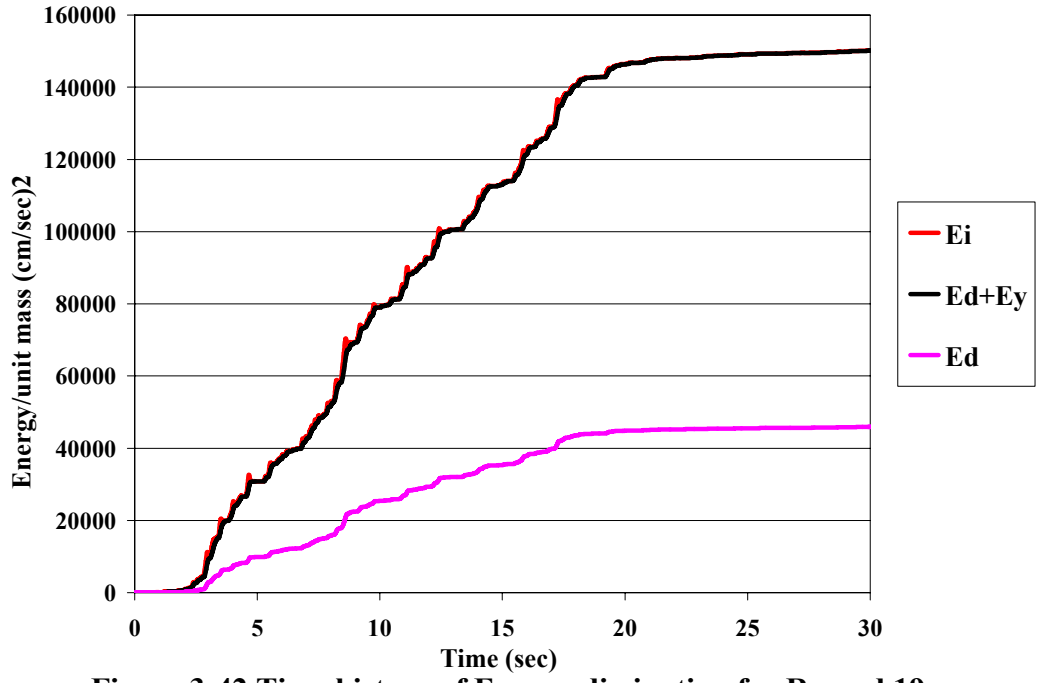

Figure 3-42 Time history of Energy dissipation for Record 19

Telcordia -T= 0.3 sec, 5% cr. damping, Cy=0.25

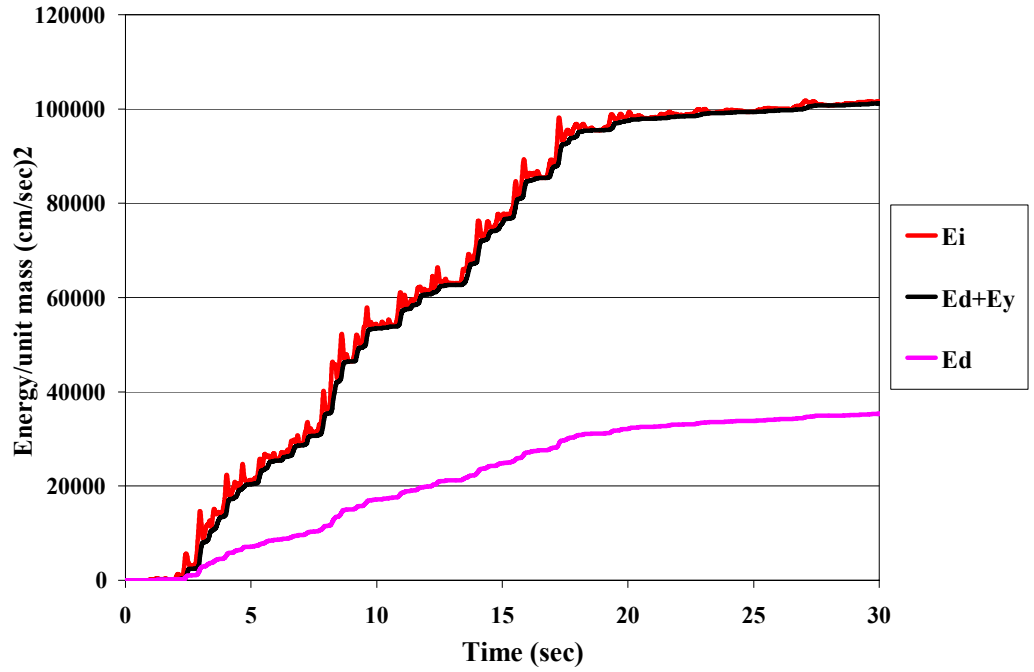

Figure 3-43 Time history of Energy dissipation for Record 19

Telcordia -T= 1.0 sec, 5% cr. damping, Cy=0.25

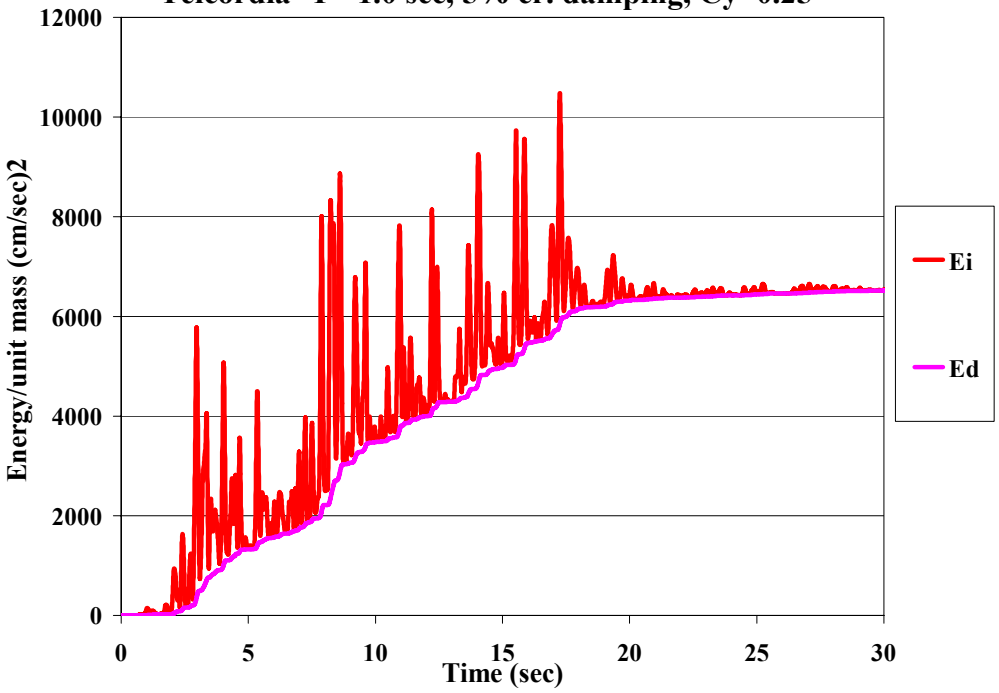

Figure 3-44 Time history of Energy dissipation for Record 19

Telcordia -T= 3.0 sec, 5% cr. damping, Cy=0.25

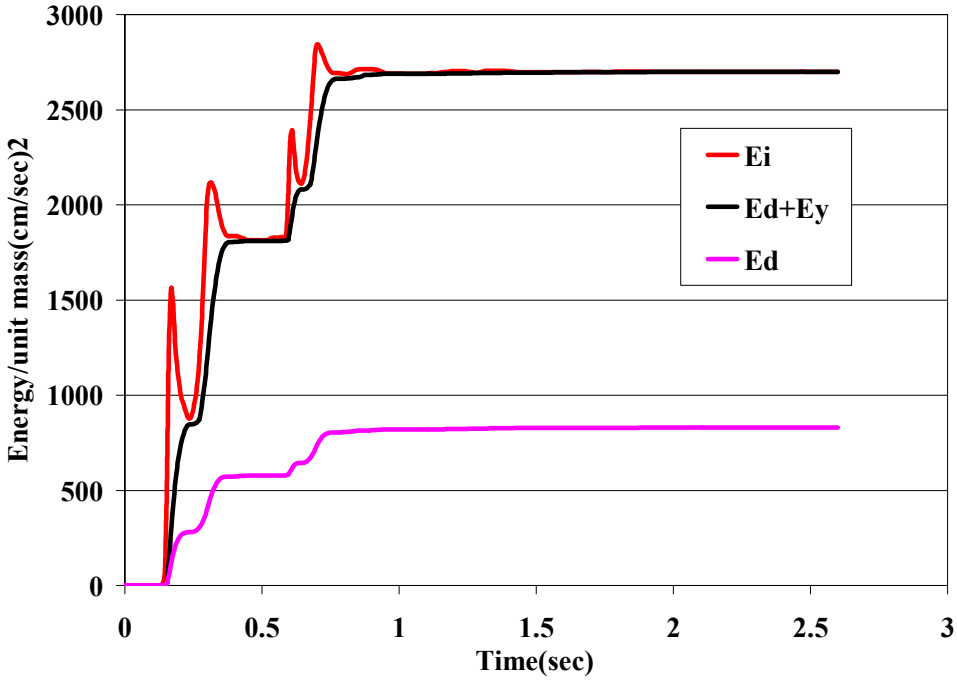

Figure 3-45 Time history of Energy dissipation for Record 20

Measured NTS-5 - T= 0.2 sec, 5% cr. damping, Cy=0.25

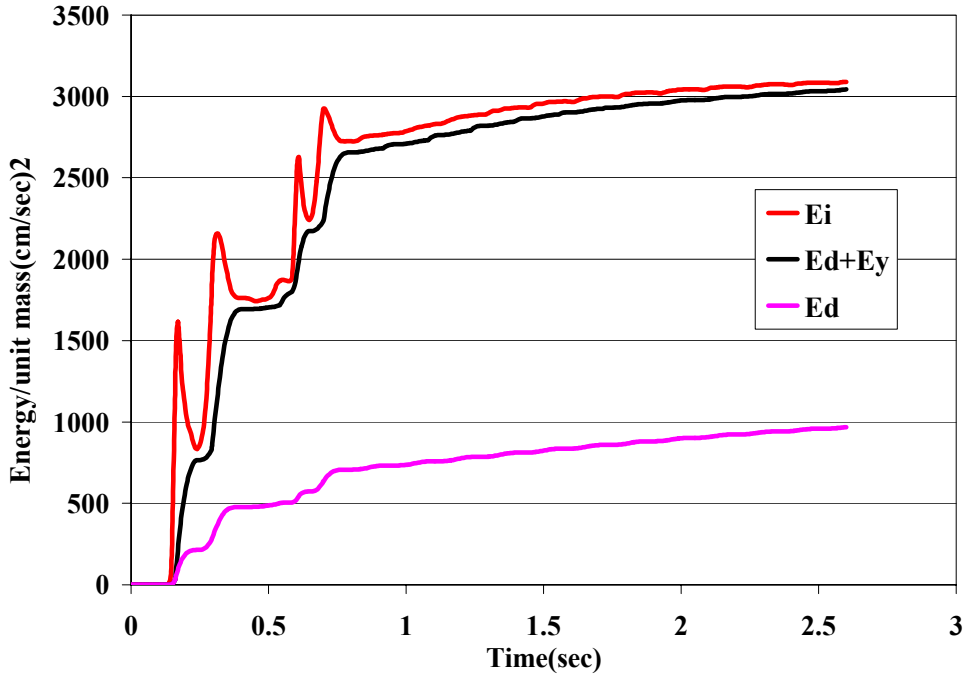

Figure 3-46 Time history of Energy dissipation for Record 20

Measured NTS-5 - T= 0.3 sec, 5% cr. damping, Cy=0.25

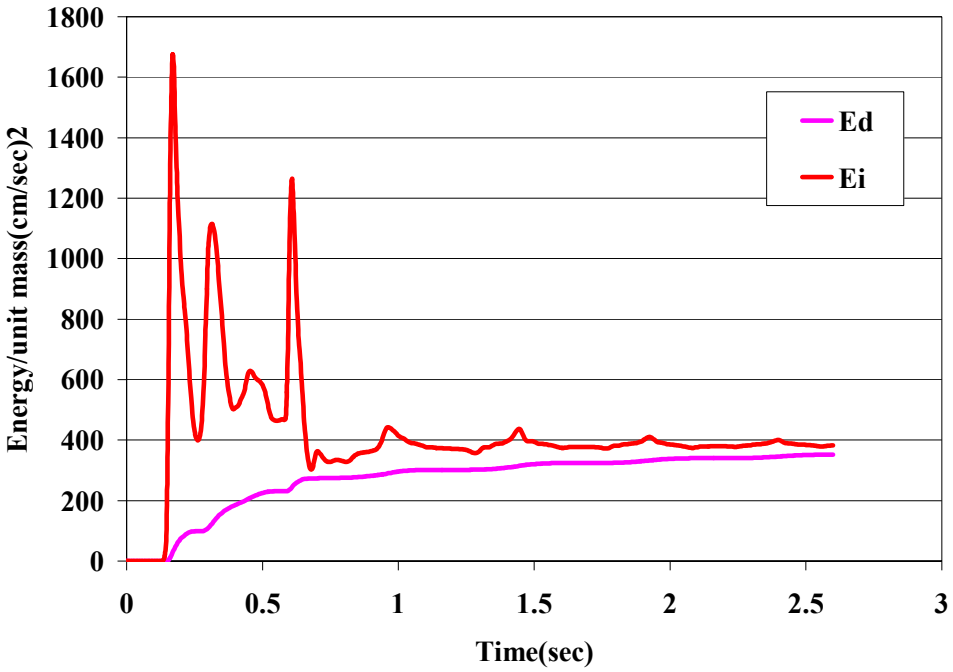

Figure 3-47 Time history of Energy dissipation for Record 20

Measured NTS-5 - T= 1.0 sec, 5% cr. damping, Cy=0.25

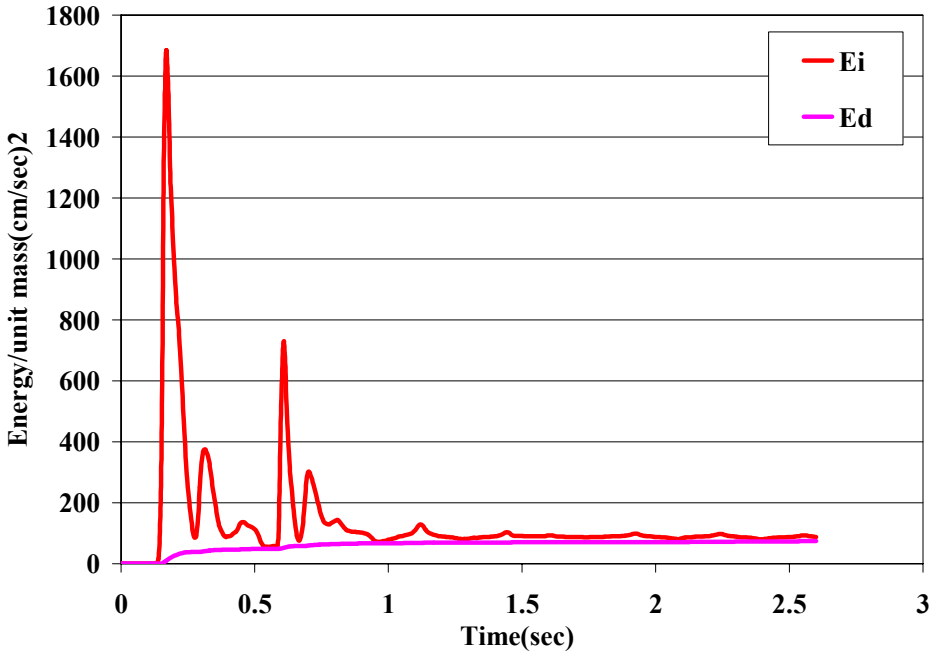

Figure 3-48 Time history of Energy dissipation for Record 20

Measured NTS-5 - T= 3.0 sec, 5% cr. damping, Cy=0.25

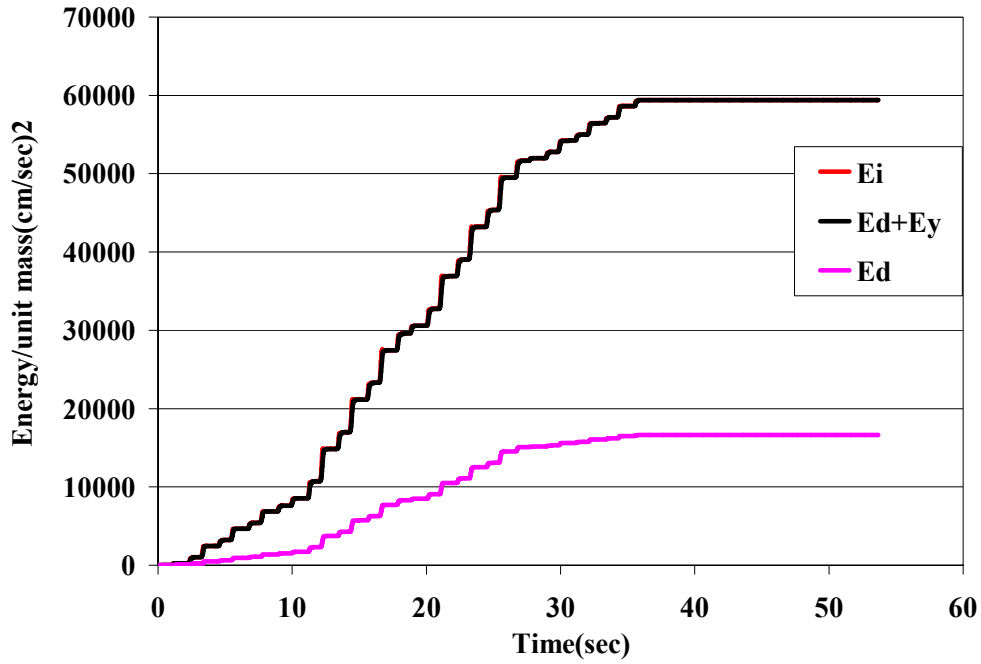

Figure 3-49 Time history of Energy dissipation for Record 22

Synthesized NTS - T=0.2 sec, 5% cr. damping, Cy=0.25

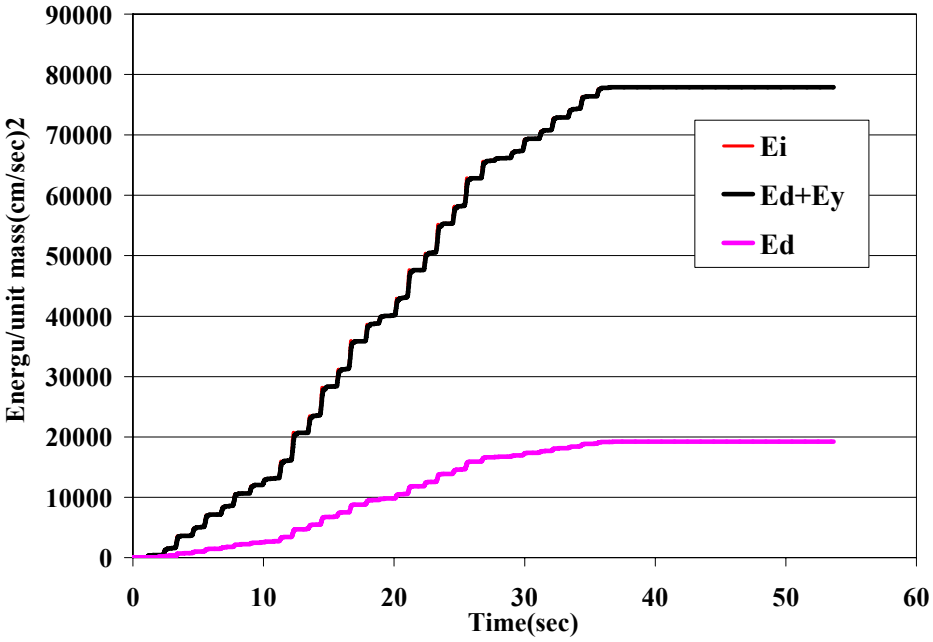

Figure 3-50 Time history of Energy dissipation for Record 22

Synthesized NTS - T=0.3 sec, 5% cr. damping, Cy=0.25

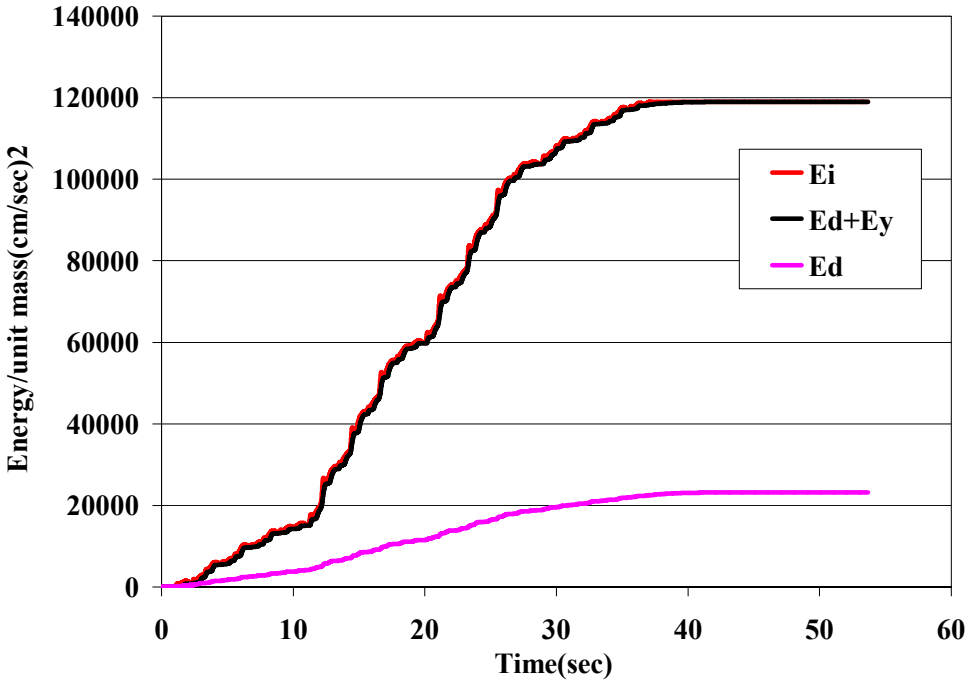

Figure 3-51 Time history of Energy dissipation for Record 22

Synthesized NTS - T=1.0 sec, 5% cr. damping, Cy=0.25

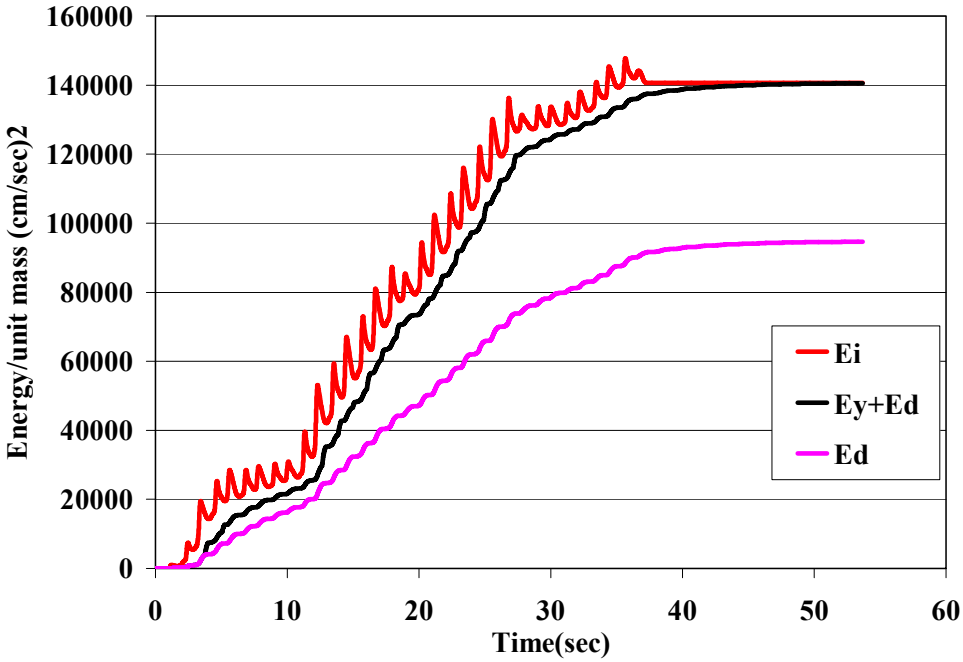

Figure 3-52 Time history of Energy dissipation for Record 22

Synthesized NTS - T=3.0 sec, 5% cr. damping, Cy=0.25

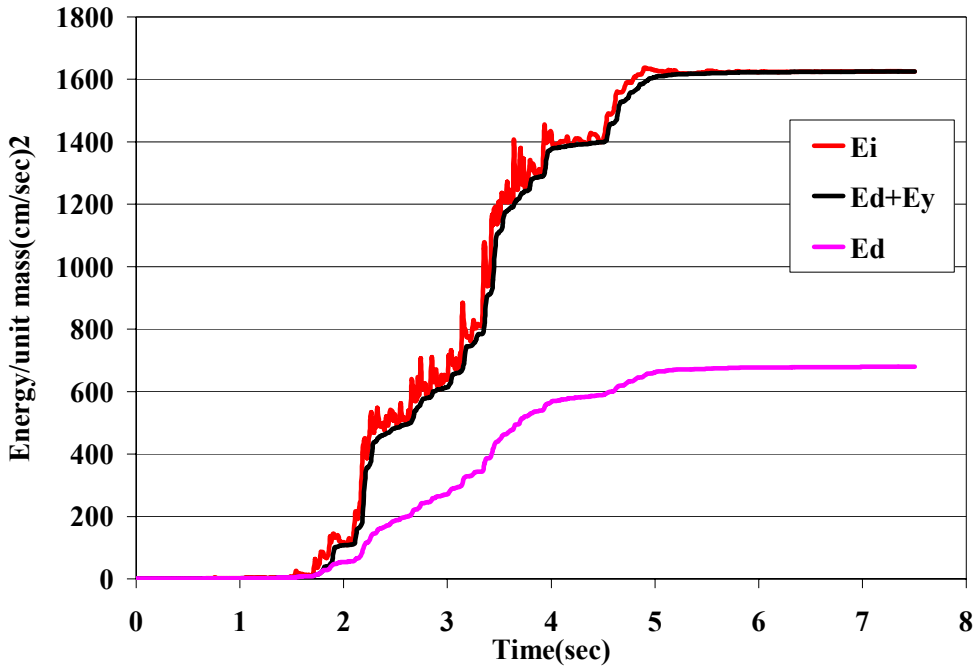

Figure 3-53 Time history of Energy dissipation for Record 23

Black Thunder Mine 50 m radial - T=0.2 sec, 5% cr. damping, Cy=0.25

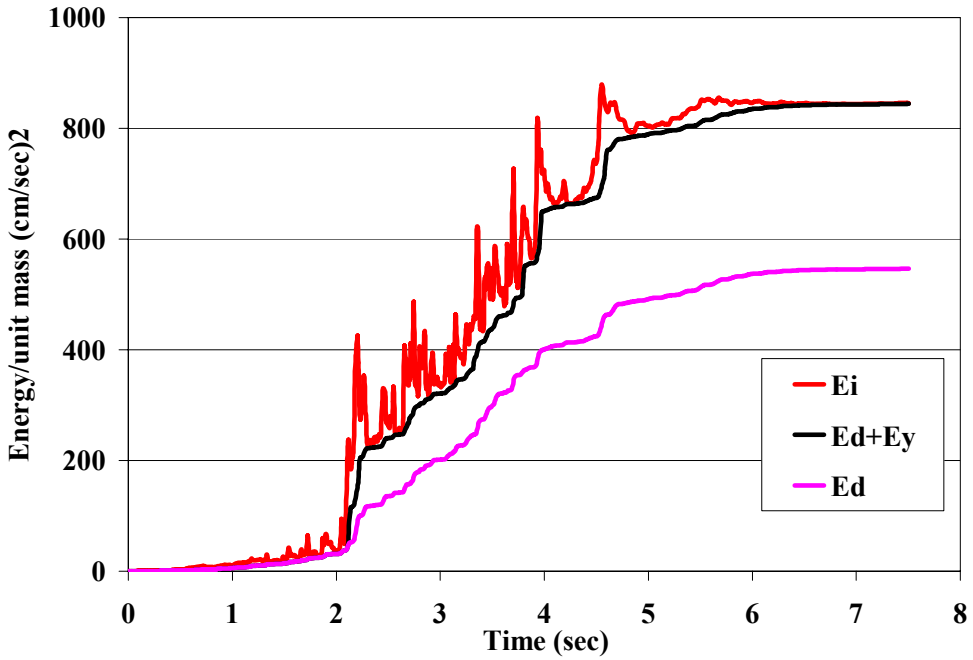

Figure 3-54 Time history of Energy dissipation for Record 23

Black Thunder Mine 50 m radial - T=0.3 sec, 5% cr. damping, Cy=0.25

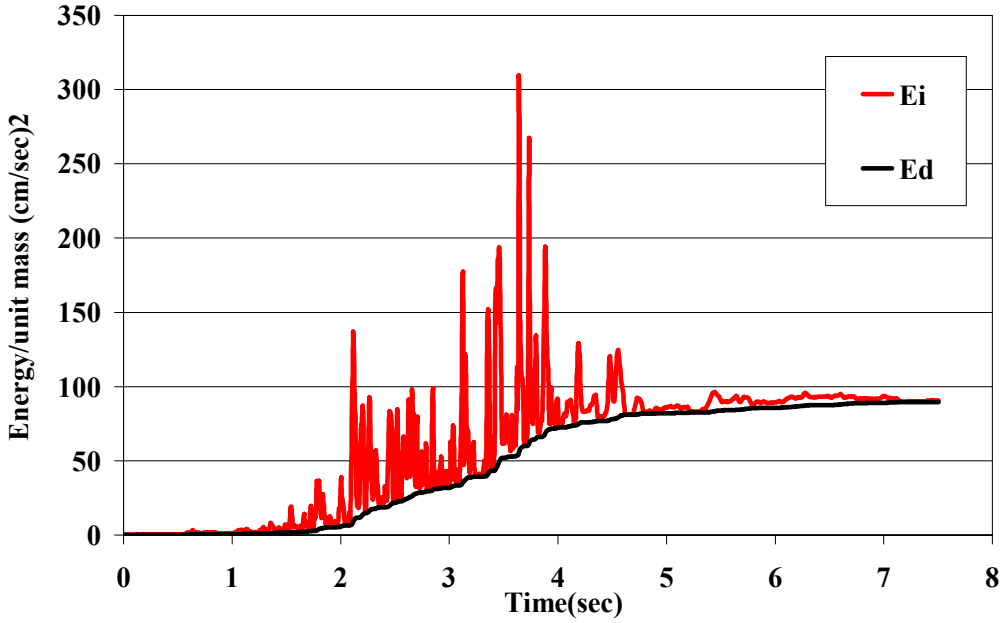

Figure 3-55 Time history of Energy dissipation for Record 23

Black Thunder Mine 50 m radial - T=1.0 sec, 5% cr. damping, Cy=0.25

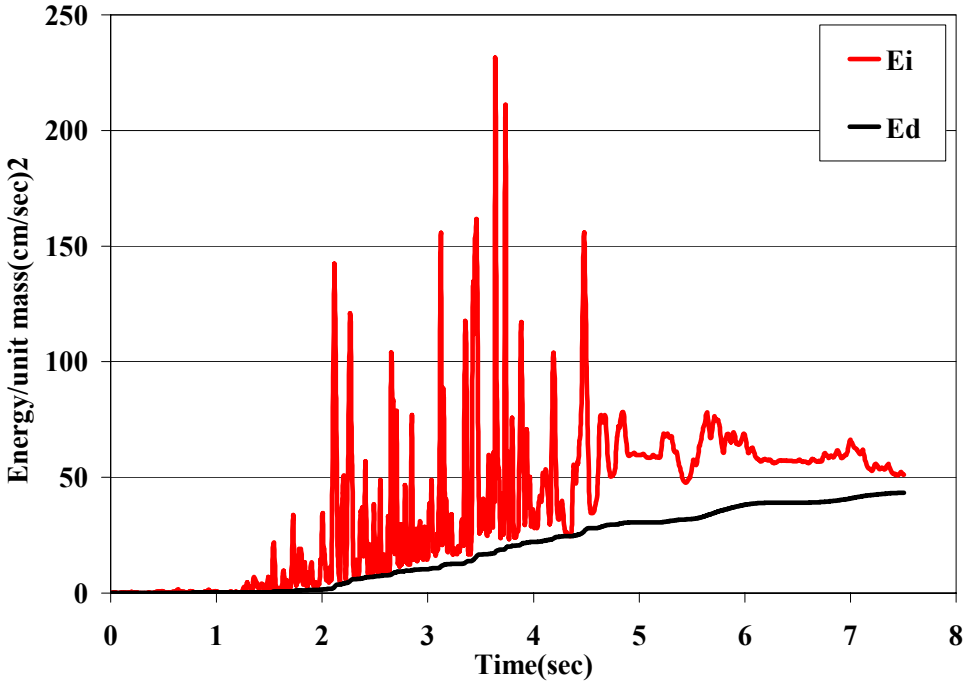

Figure 3-56 Time history of Energy dissipation for Record 23

Black Thunder Mine 50 m radial - T=3.0 sec, 5% cr. damping, Cy=0.25

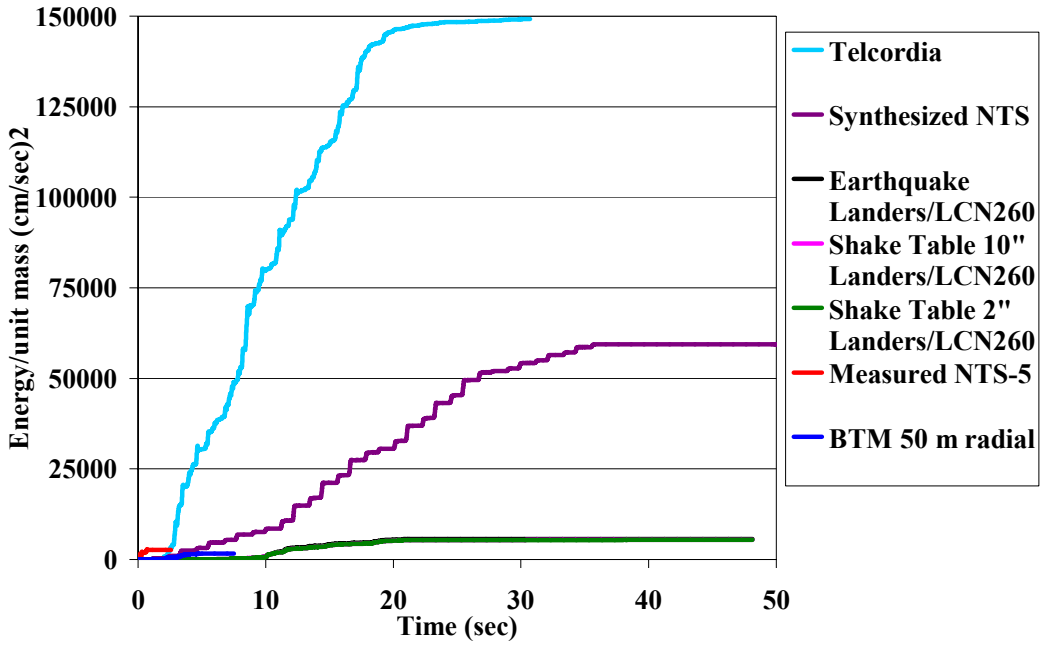

Figure 3-57 Energy input time history for selective records

T=0.2 sec, 5% cr. damping, Cy=0.25

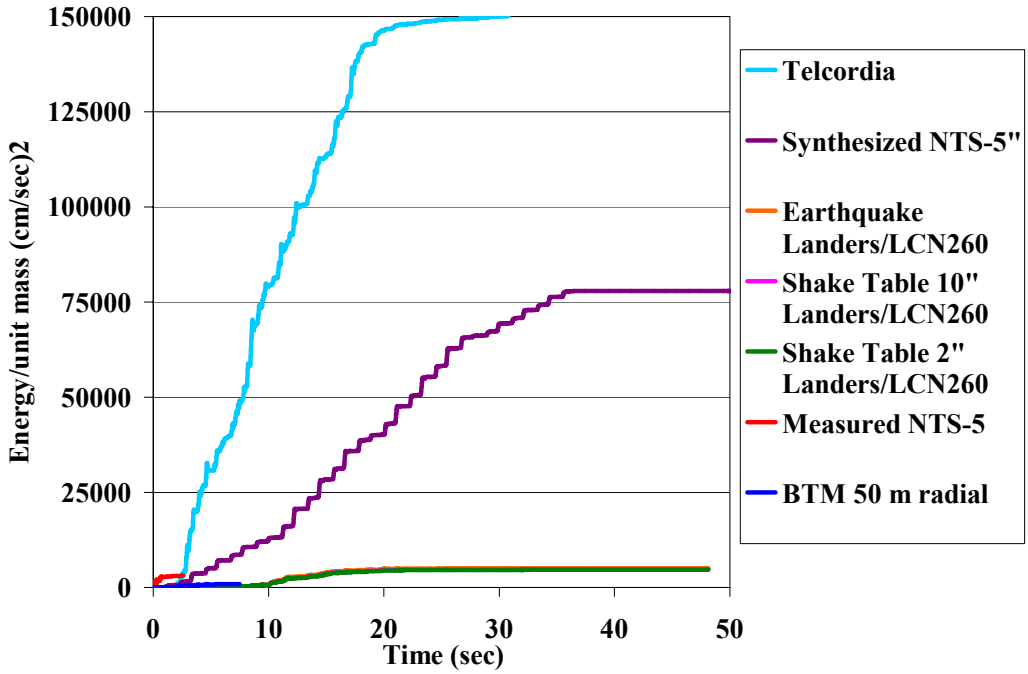

Figure 3-58 Energy input time history for selective records

T=0.3 sec, 5% cr. damping, Cy=0.25

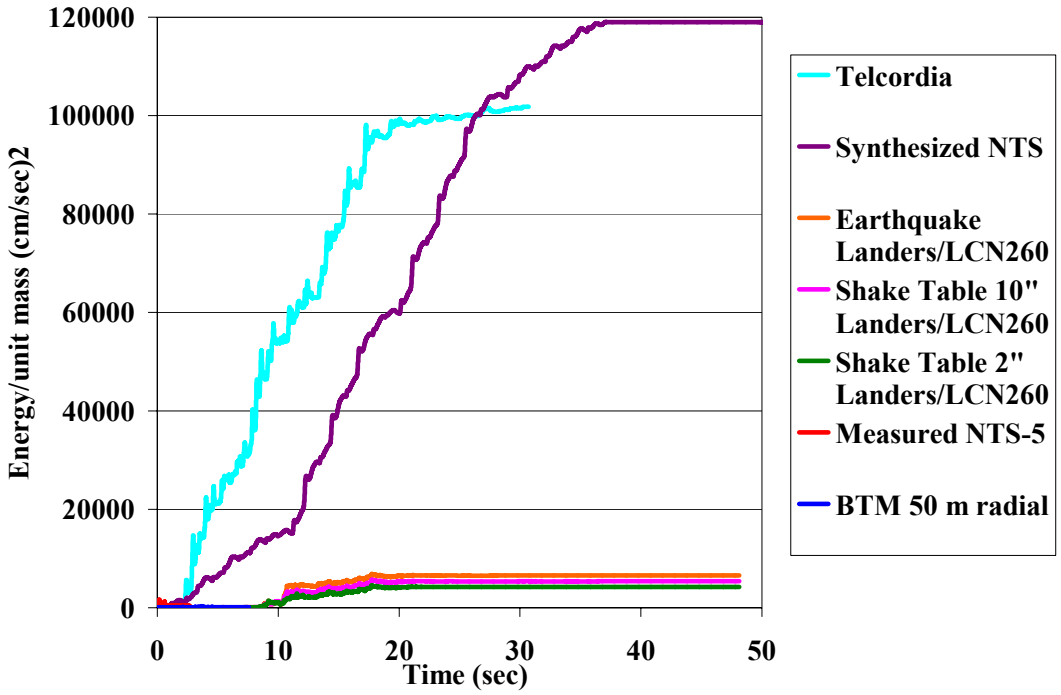

Figure 3-59 Energy input time history for selective records

T=1.0 sec, 5% cr. damping, Cy=0.25

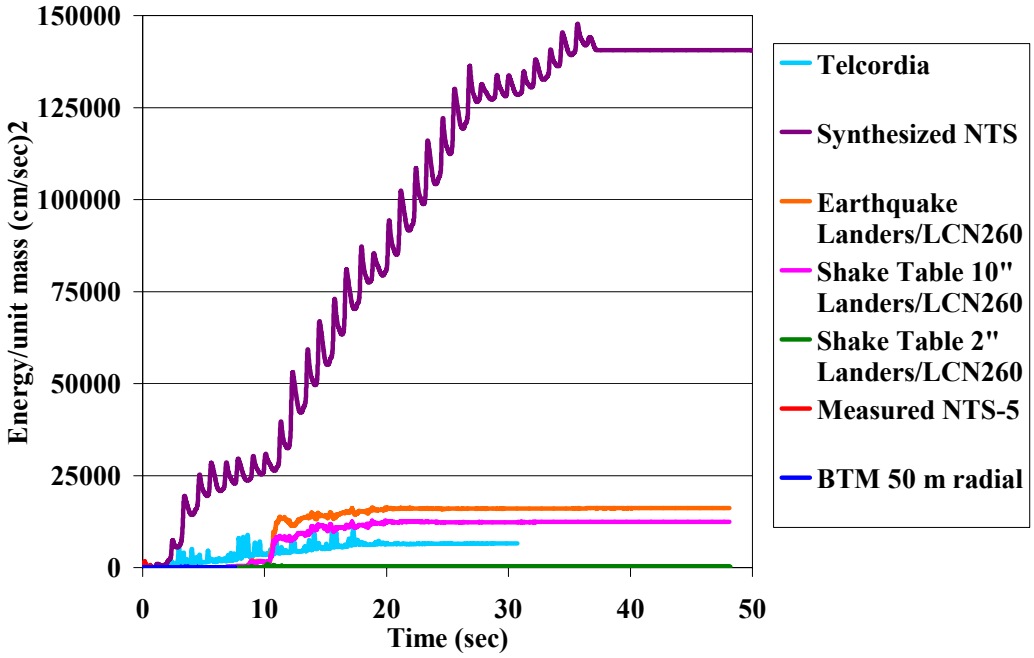

Figure 3-60 Energy input time history for selective records.

T=3.0 sec, 5% cr. damping, Cy=0.25

3.7 Conclusions

Based on the records' characteristics and the analysis results we can draw the following conclusions for the experimental testing methods under consideration:

Shake table records (10" and 2" displacement limit, Telcordia)

The earthquake records and the corresponding shake table (10" displacement limit) have almost identical values for the peak acceleration, Arias intensity and cumulative absolute velocity. Their linear response spectra values are also identical throughout the spectrum. From all the testing methods examined in this study, the results of the analysis for the large shake table (10" displacement limit) records are the closest to the results for the corresponding earthquake records. Full-scale experiments are difficult to perform with small (2" displacement limit) shake tables due to limitations of velocities and displacements.

The Telcordia record has the largest total input energy for period values 0.2 and 0.3 sec from all the records. Specimens subjected to the Telcordia excitation can reach response values beyond their elastic limit and valuable insight into their non-linear behavior can be gained. However, the Telcordia record can only be produced on large shake tables.

NETI records

More information is needed regarding the quantitative correlation between the number of the explosive RESQUE sources used at the NETI facility, the intensity of the triggered excitation and the level of the potential structural damage to the participating specimens. Due to the large input energy generated by the detonation of the explosives, it is evident that specimens will dissipate energy through non-linear cyclic response and will sustain considerable structural damage. The RESQUE technique can also be fielded around existing structures to test the dynamic characteristics of actual full-scale structures in situ.

BTM records

The total input energy for the BTM records attenuates rapidly with increasing distance from the explosive source. Only experiments in a less than 100 m. radius from the source can take place in order to have significant excitation. Full-scale experimentation remains difficult, since the total input energy from a BTM record, even the 50 m. radial, is significantly smaller than the total earthquake energy. Small excitation duration prohibits energy dissipation through many hysteretic cycles. This kind of excitation may be appropriate for small-scale experiments (1/4 scale or smaller).

4. FINITE ELEMENT ANALYSIS FOR A COUPLING CAPACITOR VOLTAGE TRANSFORMER (CCVT –TYPE EHCM-550)

4.1 Introduction

A finite element model of a coupling capacitor voltage transformer (CCVT EHCM-550) was implemented with the SAP2000 finite element computer program. The material and section properties for the CCVT were adopted from the RITZ Instrument transformer, INC brochure [Ref.22]. The CCVT FEM was subjected to the input acceleration time histories (R1-R28) presented in section 3.2 and a time history analysis was implement for each record.

The bending moment at the base of the porcelain capacitor was chosen to be the critical index to define the strength capability for the CCVT and its factor of safety against failure. The porcelain manufacturer, NGK Insulators, Ltd. of Japan, tested the breaking strength of the porcelain insulators for the CCVT Type EHMC-525 and found it to be 42.45 kip-ft. Selective time history traces for the base moment as well as the factor of safety for the record ensemble are presented in the following sections.

4.2 Description of CCVT

The Ritz Instrument Transformers Coupling Capacitor Voltage Transformer (CCVT) type EHCM-525 consists of 3 units housed in porcelain shells. An aluminum cover is placed at the top of each capacitor unit. The assembly is fitted with an aluminum terminal at the top to allow for a high voltage connection. The capacitor stack consists of a series of capacitor elements. Each element consists of the purest cellulose Kraft paper and polypropylene film soaked into synthetic oil.
A fabricated steel base tank supports the porcelain capacitor.
It serves to house the electromagNeTIc unit and related circuitry
The mineral oil in the base tank is separated from the oil in the capacitor units and is hermetically sealed from environmental influences.

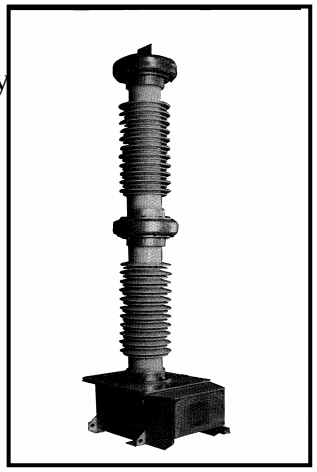

Figure 4-1 CCVT Ritz Instrument Transformers, INC.

4.3 Finite Element Model

The finite element model for the CCVT is comprised of :
- 16 joints, 15 frame elements, 5 material properties, 6 section properties.

The joint coordinates, frame section and material properties are given in the following tables. The units are kip/inches. The six degrees of freedom for joint 1 are fixed.

J O I N T C O O R D I N A T E S

JOINT	X	Y	Z
1	0.000	0.000	0.000
2	0.000	0.000	19.800
3	0.000	0.000	20.800
4	0.000	0.000	29.900
5	0.000	0.000	76.000
6	0.000	0.000	83.700
7	0.000	0.000	87.700
8	0.000	0.000	96.800
9	0.000	0.000	142.800
10	0.000	0.000	150.600
11	0.000	0.000	154.500
12	0.000	0.000	163.600
13	0.000	0.000	209.700
14	0.000	0.000	218.400
15	0.000	0.000	222.300
16	0.000	0.000	226.300

M A T E R I A L P R O P E R T Y D A T A

MATERIAL LABEL	WEIGHT PER UNIT VOL	MASS PER UNIT VOL	MODULUS OF ELASTICITY	SHEAR MODULUS	POISSON'S RATIO
STEEL	0.2830E-03	0.7324E-06	0.290E+05	0.112E+05	0.3
BOXMAT	0.3910E-03	0.1013E-05	0.300E+05	0.115E+05	0.3
PORCELAI	0.3460E-03	0.8963E-06	0.900E+04	0.346E+04	0.3
BELMAT	0.1000E-05	0.2588E-08	0.100E+05	0.385E+04	0.3
ALUMINUM	0.9600E-04	0.2985E-05	0.100E+05	0.385E+04	0.3

F R A M E S E C T I O N P R O P E R T Y D A T A

SECTION LABEL	AXIAL AREA	TORSIONAL CONSTANT	MOMENTS OF INERTIA I33	MOMENTS OF INERTIA I22	SHEAR AREAS A2	SHEAR AREAS A3
BOXPLAT	0.418E+03	0.230E+05	0.117E+05	0.193E+05	0.306E+03	0.306E+03
BASEBOX	0.306E+02	0.111E+04	0.703E+03	0.104E+04	0.562E+01	0.545E+01
PORCEL2	0.157E+02	0.201E+04	0.584E+02	0.584E+02	0.304E+02	0.304E+02
PORCEL1	0.490E+02	0.235E+04	0.640E+03	0.640E+03	0.338E+02	0.338E+02
BELLOWS	0.403E+02	0.100E+01	0.954E+03	0.954E+03	0.675E+01	0.675E+01
ALUMINU	0.195E+02	0.523E+02	0.386E+02	0.260E+02	0.163E+02	0.163E+02

F R A M E E L E M E N T D A T A

ELEMENT LABEL	JOINT END-I	JOINT END-J	ELEMENT LENGTH	SECTION LABEL	MATERIAL LABEL
F1	1	2	19.800	BASEBOX	BOXMAT
F2	2	3	1.000	BOXPLAT	STEEL
F3	3	4	9.100	PORCEL1	PORCELAI
F4	4	5	46.100	PORCEL2	PORCELAI
F5	5	6	7.700	PORCEL1	PORCELAI
F6	6	7	4.000	BELLOWS	BELMAT
F7	7	8	9.100	PORCEL1	PORCELAI
F8	8	9	46.000	PORCEL2	PORCELAI
F9	9	10	7.800	PORCEL1	PORCELAI
F10	10	11	3.900	BELLOWS	BELMAT
F11	11	12	9.100	PORCEL1	PORCELAI
F12	12	13	46.100	PORCEL2	PORCELAI
F13	13	14	8.700	PORCEL1	PORCELAI
F14	14	15	3.900	BELLOWS	BELMAT
F15	15	16	4.000	ALUMINU	ALUMINUM

T O T A L W E I G H T S A N D M A S S E S

SECTION LABEL	WEIGHT	MASS
BOXPLAT	0.1183	0.0003
BASEBOX	0.2369	0.0006
PORCEL2	0.7488	0.0019
PORCEL1	0.8731	0.0023
BELLOWS	0.0005	0.0000
ALUMINU	0.0075	0.0002
TOTAL	1.9852	0.0054

4.4 Analysis Results

Table 4.1 Modal Periods and Frequencies for the CCTV

Modes	Period (sec)	Frequency (Hz)
1	0.433	2.31
2	0.432	2.31
3	0.068	14.73
4	0.068	14.78
5	0.023	42.89
6	0.023	43.10

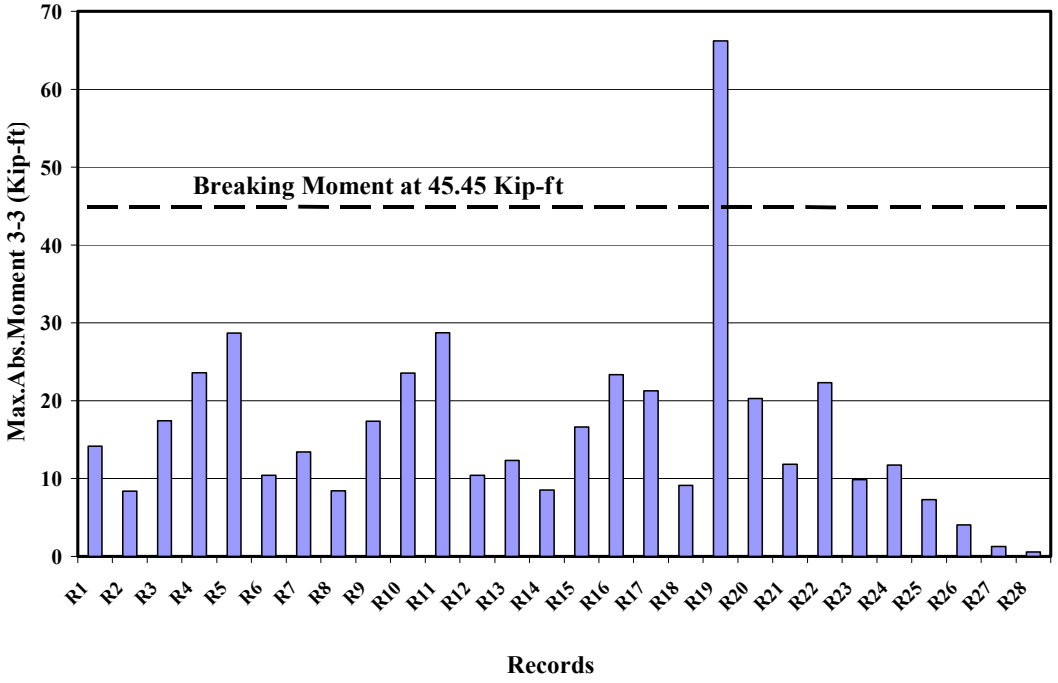

Figure 4-2 Maximum Absolute Moment 3-3 at the base of the porcelain capacitor for 2 % critical damping.

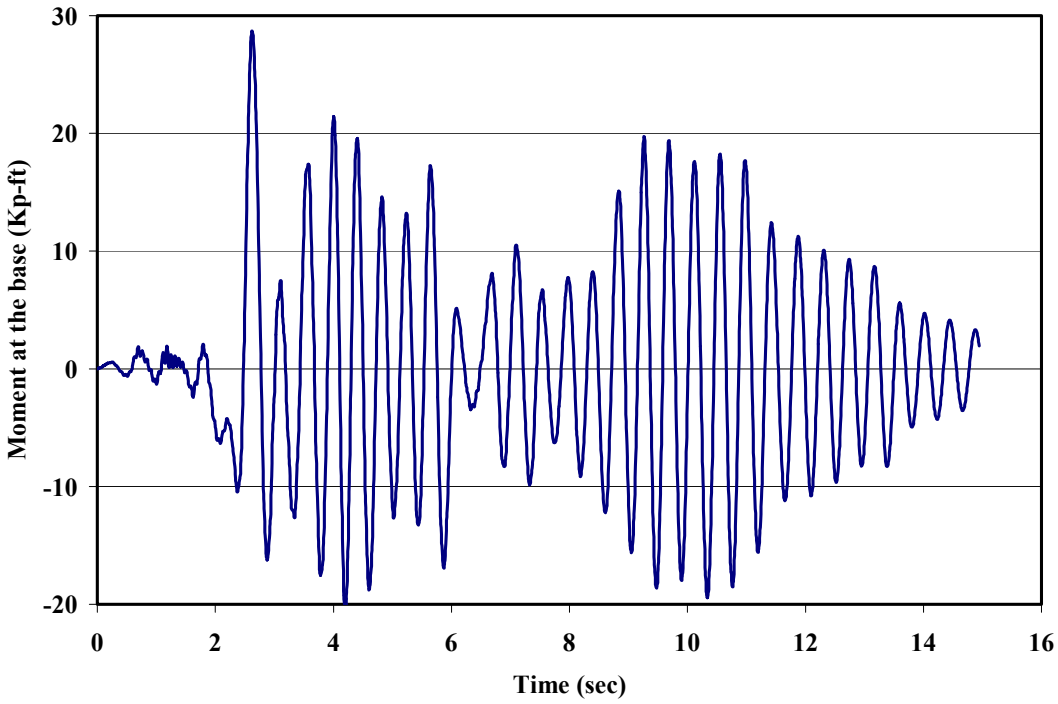

Figure 4-3 Record 5 Northr RRS-288, Time History for the moment at the base of the porcelain capacitor for 2% critical damping

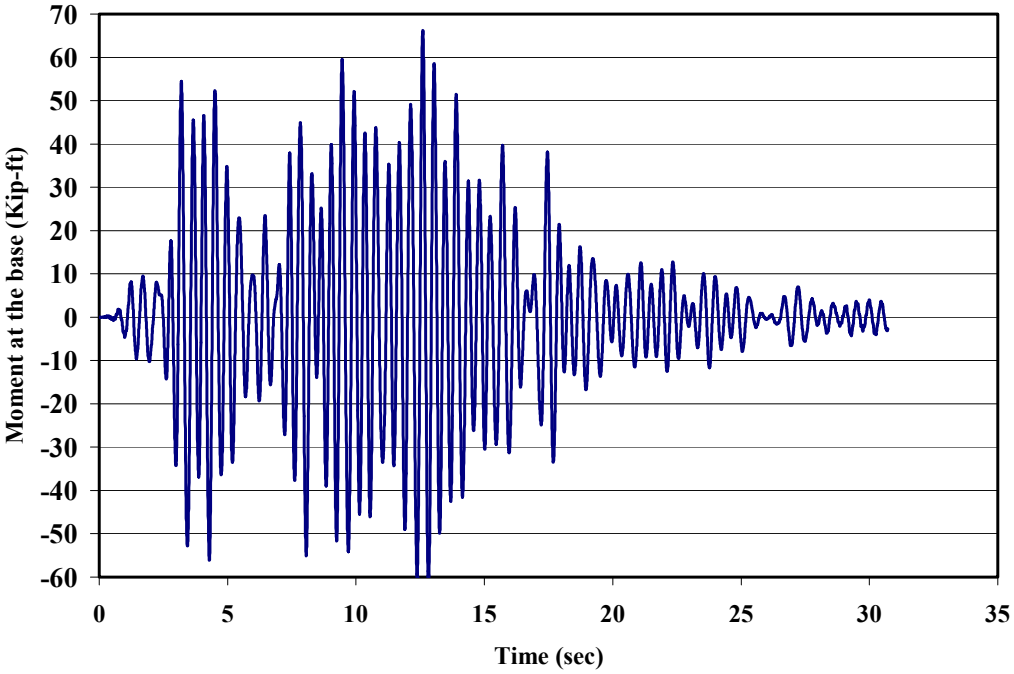

Figure 4-4 Record 19 Telcordia, Time History for the moment at the base of the porcelain capacitor for 2% critical damping.

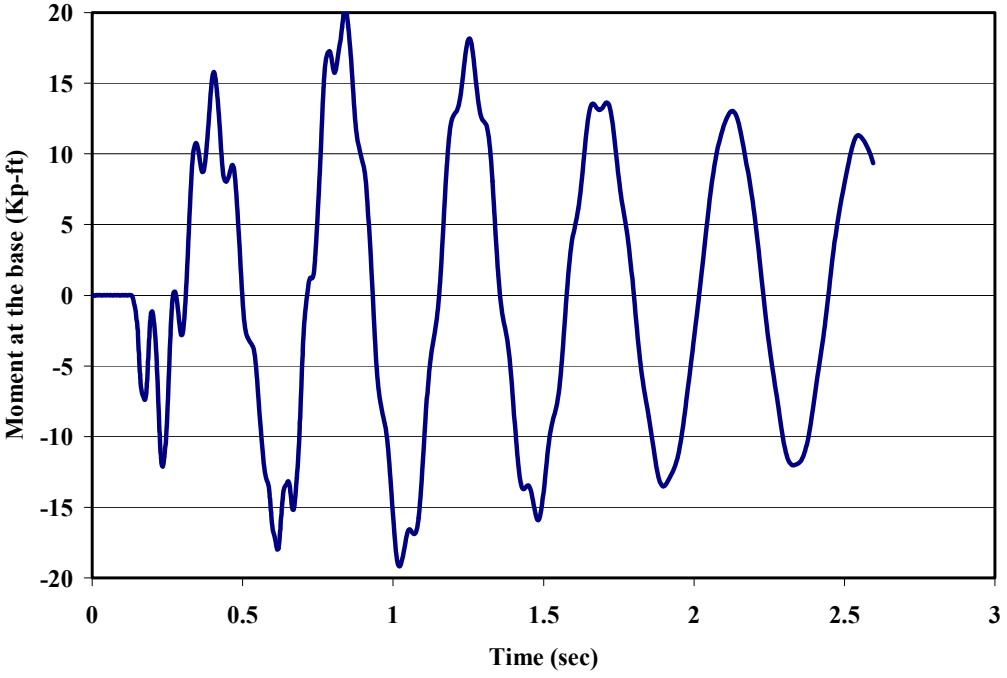

Figure 4-5 Record 20 Measured NTS-5, Time History for the moment at the base of the porcelain capacitor for 2% critical damping.

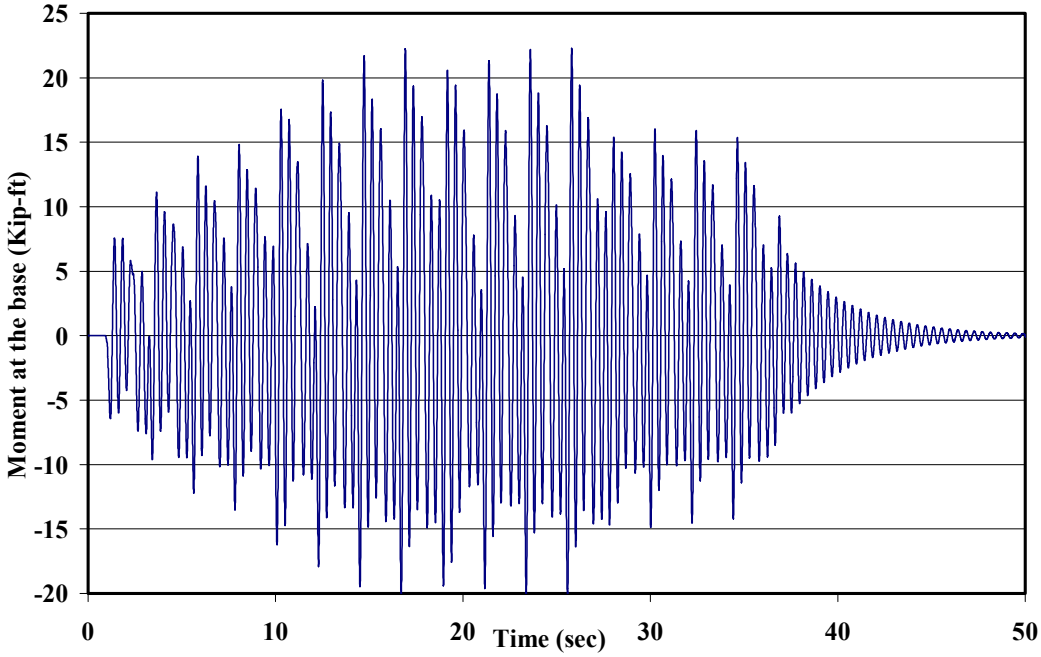

Figure 4-6 Record 22 Synthesized NETI, Time History for the moment at the base of the porcelain capacitor for 2% critical damping.

REFERENCES

1. Assessment of Earthquake Engineering Research and Testing Capabilities in the United States, Proceedings, EERI, Sept 1995, WP-01A

2. Seible, Fr and Shing B.P., "*Worldwide Survey Of Earthquake Engineering Testing Facilities*", Assessment of Earthquake Engineering Research and Testing Capabilities in the United States, Proceedings, EERI, Sept 1995, WP-01A

3. M.Watabe, *Large Scale Testing Facilities for Earthquake Engineering In Japan*, Assessment of Earthquake Engineering Research and Testing Capabilities in the United States, Proceedings, EERI, Sept 1995, WP-01A

4. Clark A.J., "*A Futuristic View Of Structural Experimental Facilities*", Assessment of Earthquake Engineering Research and Testing Capabilities in the United States, Proceedings, EERI, Sept 1995, WP-01A

5. Gefken P.R. and Curran D.R., *"Generation Of Strong Ground Motion In Support Of Development Of A Full-Scale Test Facility*", SRI International, Final Technical Report, Jan 1999

6. Blume, J.A., "*The Motion and Damping of Buildings Relative to Seismic Response Spectra",* Bull. Seism. Soc. Am. 60 (1) , Feb 1970:231-259

7. Blume, J.A., "*High-rise Building Characteristics and Responses Determined from Nuclear Seismology", ",* Bull. Seism. Soc. Am. 62 (2), April1972: 519-540

8. Bleiweis, P.B. et al., "*Simulation of Strong Ground Motion Earthquake Effects on Structure Using Explosive Blasts*", Nucl. Eng. Des. 25, 1973:126-149

9. Taylor, G.B. et al., "*Seismic Proof Tests Using Explosives to Produce Strong Ground Motion*", Nucl. Eng. Des. 29, 1974:202-217

10. Higgins, C.J. and Triantafilidis, G.E., *"The Simulation of Earthquake Ground Motions with High Explosives*", Proceedings of the Sixth World Conference on Earthquake Engineering, New Delhi, Vol.1, 1977:489-495

11. Higgins, C.J. et al.," *High Explosive Simulation of Earthquake-Like Ground Motions*", Proceedings of the 2nd Specialty Conference on Dynamic Response of Structures: Experimentation, Observation, Prediction, and Control, ASCE, 1981:126-140

12. Higgins, C.J. et al.," *A small Explosive Simulation of Earthquake-Like Ground Motions With High Explosives*", Earthquake Engineering and Soil Dynamics, Proc. ASCE Geotech. Eng. Division Specialty Conference, Vol. 2, 1978:512-529

13. Bruce, J.R. et al., "*Simulation of Strong Earthquake Motion With Contained Explosive Line Source Arrays*", Proceedings of the 2nd U.S. National Conference on Earthquake Engineering, EERI, 1979: 1134-1143

14. Bruce, J.R. and Lindberg H.E.,*"Earthquake Simulation Using Contained Explosions*", Proceedings of the 2nd Specialty Conference on Dynamic Response of Structures: Experimentation, Observation, Prediction and Control, ASCE, 1981:111-125

15. PEER Strong Motion Database [http://peer.Berkeley.edu]

16. Telcordia Technologies, *Network Equipment –Building System (NEBS) Requirements: Physical Protection,* GR-63-CORE - Issue 1, October 1995

17. Arias, A., " *A measure of earthquake intensity* " in Seismic Design for Nuclear Power Plants (R.J. HANSEN ed.), MIT Press, 1970, pp.438-483

18. EPRI,"*A criterion for determining exceedance of the operating basis earthquake* ", EPRI NP-5930, Electrical Power Research Inst., Palo Alto, CA, 1988

19. EPRI, "*Standardization of the cumulative absolute velocity*", EPRI TR-100082 (Tier 1), Electrical Power Research Inst., Palo Alto, CA, 1991

20. NEES-2 Assessment and completion of the George E. Brown, Jr. Network for Eearthquake Engineering Simulation (NEES) Major Research Equipment (MRE) portfolio , Available online at http://nees.ucsd.edu

21. Conte, J.P. et al., *"Influence of the earthquake ground motion process and structural properties on response characteristics of simple structures",* Report No. UCB/EERC-90/09, University of California at Berkeley, July 1990

22. RITZ Instrument Transformers, INC , Coupling Capacitor Voltage Transformers SHCR/SHCM 72.5…550, EHCR/EHCM 72.5…800

23. Directory of International Earthquake Engineering Research Facilities, SRI International, October 2001 [http://stpp.wdc.sri.com/earthquake].

24. Black Thunder Mine Event Of April 3, 1997 Corrected Ground Motion Records Response Spectra And Attenuation Data, Kajima Corporation Nuclear Structures

Engineering Department Tokyo, Japan, Cornelius J.Higgins, J.A. Pires and R. Guice ARA Inc., May 1997.

25. Dynamics of Structures Theory and Applications to Earthquake Engineering, Anil K. Chopra